Workshop "Characterization of Fault Zones"

EXTENDED ABSTRACTS

09th of October 2013

Salzburg Congress, Austria

Österreichische
Gesellschaft für
Geomechanik

A-5020 Salzburg
Innsbrucker Bundesstr. 67

T +43 (0)662 87 55 19
F +43 (0)662 88 67 48
E salzburg@oegg.at
www.oegg.at

Characterization of Fault Zones

CONTENT

Characterization and Classification of Fault Zones

F. Fasching [a] & R. Vanek [a]

[a] *3G Gruppe Geotechnik Graz ZT-GmbH, Graz, Austria*

1. INTRODUCTION

The characterisation of brittle fault zones is one of the essential interdisciplinary tasks in the fields of engineering geology and geotechnics. The prediction of the rock mass model and detailed knowledge about the mechanical properties of various fault rocks are of particular significance. The complexity of fault zones and their relevance for constructions make it necessary to implement a project-specific characterisation of the rock mass.

All relevant geological, hydrogeological and geotechnical conditions should be described. In addition, the construction and economic background of each project has to be taken into consideration in order to be able to deliver practical information for the designer team. Considering this, a clear path from investigation, through the development of the geological model to the geotechnical design and the construction is essential.

The talk summarizes the significant characteristics of fault zones and presents their practical implementation in a project-specific characterisation. Additional, short descriptions of different types of fault rocks and fault zones are given. The intention is to illustrate the engineering geological characterisation of fault rocks and fault zones in order to provide the data needed for geotechnical and construction design.

2. SUMMARY OF THE TALK

The considerations presented, can be summarised by the following statements:

- Fault zones represent complex geological structures that are composed of various rocks with different properties.
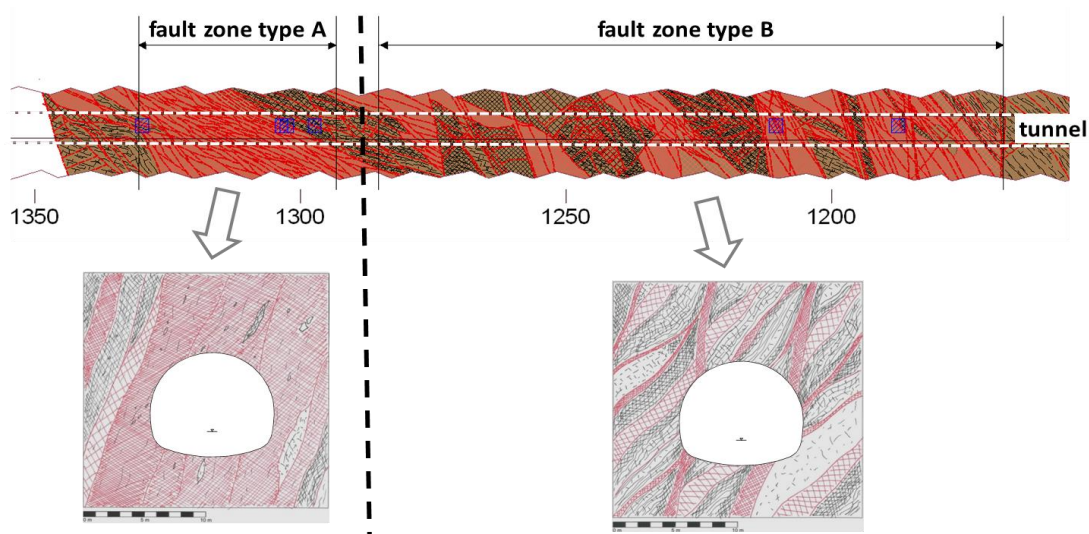
Figure 1: Longitudinal section of a tunnel drive in a fault zone; two cross sections.

- Each fault zone is unique, due to a wide range of different influencing factors, such as:

  – modes of tectonic displacement
  – stress field
  – temperature-level
  – duration of displacement (age of fault)
  – amount and rate of displacement (tectonic activity)
  – parent rock mass (lithology, mineral content, structure ...)
  – groundwater conditions

The interaction of those factors causes the special properties of each fault zone, especially:

  – size and scale of the fault zone (thickness, persistence)
  – internal structure of the fault zone
  – rock / rock mass strength
  – permeability properties
  – rock mass behaviour

- Taking into account all the specific properties of fault rocks, an unambiguous treatment as either soil material or solid rock is not possible. This gives fault rocks a certain special status.

➢ fine clastic rock (FC)

➢ coarse clastic rock (CC)

➢ block (B)

➢ damage zones (DZ)

➢ tectonic reccia (TB)
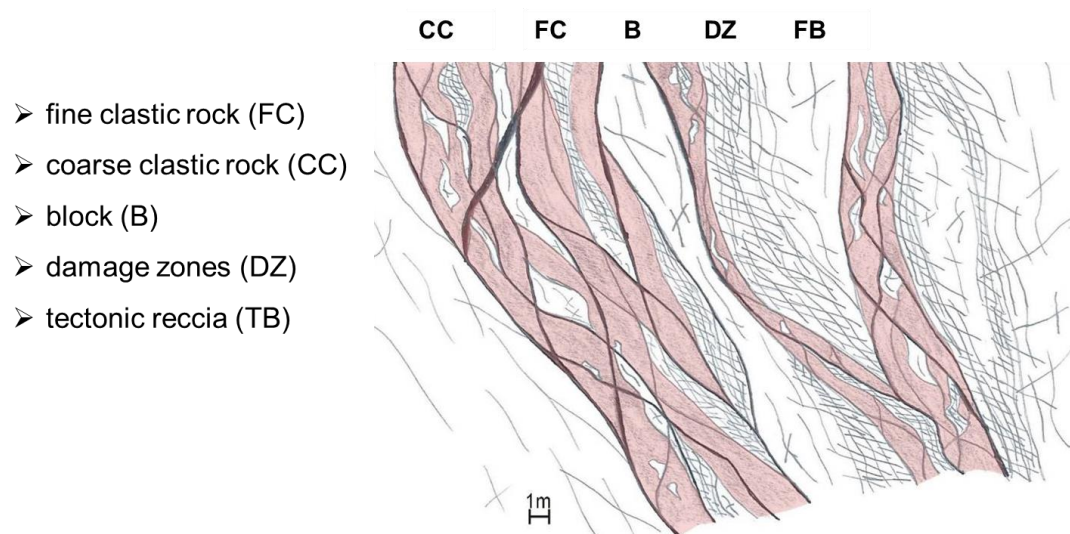
Figure 2: Zones of all kinds of fault rocks with soil and hardrock properties.

- For an appropriate characterisation of fault zones, detailed structural geological knowledge about their origin and development and the resulting internal structures are essential.

Micarelli et al./ Journal of Structural Geology 28 (2006)

Increase of shear displacement

Increase of persistence

Increase of cataclasis

Increase of deformation

Increase of thickness

Increase of complexity of internal structure

Increase and decrease of permeability

Figure 3: Evolution of a fault zone causing changes in properties.

- The complexity and variety of fault rocks demands an unmistakeable and clear use of terms and descriptions.

Figure 4: Specific classification system of fault rocks (F. Fasching & R. Vanek, 2010).

- The engineering geological and geomechanical characterisation of fault zones is essential for an adequate design and successful construction of underground structures in a faulted rock mass.

ENGINEERING GEOLOGICAL CHARACTERISATION OF FAULT ZONES [1]		*description*	*parameters*
geological environment		parent rock and geological setting	-
fault components	shear zones / fault rocks	fault rocks, particle size distribution, compaction, mineralogy, permeability, …	friction angle, cohesion, Young's modulus, …
	shear bodies / preserved rock portions [2]	rock properties, mineralogy, properties of discontinuity network, wear properties, …	strength parameters of rock, shear parameters of discontinuities, wear indices, …
internal architecture		thickness of shear zones, shape and size of shear bodies, volumetric proportion of shear bodies, anisotropy, …	size of shear bodies, block-matrix-ration, …
rock mass	rock mass parameters	description of strength und deformability properties, comment on anisotropy of rock mass properties	rock mass strength, friction angle, cohesion, Young's modulus, Poisson's ratio, …
	additional. engin. geol. information [3]	permeability, grouting properties, swelling potential, wear properties, …	(as required)

[1] according to "ground types" following the "Guideline for the Geotechnical Design for Underground Structures" (ÖGG, 2008)
[2] the properties of shear bodies usually can be characterised analogously to ground types of hard rock mass
[3] according to project requirements

Figure 5: Main aspects of a project-specific characterisation of a fault zone.

- The transfer of the engineering geological model of a fault zone into a realistic geomechanical model is a great challenge in geotechnical design. An adequate implementation requires intensive interdisciplinary collaboration between the engineering geologists and geotechnical engineers.

3. DISCUSSION

In the course of the engineering geological characterisation of fault zones, certain simplifications have to be made concerning internal architecture and rock mass properties. The requirements for a simplified model are based on one hand on the incomplete knowledge of the condition of the fault zone, as can be derived from the geological site investigation. On the other hand, the geomechanical design will need adaptations due to limited performance and system capacity of numerical models. That requires simplifications to the spatial-geometrical conditions, the rock mass parameters and the constitutive laws.

In order to ensure that no essential geotechnical criteria are lost through such simplifications, detailed engineering geological knowledge about the ground is desirable. This requires careful and systematic investigations and sampling of - if possible - all components of the fault zone (different fault rocks and shear bodies). The results of field and laboratory tests should therefore be subjected to thorough analysis, where every single result is being assigned to a specific fault material. This detailed knowledge coupled with a model of all geomechanical behaviour/failure mechanisms is essential as a precondition for the adequate determination of rock mass parameters.

The quality of both, the engineering geological model and the geomechanical model finally determine the reliability of prediction for the construction project.

References

[1] Brodie, K., Fettes, D., Harte, B. & Schmid, R. 2007. Structural terms including fault rock terms. Recommendations by IUGS Subcommission on the Systematics of Metamorphic Rocks (Web version of 01.02.2007).

[2] Brosch, F.J., Kurz, W. & Klima, K. 2006. Definition and Characterization of Faults and Fault Rocks. Felsbau 24 (5), pp.13-20, Essen: VGE.

[3] Caine, J.S., Evans, J.P., & Forster, C.B. 1996. Fault zone architecture and permeability structure. Geology Vol. 24, pp. 1025-1028.

[4] Eisbacher, G.H. 1996. Einführung in die Tektonik. Stuttgart: Enke.

[5] Fasching, F. & Vanek, R. 2011. Engineering geological characterisation of fault rocks and fault zones, Geomechanics and Tunnelling Vol. 4 (3), pp. 181–194, Berlin: Ernst & Sohn.

[6] Heitzman, P. 1985. Kakirite, Kataklasite, Mylonite – Zur Nomenklatur der Metamorphite mit Verformungsgefüge. Eclogae geol. Helv. Vol. 78 (2), pp. 273-286.

[7] Hobbs, B.E., Means, W.D. & Williams, P.F. An Outline of Structural Geology. New York: John Wiley & Sons.

[8] Mandl, G. 2000. Faulting in Brittle Rocks. Berlin / Heidelberg: Springer.

[9] Meschede, M. 1996. Methoden der Strukturgeologie. Stuttgart: Enke.

[10] Naylor, M.A., Mandl, G. & Sijpesteijn, C.H.K. 1986. Fault geometries in basement-induced wrench faulting under different initial stress states. Journal of Structural Geology Vol. 8 (7).

[11] ÖGG Fachsektion "Felsmechanik und Felsbau". 2010. Arbeitskreis „Geomechanik tiefliegender Tunnel". Österreichische Gesellschaft für Geomechanik. Unpublizierte Arbeitsunterlagen.

[12] Riedmüller, G., Brosch, F.J., Klima, K. & Medley, E.W. 2001. Engineering Geological Characterization of Brittle Faults and Classification of Fault Rocks. Felsbau 19 (4), pp. 13-18, Essen: VGE.

[13] Schmid, S.M. & Handy, M.R. 1991. Towards a Genetic Classification of Fault rocks: Geological Usage and Tectonophysical Implications. Controversies in Modern Geology, Chapter 16, London: Academic Press.

[14] Tchalenko, J.S. 1970. Similarities between shear zones of different magnitudes. Geological Association of America Bulletin Vol. 81, pp. 1625–1640.

[15] Twiss, R.J. & Moores, E.M. 1992. Structural Geology. New York: Freeman & Co.

[16] Wibberley, C.A.J., et.al. 2008. The Internal Structure of Fault Zones. Geological Society Special Publication, NO. 299, London: The Geological Society.

Authors

Dipl.-Ing. Florian Fasching
3G Geotechnik Gruppe Graz ZT-GmbH
Triester Straße 478 a
8055 Graz-Seiersberg
Austria

florian.fasching@3-g.at

Mag. Robert Vanek
3G Geotechnik Gruppe Graz ZT-GmbH
Triester Straße 478 a
8055 Graz-Seiersberg
Austria

vanek@3-g.at

Ingenieurgeologische Charakterisierung von Störungszonen im Innsbrucker Quarzphyllit

A. Töchterle [a], H. Schierl [a] & C. Reinhold [a]

[a] *Brenner Basistunnel BBT SE, Innsbruck, Austria*

Der Brenner Basistunnel (BBT) wird zwischen Tulfes bei Innsbruck (A) und Franzensfeste (I) errichtet (64 km). Teil des Gesamtprojekts ist ein durchgehender Erkundungsstollen unterhalb und mittig zwischen den beiden Haupttunnelröhren. Wesentliche Erkundungsziele sind die Lokalisierung, Bestimmung der Raumlage und geomechanische Charakterisierung von Störungszonen in den zu durchörternden Einheiten.

1. GEOLOGISCHE ÜBERSICHT

Der BBT durchörtert von N nach S den ostalpinen Innsbrucker Quarzphyllit, die emporgewölbten penninischen Einheiten des Tauernfensters nahe an dessen westlichen Rand, ein schmales ostalpines Segment (OA) im S des Tauernfensters, die Periadriatische Störungszone und anschließend den südalpinen Brixner Granit (Abbildung 1). Die penninischen Einheiten des Tauernfensters lassen sich grob untergliedern in Obere und Untere Schieferhülle und die Zentralgneise mit dem Alten Dach. Die Trasse des gesamten BBT zwischen Innsbruck und Franzensfeste verläuft zu ca. 75% in Gesteinen mit einer meist stark ausgeprägten Schieferung, bestehend aus Phylliten und Schiefern der ostalpinen Einheiten sowie der Oberen und Unteren Schieferhülle. Die restlichen 25% verteilen sich auf kaum bis deutlich geschieferte Orthogneise und auf ungeschieferten Granit. Bisher wurden im N überwiegend Tunnelbauwerke im Innsbrucker Quarzphyllit aufgefahren (IQP), wobei hier in erster Linie der Erkundungsstollen mit einer derzeitigen Länge von ca. 4,8 km zu erwähnen ist.
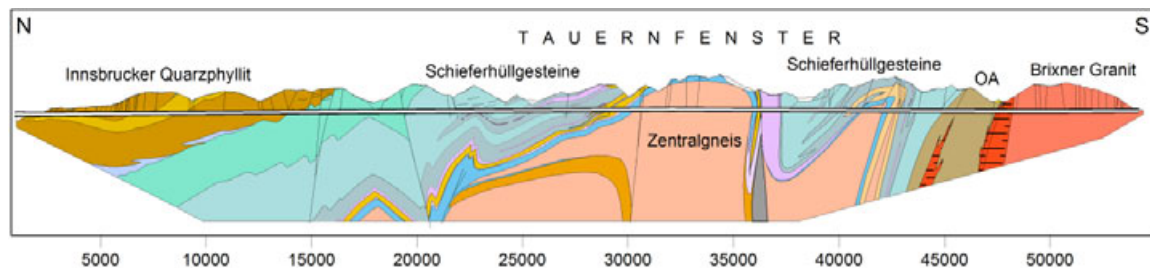
Abbildung 1: Geologischer Übersichtslängsschnitt des BBT zwischen Innsbruck und Franzensfeste.

2. SPRÖDE STÖRUNGSGESTEINE UND GEBIRGE UNTER STÖRUNGS-EINFLUSS – NOMENKLATUR FÜR DIE CHARAKTERISIERUNG VON TYPISCHEN STÖRUNGSGESTEINEN IM BBT-PROJEKTRAUM

Eine Störung wird als spröd bezeichnet, wenn es im Zuge der Deformation zu bruchhaften Verformungsprozessen im Gestein gekommen ist. Diese Prozesse können sich entweder auf einzelne isolierte Bruchflächen konzentrieren oder ganze Gesteinsabschnitte penetrativ erfassen und zur Bildung sogenannter „Störungsgesteine" führen. Zu beachten ist hier, dass diese Beschreibung maßstabsabhängig ist und immer im Zusammenhang mit der Größe des betrachteten Gebirgsausschnittes zu sehen ist. Unabhängig davon ist mit der Bruchbildung generell eine Herabsetzung der Festigkeit des Materials verbunden, wobei es durch nachfolgende Zementationsprozesse zu einer „Ausheilung" und zumindest teilweisen Wiederverfestigung der Bruchzone kommen kann. Aufgrund der Verminderung der Materialfestigkeit sind spröde Störungen jedenfalls von besonderer bautechnischer Relevanz im Tunnelbau.

Zur Beschreibung der Störungsgesteine können verschiedene Klassifikationssysteme aus der Fachliteratur herangezogen werden [1, 2, 3, 4]. Zudem wurde im Zuge der intensivierten geologischen Vorerkundungen für den BBT zwischen 1999 und 2006 bereits besonderes Augenmerk auf die Charakterisierung der im Projektgebiet auftretenden Störungen gelegt. Die verschiedenen Störungsgesteine wurden neben weiteren geotechnisch relevanten Strukturen beschrieben, fotographisch dokumentiert und in einem Klassifikationsschema untergliedert [5], und die im Projektgebiet auftretenden Störungen wurden anhand von Obertage-Aufschlüssen im Detail beschrieben [6]. Es zeigte sich im Zuge der fortlaufenden Dokumentation im Erkundungsstollen allerdings zunehmend, dass mithilfe der bestehenden Modelle die Kategorisierung der aus geschieferten Ausgangsgesteinen gebildeten Störungsgesteine nicht in befriedigendem Maße möglich war.

Deshalb wurde aufbauend auf den Grundlagen aus der Fachliteratur (insbesondere [3]) und den Ergebnissen aus der Vorerkundung ein projektspezifisches Klassifikationsschema für Störungsgesteine zusammengestellt (Tabelle 1 & 2). Es hat sich zudem als nützlich erwiesen, auch das unter Störungseinfluss stehende Nebengebirge hinsichtlich des Beeinflussungsgrades durch die Störung in Form eines einfachen Schemas zu untergliedern (Tabelle 3). Alle Definitionen haben dabei folgende Bedingungen zu erfüllen:

- gute Anwendbarkeit in den für den gesamten Projektraum zu erwartenden Gesteinen
- gute Anwendbarkeit im Zuge der Vortriebsdokumentation
- größtmögliche Eingliederung des Klassifikationsschemas aus der Vorerkundung [5, 6]
- kein Widerspruch zu allgemein anerkannten Definitionen der Struktur- und Ingenieurgeologie [1]

Tabelle 1: Lockergesteinsartige Störungsgesteine.

---

[1] Insbesondere dieser Punkt beherbergt das meiste Diskussionspotential. Gründe dafür sind bestehende Unterschiede in den etablierten Definitionen, die einerseits traditionell begründet sein können [2] und andererseits auch auf die unterschiedliche Herangehensweise an die Thematik verschiedener Fachbereiche zurückgeführt werden können.

Tabelle 2: Festgesteinsartige Störungsgesteine.

Festgesteinsartige Störungsgesteine - Kataklasite		
Unterschiedliche sprödtektonische Störungsgesteine mit Festgesteinscharakter und geringen bis hohen Festigkeiten. Die jeweilige Festigkeit ist zurückzuführen auf Restfestigkeit, auf Mineral-Einregelung anstelle völligen Zerbrechens oder auf Zementation. Das Maß der Entfestigung ist durch zusätzliche Begriffe wie *stark*, *mäßig* oder *gering entfestigt* näher zu beschreiben, also z.B.: *Protokataklasit, mäßig entfestigt* Das Maß der Zementierung ist durch zusätzliche Begriffe wie *stark*, *mäßig* oder *gering* näher zu beschreiben, also z.B.: *Kataklasit, stark zementiert*		

Gestein	Beschreibung	Fotos / Skizzen	
Protokataklasit (prc)	Sprödtektonisch mäßig durchbewegtes Gestein; geprägt durch eine gegenüber dem Umgebungsgestein wesentlich erhöhte Dichte an Kluft- und Scherflächen mit meist mehreren Vorzugsorientierungen; bei den Scherflächen handelt es sich meist um diskrete Harnischflächen bzw. geringmächtige Scherbahnen; Primärgefüge noch reliktisch vorhanden; Matrixanteil<10% (ca.); Festigkeit in Form von Restfestigkeit		
Geschieferter Protokataklasit (fprc)	Sprödtektonisch mäßig bis stark durchbewegtes Gestein; geprägt durch engständige Schieferungs- und Scherflächen mit einer dominanten Vorzugsorientierung bei stark streuenden Orientierungswerten der einzelnen Flächen; typisches Sigmoidalgefüge; deutliche Entfestigung entlang dieser Trennflächen; oft intensiv und unregelmäßig verfaltet; Primärgefüge evt. noch reliktisch vorhanden; Matrixanteil<10% (ca.); Festigkeit in Form von Restfestigkeit und untergeordnet durch Kornverband infolge von Mineral-Einregelung anstelle völligen Zerbrechens		
Geschieferter Kataklasit (fol)	Sprödtektonisch stark bis sehr stark durchbewegtes Gestein; geprägt durch eine intensive Schieferung; die tektonische Verformung passierte v.a. entlang neugebildeter bzw. völlig überformter Schieferungsflächen; Festigkeit durch Kornverband infolge von Mineral-Einregelung anstelle völligen Zerbrechens		
Kataklasit, zementiert (cat)	Verschiedene Typen von spröden Störungsgesteinen; durch Zementation verfestigt; sehr vielfältig hinsichtlich Ausbildung und Festigkeit		
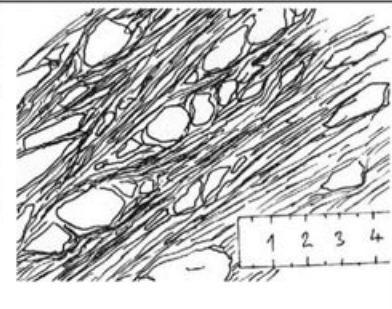
Tabelle 3: Nebengebirge unter Störungseinfluss.

Nebengebirge unter Störungseinfluss		
Bezeichnung	**Beschreibung**	**Skizze**
Erhöhte Trennflächendichte (jrm)	Gebirge mit erhöhter Trennflächendichte, sowie vermehrtem Auftreten von Harnischflächen. Ein direkter Störungseinfluss ist nicht sofort zu erkennen. Die erhöhte Dichte an Trennflächen zeigt sich oft erst im Zuge der graphischen Darstellung oder nachfolgenden Auswertung des betreffenden Abschnittes (Tunnelband, GSI,…). (gelb markierter Bereich in der Skizze)	
Zerrüttungszone (frac)	Gebirge mit deutlich erhöhter Trennflächendichte und schieferungsparalleler Entfestigung, sowie deutlich vermehrters Auftreten von Harnischflächen. Das Gebirge ist zerrüttet und bereits an der Ortsbrust als deutlich gestört erkennbar. (rot markierter Bereich in der Skizze)	

3. GEOLOGISCH-GEOTECHNISCHE VERHÄLTNISSE IN DEN VORTRIEBEN IM INNSBRUCKER QUARZPHYLLIT

Im Februar 2010 starteten die Vortriebsarbeiten im Erkundungsstollenabschnitt Innsbruck-Ahrental in der Sillschlucht bei Innsbruck. Noch im selben Jahr begannen die Arbeiten beim Zufahrtstunnel Ahrental, und im Mai 2012 erfolgte der Anschlag des Fensterstollen Ampass als Zugangsstollen für den geplanten Rettungsstollen Tulfes. Im Sommer 2013 konnten alle Vortriebsarbeiten erfolgreich fertiggestellt werden. Insgesamt wurden dabei über 9 km Stollen und Tunnel im Innsbrucker Quarzphyllit hergestellt.

Der Erkundungsstollen Innsbruck-Ahrental (4,8 km) wurde konventionell vorgetrieben und weist eine Querschnittsfläche von ca. 30 m^2 auf. Die maximale Überlagerung beträgt ca. 900 m. Der Ausbruch erfolgte praktisch vollflächig, in den größeren, alle 250 m angeordneten Ausweichnischen wurde der Querschnitt in Kalotte und Strosse unterteilt. Aufgrund der Distanz zum Wipptal ist der Einfluss der Wipptalstörung bzw. die Tektonisierung des Gebirges hier deutlich weniger stark ausgeprägt als das Gebirge im Zufahrtstunnel Ahrental. Die Hauptkluftscharen fallen hier ebenfalls steil ost- und westwärts ein, aufgrund der annähernd Nord-Süd verlaufenden Tunnelrichtung aber nicht direkt aus der Ortsbrust, sondern seitlich zu den Ulmen hin. Über weite Strecken war das Gebirgsverhalten nur durch kleinvolumige, gefügebedingte Nachfälle geprägt. In drei Abschnitten wurden durch schleifend bis achsparallel bzw. spitzwinkelig streichende Störungen schwach druckhafte Verhältnisse generiert. Nachstehend werden exemplarisch zwei geotechnisch relevante Störungszonen im Erkundungsstollen Innsbruck-Ahrental beschrieben:

Störungszone ESI-f2088:

Von Stollenmeter ca. 1850 m bis 2100 m begleitete ein Längsstörungssystem mit einer Mächtigkeit der Hauptstörung von ca. 3 m den Tunnelquerschnitt am linken bzw. östlichen Ausbruchsrand.

Diese mit ca. 60° nach ENE einfallende Störung löste in Folge lang anhaltende, asymmetrische Kriechbewegungen mit gegenüber der Setzungskomponente erhöhten horizontalen Querverschiebungen bis max. 160 mm Absolutverschiebung aus. Als Folge traten Schäden am Ausbau (Risse und Abplatzungen der Spritzbetonschale) auf, welche Sanierungsmaßnahmen und den nachträglichen Einbau eines Sohlgewölbes erforderlich machten.

Störungszone ESI-f4158:

Eine weitere Störungszone mit schwach druckhaftem Gebirgsverhalten trat bei Stollenmeter 4140-4180 auf. Diesmal war ein westfallendes, annähernd spitzwinkelig streichendes Störungssystem Auslöser dafür. Die

Hauptstörung ist hier ca. 5 m mächtig bestehend aus dm-mächtigen Scherbahnen mit Fault gouge neben veruschelten und mürbfesten Quarzphyllit (geschieferter Protokataklasit bis Kataklasit). Je nach Position des Störungssystems wurden die größten Verschiebungsbeträge beim Hereinstreichen und beim Herausstreichen der Störung in bzw. aus dem Querschnitt beobachtet. Auch hier traten Schäden am Ausbau mit Rissbildungen, Ausknicken der Gitterträger und Aufbiegen der Ankerplatten auf, welche im Nachgang saniert werden mussten.

Bei beiden Abschnitten war an der Ortsbrust selbst kein unmittelbares Standfestigkeitsproblem mit verstärkten Nachfällen gegeben. Die augenscheinliche Gebirgsverschlechterung war nicht gravierend. Auch aus den gemessenen Erstverschiebungen ließ sich nicht sofort ein druckhaftes Gebirgsverhalten ableiten. Aus den gemachten Erfahrungen wurde aber für den weiteren Vortrieb eine Verstärkung des Ausbaus beschlossen, sobald an der Ortsbrust erste Indizien für ungünstig streichende, auch nur geringmächtige Störungssysteme auftraten. Neben einem dichteren Radialankerungsschema und je nach Position der Störung unterschiedlichen, zumeist asymmetrischen Ankerlängen waren auch. Verformungsschlitze in der Spritzbetonschale und eine baubetriebliche Abstimmung für einen raschen Sohlschluss vorgesehen.

4. ERMITTLUNG DER GEOMECHANISCHEN KENNWERTE DER STÖRUNGSZONEN

Für die geologisch-geotechnische Prognose ist neben Lage, Orientierung, Abmessungen und Gebirgsverhalten der Störungszonen auch die Angabe zutreffender geomechanischer Kennwerte, mit denen die Störungszonen beschrieben werden können, entscheidend. Üblicherweise wird dabei so vorgegangen, dass Gesteins- bzw. Bodenproben entnommen werden, diese im Labor bezüglich ihrer mechanischen Eigenschaften untersucht werden und aus diesen Ergebnissen schlussendlich auf die Kennwerte der Störungszone geschlossen wird.

Bei den im Innsbrucker Quarzphyllit im Erkundungsstollen angetroffenen bestimmenden Störungsgesteinen handelte es sich im Wesentlichen um geschieferte Protokataklasite (fprc). Solche Gesteine können als Festgestein mit geringen bis sehr geringen Festigkeiten beschrieben werden (UCS < 1…5 MPa). Gesteinsproben in Form von Handstücken aus dem Vortrieb lassen sich mit einem leichten Hammerschlag oder sogar schon mit der Hand brechen. Aufgrund dieser geringen Festigkeiten war es derzeit noch nicht möglich überhaupt Kerne für einaxiale oder triaxiale Druckversuche zu gewinnen.

Aufgrund der im Labor derzeit noch nicht ermittelbaren mechanischen Eigenschaften der Protokataklasite, musste eine andere Möglichkeit zur Abschätzung der geomechanischen Eigenschaften der Störungszonen im Innsbrucker Quarzphyllit gefunden werden. Durch den vorlaufenden Erkundungsstollen besteht die Möglichkeit der Rückrechnung der im Erkundungsstollen Innsbruck-Ahrental gemessenen Verformungen und somit der Abschätzung der Gebirgskennwerte der Störungszonen. Auf Basis des geologischen Modells der Störungszonen, welches auf den Erfahrungen beim Auffahren des Erkundungsstollens basiert, werden die Verhältnisse im Bereich der Störungszonen mit verschiedenen Berechnungsverfahren nachvollzogen. Dafür kommen sowohl einfache Berechnungen mit der Kennlinie, als auch komplexe 2- und 3-dimensionale numerische Berechnungen zur Anwendung.

Das prinzipielle Vorgehen sieht in drei Schritten die Erstellung des geologischen Modells, die darauf folgende Erstellung des geotechnischen Modells und schlussendlich die Erstellung des Berechnungsmodells der Störungszone vor (Abbildung 2). Aus den geologischen Daten welche aus dem Vortrieb des Erkundungs-stollens gewonnen wurden (Ortsbrustdokumentation, Tunnelbänder) wird im ersten Schritt ein geologisches Modell der Störungszone erarbeitet. Im folgenden Schritt wird daraus ein vereinfachtes geotechnisches Modell erarbeitet, welches unter anderem die Aufteilung in Core Zone (CZ) und Damage Zone (DZ) umfasst. Dieses geotechnische Modell der Störungszone wird dann lagemäßig in das Berechnungsmodell integriert. Weiterhin werden die Vortriebshistorie sowie die verwendeten Stützmittel detailliert ausgewertet und in das Berechnungsmodell integriert.

Tabelle 4 zeigt beispielhaft die Kennwerte für zwei Störungszonen im Innsbrucker Quarzphyllit die bereits im Erkundungsstollen aufgefahren und deren Kennwerte über Rückrechnungen abgeschätzt wurden. Das Verhalten beim Vortrieb dieser beiden Störungszonen ist unter Punkt 3 beschrieben. Aus den angegebenen Core Zone Kennwerten wird unter anderem die Tiefenabhängigkeit der Parameter Elastizitätsmodul und Kohäsion ersichtlich. Beide Störungszonen sind dem gleichen regionalgeologischen Störungssystem (Wipptal-System) zuzuordnen und zeigen auch annähernd einen vergleichbaren geologischen Ausbau. Lediglich die Mächtigkeiten und Überlagerungshöhen sind unterschiedlich. Die Rückrechnungen haben

eine Zunahme von E-Modul und Kohäsion mit steigender Überlagerung ergeben. Dieser Sachverhalt ist insbesondere für Lockergestein hinreichend bekannt.
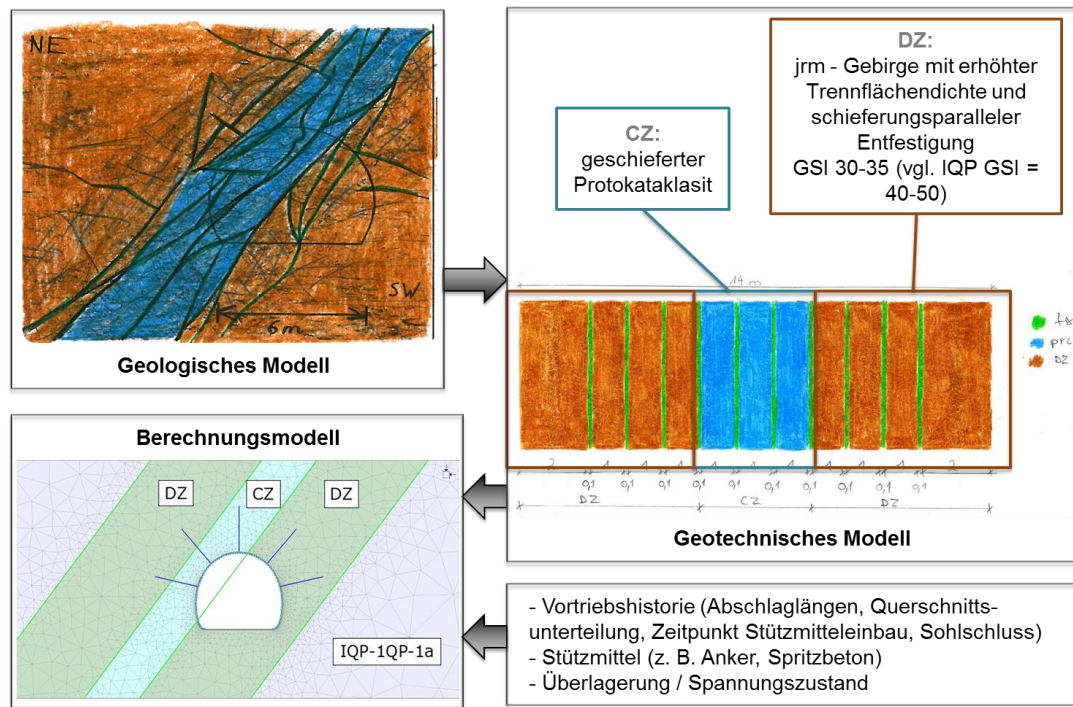
Abbildung 2: Beispiel für die Überführung des geologischen Modells in ein Berechnungsmodell.

Tabelle 4: Geomechanische Kennwerte ausgewählter Störungszonen die im Erkundungsstollen Innsbruck-Ahrental aufgefahren wurden.

Bezeichnung	Kurzbeschreibung	Abmessungen (DZ: Hangend / Liegend der CZ)	Über-lagerung	Parameter Core Zone	Parameter Damage Zone
ESI-f2088	CZ: fprc 90%, fg 10% DZ: jrm 70%, fprc 20%, fg 10% (GSI 25-30)	CZ: 3 m DZ: 5,5 m / 5,5 m	300 m	E = 400 MPa c = 0,15 MPa φ = 25°	E = 1000 MPa c = 0,45 MPa φ = 26°
ESI-f4158	CZ: fprc 90%, fg 10% DZ: jrm 80%, fprc 10%, fg 10% (GSI 30-35)	CZ: 5,5 m DZ: 10,5 m / 1 m	690 m	E = 600 MPa c = 0,30 MPa φ = 26°	E = 1000 MPa c = 0,50 MPa φ = 28°

5. RESÜMEE

Für die Planung und den Bau der Hauptröhren des BBT ist die möglichst genaue Charakterisierung von potentiell den Vortrieb und insbesondere auch die Wahl des Vortriebsverfahrens (konventionell-maschinell) beeinflussenden Störungszonen von maßgeblicher Bedeutung. Bei der geomechanischen Prognose für tiefliegende Tunnelbauwerke ohne Erkundungsstollen werden die Eigenschaften von Störungszonen im Normalfall aus Oberflächenkartierungen und Tiefbohrungen abgeleitet. Dabei können sich bedeutende Schwankungsbreiten in den prognostizierten geologisch-geotechnischen Daten ergeben. Im geologisch-geomechanischen Modell des BBT aus der Vorerkundung (basierend auf Bohrungen und Ober-flächenkartierungen) bezog sich beispielsweise die Angabe der Störungszonen auf eine Anzahl je geotechnischem Homogenbereich mit globalen Gebirgsparametern für die Störungszonen. Für das geologisch-geomechanische Modell der Hauptröhren kann nun basierend auf den Erkenntnissen aus dem

Erkundungsstollen eine diskrete Angabe der Einzelstörung mit jeweils bezogenen Gebirgsparametern erfolgen. Ziel des vorauseilenden Erkundungsstollens beim BBT ist unter anderem, die notwendigen Daten der Störungszonen präziser und mit geringeren Schwankungsbreiten für die Haupttunnel prognostizieren zu können. Damit soll das geologisch-geomechanische Risiko beim Bau der Hautröhren erheblich reduziert werden.

References

[1] Brodie, K., Fettes, D., Harte, B. & Schmid, R. 2007. Structural terms including fault rock terms. Recommendations by IUGS Subcommission on the Systematics of Metamorphic Rocks (Web version of 01.02.2007).

[2] Fasching, F. & Vanek, R. 2011. Engineering geological characterisation of fault rocks and fault zones / Ingenieurgeologische Charakterisierung von Störungsgesteinen und Störungszonen. *Geomechanics and Tunnelling* 4 (3), pp. 181-194, Berlin: Ernst & Sohn.

[3] Heitzmann, P. 1985. Kakirite, Kataklasite, Mylonite - Zur Nomenklatur der Metamorphite mit Verformungsgefügen. *Eclogae geol. Helv.* 78 (2), pp. 273-286.

[4] Riedmüller, G., Brosch, F.J., Klima, K. & Medley, E.W. 2001. Engineering Geological Characterization of Brittle Faults and Classification of Fault Rocks. *Felsbau* 19 (4), pp. 13-18, Essen: VGE.

[5] BBT EWIV. 2001. Geologie, Erkundung, Strukturtektonik, Schlußbericht. Unveröffentl. Bericht von Brandner, R., Decker, K., Ortner, H., Reiter, F., Bistacchi, A. & Massironi, M.

[6] BBT SE. 2005. Charakterisierung von Störungszonen. Unveröffentl. Bericht von Brandner, R., Dal Piaz G.V., Bistacchi, A., Decker, K. & Reiter, F.

Authors

Dr. Andreas Töchterle
Brenner Basistunnel BBT SE
Amraser Str. 8
6020 Innsbruck
Austria
andreas.toechterle@bbt-se.com

Mag. Heimo Schierl
Brenner Basistunnel BBT SE
Amraser Str. 8
6020 Innsbruck
Austria
heimo.schierl@bbt-se.com

Dr.-Ing. Chris Reinhold
Brenner Basistunnel BBT SE
Amraser Str. 8
6020 Innsbruck
Austria
chris.reinhold@bbt-se.com

Results of Laboratory Tests on BIM-rocks

T. Pilgerstorfer [a]

[a] *Graz University of Technology, Institute for Rock Mechanics and Tunnelling, Graz, Austria*

When dealing with tunnels in difficult ground conditions, e.g. fault zones, the knowledge of the rock mass parameters is of utmost importance to ensure a safe and economical tunnel design. Sections with a high content of cataclasites form the most challenging stretches during tunneling, and a proper geomechanical characterization is imperative. However, investigating the overall-properties is currently a challenging task, originating from difficulties in sample acquisition, sample preparation and laboratory testing.

In order to gain insight into the overall mechanical properties of cataclasite-like material and to study the basic mechanical behavior of BIM-rocks an extensive laboratory program was carried out. Artificial block-in-matrix rocks were fabricated for both direct shear tests and large oedometer tests. For the direct shear tests models with six different block orientations, related to the shear direction, and three different block proportions were created. The large oedometer tests feature samples with three different block arrangements, with regard to the loading direction. A straight forward evaluation method is presented and the results are discussed in detail, highlighting the effect of block orientation and block proportion on the shear behavior, shear strength and deformation behavior of BIM-rocks.

1. INTRODUCTION

Tectonic faults are usually composed of lens-shaped, relatively competent rock blocks surrounded by finely grained cataclastic material [1, 2]. Hence, their properties are highly anisotropic and depend on the degree of the regularity of the block orientation, the total volumetric amount of the competent lenses as well as the properties of the matrix.

To study the principle mechanical properties of fault material an extensive laboratory program was conducted on artificial block-in-matrix rocks. Tunneling in weak rock mass is often accompanied by large displacements, hence an intended issue was to investigate the behavior of BIM-rocks exposed to large strains. Lindquist [3] provided a comprehensive study of triaxial tests on artificial BIM-rocks. However, being a characteristic of triaxial tests large strains are difficult to achieve and the investigation of failure surfaces is rarely possible. Hence it was decided to examine the mechanical behavior of artificial BIM-rocks in direct shear tests. Another important issue is the knowledge about the stress dependency of the deformation properties, especially for TBM-advances in weak rock masses. The amount of displacements which are expected and the risk for a shield-TBM getting stuck should be known a priori.

2. ARTIFICIAL BLOCK-IN-MATRIX ROCKS

2.1. Matrix material

A special issue was finding a proper matrix material, meeting following goals:

- A relatively short curing time, to ensure prefabrication of samples within a tight timetable, and
- Limited, controllable strength and deformation properties in order to ensure high contrast between matrix and block properties.

After performing several tests, including uniaxial and triaxial compression tests, visual inspection of curing behavior (onset of cracking due to shrinkage) it turned out that a mixture of finely crushed rock material (limestone), cement and water meets the intended properties best. A crushed rock/cement ratio of 5:1 was used, the water/cement ratio was set to 1.8, allowing a good workability. This obvious high ratio is required due to the fact that the mixture contains almost no coarse aggregates. The properties of the matrix material, gained by triaxial tests, are a uniaxial compressive strength of approximately 3 MPa and a Young's modulus of 4000 MPa, respectively.

2.2. Block material

The blocks were made of cement-stone and feature an ellipsoidal shape, being slightly tapered in y-direction (see Table 1, block sketch at bottom left). The length is 95/100 mm (z-direction), the width is 40/45 mm (in x-direction) and the depth is 15 mm (in y-direction), respectively. A Portland cement type CEM II 42.5 was used, the water/cement ratio was set to 0.4. The blocks were prefabricated in silicone molds. Triaxial tests were performed on the block material to gain the strength and deformation properties, yielding a uniaxial compressive strength of 37 MPa after seven days curing time, a friction angle of 30° and a Young's Modulus of about 16,000 MPa. The strength ratio between matrix material and block material is about 12, and the deformation ratio amounts to the factor 4.

3. DIRECT SHEAR TESTS ON BIM-ROCKS

3.1. Sample preparation

The samples were prefabricated in two quadratic steel shear boxes. The boxes have a height of 18 cm and a length/width of 20 cm. The gap between the boxes is 2 cm, which was sealed with polystyrene bars during sample preparation. First the lower box was filled with matrix material. After a curing time of about one hour the blocks were placed in the matrix in the intended orientation and block proportion. With the help of stencils it was ensured that the blocks remained in the desired position. After the matrix had stiffened a little, and thus the blocks would stay in place, the upper box was filled up with matrix material. The samples were left to cure for seven days.

3.2. Orientation of blocks and volumetric block proportion

It was tried to cover a broad range of possible block orientations with regard to the shear direction. Specimen with four different block orientations, each with three different volumetric block proportions were fabricated, along with pure matrix and pure block samples (Table 1). In order to account for the natural scatter of strength properties and the variability in sample preparation quality three tests of each block orientation/block proportion combination were performed.

Table 1: Compilation of performed shear tests.

Block proportion	Orientation	Symbol	No. of tests	Block proportion	Orientation	Symbol	No. of tests
0%	pure matrix	n/a	3	100%	pure block	n/a	3
25%	90°	→ |||	3	75%	90°	→ |||	3
25%	90°	→ ||| par.	1	75%	90°	→ ||| par.	1
25%	60°	→ / / /	3	75%	60°	→ / / /	2
25%	30°	→ / / /	2	75%	60°	→ \ \ \	1
25%	30°	→ \ \ \	1	75%	30°	→ / / /	2
25%	0°	→ ---- long.	2	75%	30°	→ \ \ \	1
25%	0°	→ ---- trans.	1	75%	0°	→ ---- long.	2
50%	90°	→ |||	3	75%	0°	→ ---- trans.	1
50%	90°	→ ||| par.	1	**legend:**			
50%	60°	→ / / /	2	→	shear direction		
50%	60°	→ \ \ \	1	|||	blocks vertically aligned, shear in y-direction		
50%	30°	→ / / /	2	||| par.	blocks vertically aligned, shear in x-direction		
50%	30°	→ \ \ \	1	/ / /	blocks inclined in pos. y-direction		
50%	0°	→ ---- long.	2	\ \ \	blocks inclined against pos. y-direction		
50%	0°	→ ---- trans.	1	---- long.	blocks horizontally aligned, shear in z-direction		
				---- trans.	blocks horizontally aligned, shear in x-direction		

3.3. Test procedure and evaluation

The tests were performed under constant normal stiffness conditions. Due to the fact that intact samples were tested, special attention was paid to the determination of mobilization of cohesion, dilation and friction over the shear displacement. It is stated by several authors that there is no permanent cohesion in rocks, at least at relatively low confinement, where the cohesional strength component is gradually lost when the rock is strained beyond its peak strength [4, 5]. The evaluation method in principle is based on a cohesion-weakening – frictional strengthening (CWFS) model, meaning that the mobilized strength components (cohesive, frictional and dilational) are strain dependent.

3.4. Results

Figure 1 shows the maximum shear strength, which is normalized by the matrix' shear strength, versus block proportion. The results depict a conclusive picture. The shear strength almost linearly increases with increasing block proportion. The samples with 30° and 90° block orientation feature nearly the same factors of strength increase (25% - factor of 1.6, 50% - factor of 2.2, 75% - factor of 2.8). Up to 50% block proportion the samples with 60° block orientation yielded the highest contribution to the shear strength, while a decrease of shear resistance for 75% block proportion was observed.
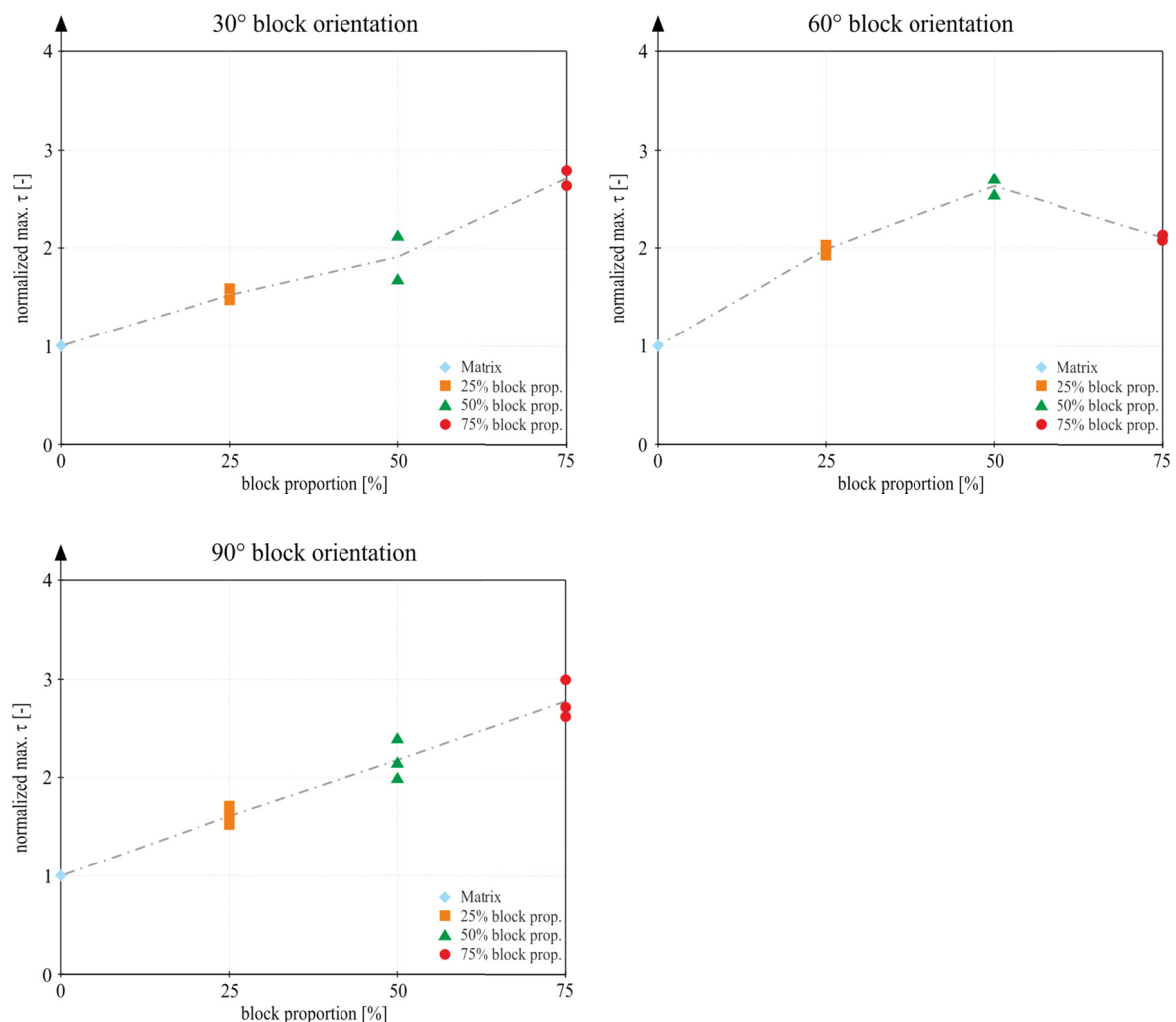
Figure 1: Max. shear strength (normalized by matrix strength) versus block proportion for 30° block orientation (top left), 60° block orientation (top right) and 90° block orientation (bottom left).

A closer inspection of the shear surfaces after the tests backs the above mentioned findings (Figure 2). Samples with 90° block orientation experience during the shearing process a sudden, brittle failure of blocks, which results in smooth cracks and thus providing low values for dilatancy. The failure plane for the 30° block orientation samples features also a smooth surface. However, in those cases pure sliding along blocks takes place, which yields relatively high values for dilatancy. The 60° block orientation arrangement yields a contrary picture. At the onset of the shearing process slight sliding along blocks is present, which leads to grinding and crushing of the blocks with ongoing shear displacement. This results in an increased shear surface roughness, which further yields a higher contribution to shear resistance.

Figure 2: Failure surfaces after the test shown for 30° block proportion (top left and right), 90° block proportion (bottom left) and 60° block proportion (bottom right).

The effect of block inclination with regard to the shear direction (blocks inclined towards or against shear direction) is nicely shown in Figure 3. Depicted therein is the accumulated shear energy over the shear displacement, which is defined by equation 1.

$$W_{(u)} = \int_0^u \tau_{(u)} \cdot du \qquad (1)$$

The shear energy is normalized by the accumulated shear energy development of the pure matrix sample. Exemplarily shown are the results of the 30° and 60° block orientation samples (Figure 3). It becomes evident that samples with blocks inclined against shear direction feature a pronounced ductile behaviour, which is represented by a steady, mostly linear increase of shear energy development over the shear displacement. A contrary picture is given for samples with blocks being inclined towards shear direction. A much more brittle behavior is observed, featuring a peak shear strength value after relatively low shear displacement, followed by a continuous decrease of shear resistance over the remaining shear displacement. This particular feature holds true for all tested samples, hence this behavior is not influenced by block proportion.
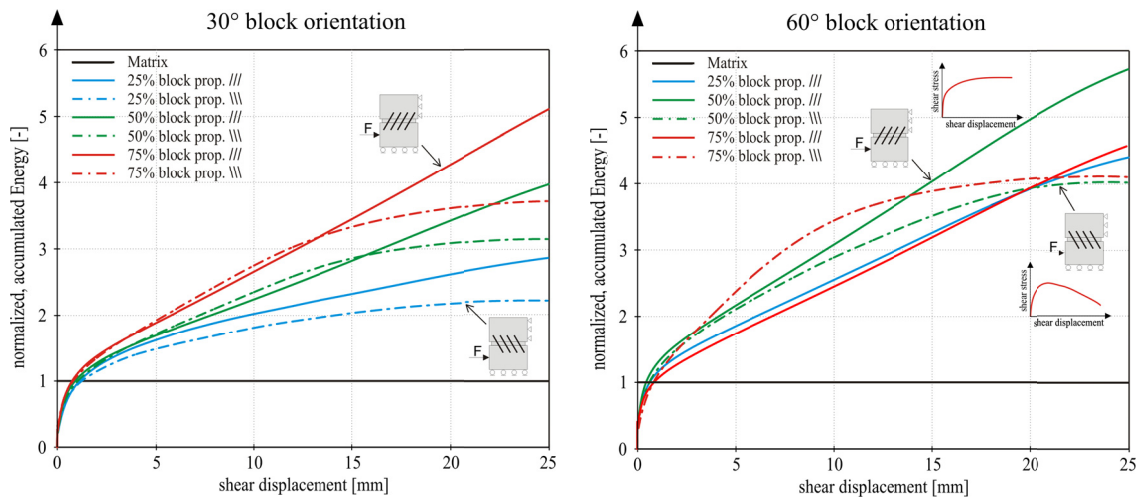
Figure 3: Normalized accumulated shear Energy versus shear displacement, shown for 30° block proportion (left) and 60° block proportion (right).

4. LARGE OEDOMETER TESTS ON BIM-ROCKS

Large oedometer tests were performed on artificial block-in-matrix rocks, in order to study the influence of block orientation and block proportion on the overall deformation properties and to gain knowledge about the stress dependency of moduli.

Current laboratory techniques for the determination of Young's moduli or constrained moduli are afflicted with restrictions. Standard oedometer tests, as characteristically used for soil testing are not adequate due to the small sample size and relatively low stress levels. Hence, those conditions do not reflect the stress conditions found at tunnel level and standard oedometer tests do not allow obtaining reliable data about the stress dependency of moduli at high depths. In order to circumvent these shortcomings a large oedometer test apparatus was developed, accounting for the issues mentioned above. A detailed description of the large oedometer test apparatus is given in [6].

4.1. Sample preparation

The artificial block-in-matrix samples were fabricated in custom-tailored shutterings. All specimen featured a diameter of 300 mm. The initial height was between 128 and 156 mm. Three different block arrangements in three different block proportions, as well as a pure matrix and pure block sample were tested. The specified block arrangements were (Figure 4):

- Blocks horizontally aligned (loading in y-direction of blocks)
- Blocks vertically aligned (loading in z-direction of blocks)
- Blocks twisted (loading in x-direction of blocks)
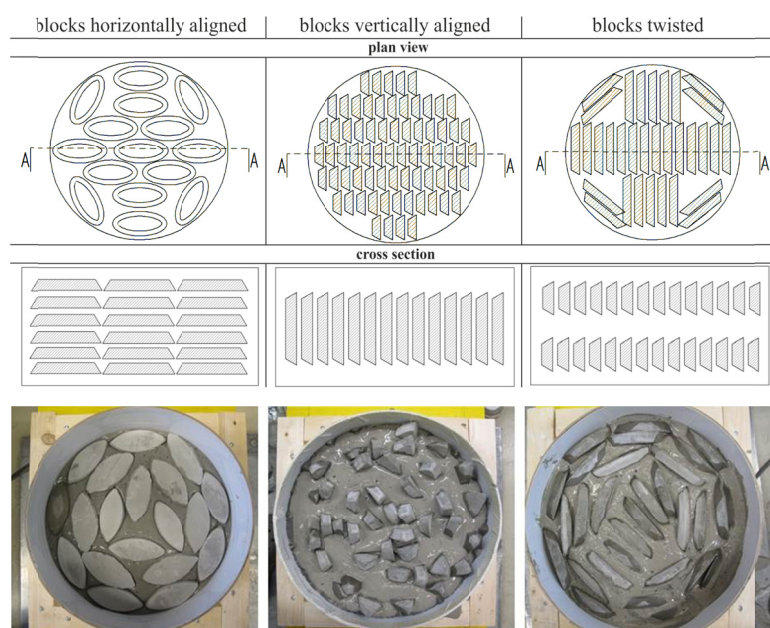
Figure 4: Different types of block arrangement for large oedometer tests; blocks horizontally aligned (left), blocks vertically aligned (middle), blocks twisted (right).

4.2. Test procedure and data evaluation

A compression test machine with a maximum load of 3000 kN was utilized as loading device. The vertical load acting on the specimen is measured by a load cell with a nominal load of 2000 kN. A floating ring configuration was used for the tests, allowing the determination of friction forces between oedometer ring surface and specimen. The measurement of friction forces was accomplished by three load cells. For the determination of vertical displacements three inductive displacement transducers were used.

The samples were repeatedly loaded and unloaded. Each loading and unloading cycle was kept constant until displacement rates became almost zero. After each loading-unloading loop the load was increased to a higher level, which was in most cases the double amount of the previous level.

The starting points of each loading and unloading loop were identified and the axial stress and appropriate axial strain were determined. Semilogarithmic stress-strain diagrams were plotted and the constrained modulus (E_s), also known as oedometer modulus, was obtained as secant modulus for each loading and unloading loop. Based on Hooke's law the Young's Modulus was calculated by using a Poission's ration ν of 0.30, based on the results of triaxial tests on the matrix.

4.3. Results

The unloading-moduli for horizontally aligned blocks feature about ten to approximately thirty times higher values than the loading-moduli. A slight hardening behavior (with increasing stress level) can be observed in the unloading loops, being more pronounced for samples with higher block proportions. The ratios of unloading moduli to reloading moduli show values of about 1.3 to 2.0.

The samples with vertically aligned blocks show a much higher ratio of loading moduli to unloading moduli (~ 20 to 50), compared to the specimen with horizontally aligned blocks. On the other hand, the hardening behavior (increase of unloading moduli with increasing stress level) is much less pronounced than in the horizontally aligned block arrangement. The ratio of unloading moduli to reloading moduli features approximately the same values as the samples with horizontally aligned blocks.

The ratios of unloading moduli to loading moduli for the twisted block arrangement feature factors of about 15 to 30, being in the range between the horizontally and vertically aligned block specimen. Again, a hardening behavior is less pronounced, and is only observed for higher block proportions. The ratio between unloading and reloading moduli yielded factors of approximately two. The values for the loading moduli are lower than those of the horizontally aligned block samples.

The ratio of loading moduli of pure block and pure matrix samples is between 8 (for low stress states) and 60 (for high stress states), hence it can be observed that the stress dependency of moduli is much more pronounced for the pure block material. However, it cannot be stated that this is a general behavior, that harder materials feature a much higher stress dependency of deformability. It is the case that the stress dependency and its occurrence is much more a question of the current degree of porosity, which is governed by the applied stress level. Furthermore, imposing stress levels exceeding the strength of a material yields plastic deformations, hence evaluation of deformation moduli consists of elastic and plastic strains, which decrease the appearance of stress dependent deformation behavior.

A quite clear picture is given if the individual data points of evaluated moduli are plotted in a Young's modulus versus axial stress diagram, allowing the observation of stress dependent deformation behavior. The results are depicted for each block arrangement in a separate diagram, given in Figure 5. In order to determine an empirical relationship governing the development of the deformation behavior with increasing stress level a mathematical relationship fitting the discrete data points was required. It was found that the exponential function shown in equation 2 is able to yield an almost perfect fit.

$$y = \kappa \cdot e^{\eta/x} \tag{2}$$

Introducing the Young's Modulus E and the axial stress σ_v equation 2 rewrites to (Eqn. 3):

$$E = \kappa \cdot e^{\eta/\sigma_v} \tag{3}$$

A closer inspection of the function parameters κ and η, describing the shape of the exponential function curve, showed that they are dependent on the volumetric block proportion. Moreover, it turned out that κ and η nearly feature a linear dependency on the block proportion. This was achieved by slight modifications of the best-fit curves for each block proportion sample, however, still yielding regression coefficients above 0.9. This approach was deemed to be valid, since one is dealing with a "given" material featuring a natural scatter in its properties. The function parameters κ and η and their dependence on the volumetric block proportion for the different block arrangements are shown in Table 2. The great advantage of this approach lies in its simplicity: Merely the knowledge of the volumetric block proportion is needed as input, in order to calculate the development of the overall stiffness for a desired stress range.

Table 2: Function parameters κ and η for different block arrangements.

function parameter	Block arrangement		
	horizontally aligned	vertically aligned	twisted
κ	for VBP < 50	$\kappa = 5 \cdot VBP + 235$	$\kappa = 11 \cdot VBP + 58$
	$\kappa = 4.8 \cdot VBP + 370$		
	for VBP $\geq$ 50		
	$\kappa = 0.000032 \cdot VBP^{4.28}$		
η	$\eta = 0.032 \cdot VBP - 5.4$	$\eta = 0.025 \cdot VBP - 5.7$	$\eta = 0.15 \cdot VBP - 8.3$

VBP ... volumetric block proportion in [%]

If one compares the diagrams shown in Figure 5 it can be nicely seen that the samples with horizontally aligned blocks feature values for the Young's modulus which are about the double amount of the vertically aligned or twisted block samples. Moreover, for the vertically aligned and twisted block arrangements a linear increase of stiffness with increasing block proportion can be observed, while for the horizontally aligned block assembly this is only the case for block proportion up to 42%. Above 42% block proportion stiffness is disproportionately increasing.
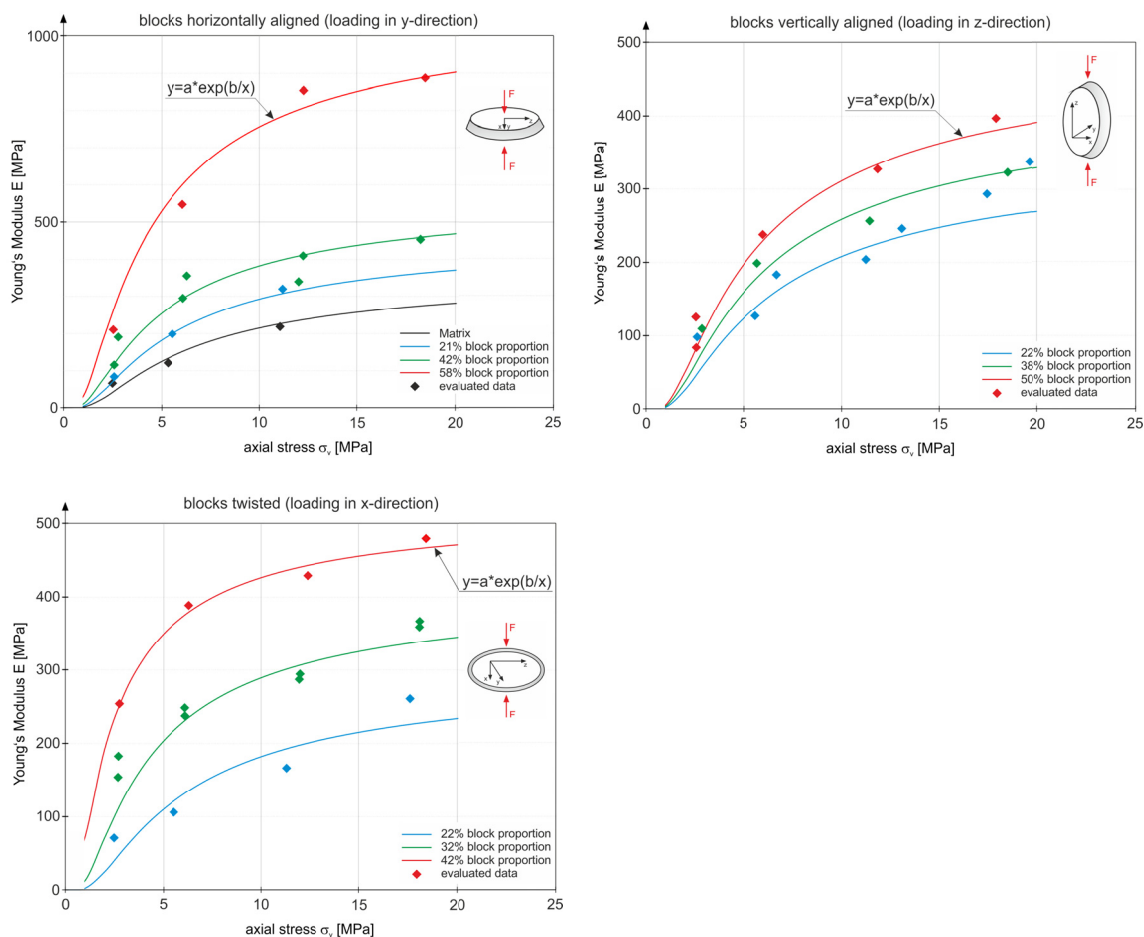
Figure 5: Evaluated Young's moduli vs. axial stress and fitting function for horizontally aligned block arrangement (top left), vertically aligned blocks (top right) and twisted block assembly (bottom left).

5. CONCLUSION

The performed direct shear and large oedometer tests on BIM-rocks provided valuable information about the mechanical behavior of fault material and yielded a deeper insight on the factors and properties influencing the strength and deformation behavior. Further research will focus on an extension and quantification of the findings to a broad range of the individual input properties, like pure matrix and pure block strength and deformability. However, still putting emphasis on meeting the requirements of a simple application, based on easily determinable geological and geotechnical information, to allow a proper and sound characterization for fault rocks.

References

[1]   Medley, E. 2001. Orderly Characterization of Chaotic Franciscan Melange. *Felsbau Rock and Soil Engineering* Vol. 12 (4), pp. 20-33, Essen: VGE.

[2]   Riedmüller, G., Brosch, F.J., Klima, K. & Medley, E. 2001. Engineering Geological Characterization of Brittle Faults and Classification of Fault Rocks. *Felsbau Rock and Soil Engineering* Vol. 19 (4), pp. 13-18, Essen: VGE.

[3]   Lindquist, E.S. 1994. The strength and deformation properties of mélange. Ph.D. Dissertation, University of California at Berkeley, USA.

[4]   Hajiabdolmajid, V., Kaiser, P.K. & Martin, C.D. 2002. Modelling brittle failure of rock. *Int. J. Rock Mech. Min. Sci.* 39 (6), pp. 731-741.

[5]   Scholfield, A.N. 1998. Don't use the C word – Mohr Coulomb error correction. *Ground Engineering*, pp. 29-32.

[6]   Wieser, P., Pilgerstorfer, T. & Schubert, W. 2012. Development of a Large Oedometer Test for the Determination of Stress Dependent Moduli on Fault Rocks. In: *Proc. EUROCK 2012 - Rock Engineering & Technology for Sustainable Underground Construction*. 28 - 30 May 2012, Stockholm, Sweden.

Author

Dipl.-Ing. Thomas Pilgerstorfer

Graz University of Technology

Institute for Rock Mechanics and Tunnelling

Rechbauerstraße 12

8010 Graz

Austria

pilgerstorfer@tugraz.at

Triaxial Tests on Cataclasites

A. Goricki [a] & E. Pimentel [b]

[a] *Gruppe Geotechnik Graz ZT GmbH, Graz, Austria*

[b] *ETH Zürich, Institute for Geotechnical Engineering, Zürich, Switzerland*

Cataclasites are highly fractured and crushed fault zone materials with generally poor mechanical properties. They origin from tectonic activities with very high stress levels and in case of deep tunnels the cataclasites are excavated in depth with high in situ stress. To investigate the behaviour of the low strength cataclasites in high stress ground conditions triaxial tests with stress levels comparable to the in situ stress are performed. The focus is set on the evaluation of the mechanical properties for the geotechnical tunnel design of the fault zone sections. The testing procedure and the results are described in this extended abstract.

1. TESTING MATERIAL

The ground material tested in the triaxial test consists of highly crushed and faulted phyllites and schists and was explored during the ground investigations for the Semmering Base Tunnel project. The fault zone material is highly heterogeneous with generally poor geotechnical properties while the described triaxial tests focus on the very weak portions of the fault zones which are predicted with thicknesses of several meters to tens of meters. Figure 1 shows the typical testing material.

Special care was taken during drilling procedure and handling of the samples to reduce the disturbance before testing to a reasonable minimum. This includes drilling with triple core barrel (including core liner), immediate vacuum sealing and protection with core liner and air bubble film. The result was a very high quality of core samples even in heavily sheared rock mass and fault zones.

Figure 1: Examples of typical testing material; cataclasites from phyllite and schist. The material can easily be broken by hand.

2. SPECIMEN PREPARATION

Depending on the degree of shearing, cataclasites can show different structures. For example, they can be described as bands of sheared rock or hard particles embedded in a relatively soft matrix. Therefore, the specimen preparation is very demanding, since cutting the sample with a conventional water flushed diamond disc saw leads to very irregular cutting surfaces. For this reason, the samples are cut on an electronically controlled air flushed diamond band saw. The saw consists of an endless metal band which has diamonds both on its cutting edge and on the lateral sides (for polishing while cutting). The sample is fastened with a prismatic adapter on a table which moves towards the rotating band saw. This equipment allows vibration less cutting of the hard inclusions without disturbing the matrix (Figure 2). After cutting one end of the specimen a parallel cut of the other end can be done by rotating the prismatic adapter by 180⁰. During cutting, the samples are protected against drying by covering them with plastic foil. Since the end surfaces are directly polished, no further treatment is necessary (Figure 3). After cutting, the specimen is weighed, photographed and measured.
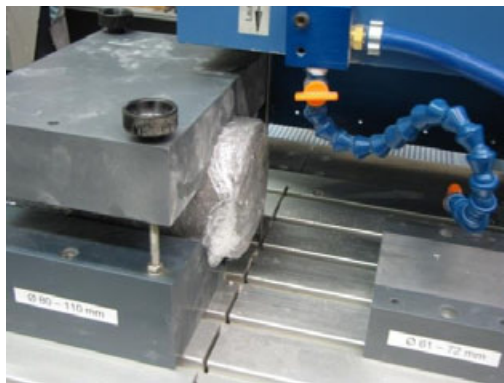
Figure 2: Diamond band saw.

Figure 3: Top view of sample after cutting.

3. TESTING EQUIPMENT

Triaxial tests on cylindrical specimens are the most frequently used laboratory tests to determine the strength and deformability of geomaterials. The standard equipment varies based on the type of material to be tested. For rock, high loads and pressures are required, whereas the pore water pressure is not controlled. On the other hand, low loads and pressures are applied for soils (about one to two orders of magnitudes lower than for rock), while controlling the pore pressure.

Since the samples of the cataclasites were recovered at depths of more than 350 m, high loads and pressures must be applied in order to test the specimen at confining pressures similar to the in-situ stresses. Due to the fact that most pores of the fault material build an interconnected system, the results need to be interpreted according to the principle of effective stresses. Therefore, the rock testing equipment must be improved in order to consider the effect of the pore pressure during the execution of the tests. The first experiences on triaxial testing of fault rock specimens under controlled pore pressure were gained at the ETH Zurich with the kakirites of the Gotthard Base Tunnel during the exploratory campaign [1]. As a consequence of the experiences of further investigations on weak rocks from other tunnelling projects, such as kakirites (from the Gotthard Base Tunnel during the construction stage and from the Ceneri Base Tunnel, Switzerland), graphitic phyllites (Visp tunnel, Switzerland, and Seich Sou tunnel, Greece) and breccias from the Straits of Gibraltar, the equipment was replaced and improved.

The used equipment consists of an electromechanical load frame with a nominal load of 600 kN (2 in Figure 4) and was designed for applying deformation rates down to 0.1 μm / min. In the triaxial cell specimens with dimensions up to 104 mm diameter and 210 mm height can be tested (1 in Figure 4 and Figure 5). The cell can withstand confining pressures up to 220 bars, which is generated with an electro-mechanical actuator with a nominal pressure of 250 bars (4 in Figure 4). The pore pressures at both ends of the specimen are controlled with two electromechanical actuators (5 and 6 in Figure 4) with a nominal water pressure of 30 bars. The axial load is measured with a high precision load cell (3 in Figure 4).

Furthermore, and in order to increase the accuracy of the measurements, the deformations of the specimen are measured close to the specimen (1 in Figure 5), i.e. inside the cell. The axial deformation is measured as the change of the distance between two magnets placed at both ends of the specimen (3 in Figure 4) with a non-contact position sensor based on the magnetostrictive principle (2 in Figure 5). The radial deformation is measured contactless with a linear magnetic encoder fixed on a chain extensometer (4 in Figure 5) and redundantly by measuring the change of the oil volume in the cell (4 in Figure 5). The latter is done by measuring the position of the piston of the actuator with a further linear magnetic encoder. Both ends of the specimen are connected with the respective pore pressure devices (5 and 6 in Figure 4 and 5). These allow applying a hydraulic gradient prior to the deviatoric loading of the specimen, in order to increase the degree of saturation. Watering the specimen enables the determination of its permeability by measuring the amount of water pressed in the specimen over time. After watering backpressure for saturating the specimen can be applied.

Figure 4: **Testing equipment.**   **Figure 5**: **Triaxial cell without hollow cylinder.**
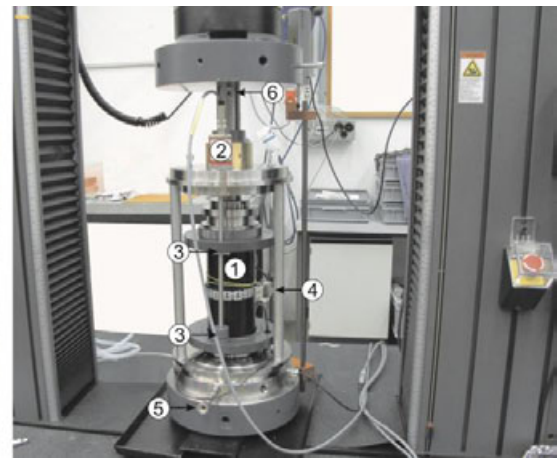
4. TRIAXIAL TEST

4.1. Testing procedure

The consolidated drained triaxial tests (CD) are performed as multi stage tests with three load stages with confining stresses in the range of the in-situ stresses and a maximum of approx. 20 MPa. The typical testing procedure consists of the following main phases.

- Hydrostatic loading up to 1 MPa.
- Water flow through the sample with hydraulic potential at both sides to increase saturation and measurement of the permeability
- Slow increase of the hydrostatic loading and consolidation at a hydrostatic stress level of 5 MPa.
- Slow increase of the axial stress (σ_1) until failure.
- Second and third loading stage with consolidation at 10 MPa and 15 MPa.
- Additionally two unloading/reloading cycles during each load stage.

Additionally, for some samples variations of the testing procedure are done as described below.

- Increase of the consolidation pressure (from 5 to 10 MPa) before the triaxial test (representing approx. 400 m of overburden and a k_0 of 1.0).
- Variation of the hydrostatic stress level of the different load stages (from 1 to 18 MPa).
- Hydrostatic unloading/reloading cycle to measure the compression (bulk) modulus.
- Testing of the specimen according to a special stress path by reduction of the axial stress (σ_1) starting from the assumed in-situ stress condition until failure of the specimen.

A full saturation of the specimen cannot be reached. But systematic investigations with kakirites from Gotthard Base Tunnel [1] show, that partially saturated material behaves almost similar in case of an interconnected pore system, which is gained by water flow through the specimen before consolidation. The collected test data are presented by stress-strain diagrams (deviator stress vs. axial strain) and the relation between volumetric strain ε_v and axial strain ε_1. In this paper the result of all tests are discussed while the result plots of only one selected sample is presented; Figure 6 shows the results for the load stage $\sigma_3 = 15$ MPa.
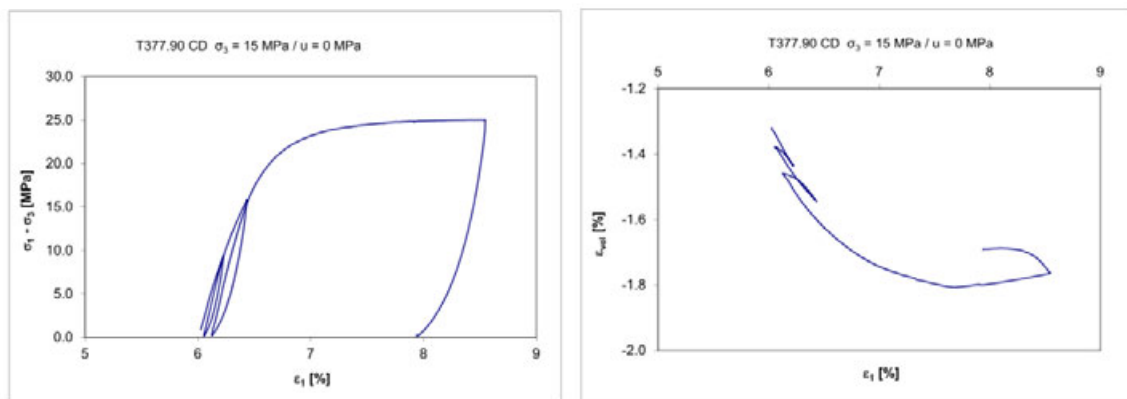
Figure 6: Results of the CD triaxial test for one load stage with confining stress of 15 MPa.

Additionally to the triaxial test geotechnical index tests such as density, water content, porosity and saturation are performed after the test. The grain size distribution is used to classify the fault material according to the specified ground types.

4.2. Results - Shear parameters

The tests show friction angles of approx. 24 to 28°. These results are comparable with CU triaxial tests done with typical low stress level of $\sigma_3 < 0.7$ MPa.

The tests show cohesions within a range of approx. 0.1 to 0.8 MPa. A correlation between cohesion and stress level can be seen where cohesion increases with higher stress levels. Furthermore the values are significantly higher than the cohesion values gained from CU triaxial tests with low stress level, which are in a range of 0.10 to 0.14 MPa for similar material. The main reason for this difference can also be related to the variation of the stress level. It can be stated that the CD tests show an increase of the cohesion with the increase of the stress level while the Mohr Coulomb failure criterion assumes a linear development of the failure envelope.

4.3. Results - Deformation parameters

The deformation behaviour is evaluated based on the stress-stain relations from the CD triaxial test results. For better interpretation of the test results the deviator stresses and the axial strains are normalised by the confining stress σ_3. Additionally the axial stains are set to zero after each load stage. Figure 7 shows the results of one multi stage triaxial test. It can be seen, that the specimen behaves differently in the initial load stage, which is related to the contraction of the material due to the generally low consolidation stress.

It can be seen that the deformation parameters depend significantly on the stress level and the loading history. With increase of the confining stress also the E-modulus increases. Furthermore the unloading/reloading modulus increases with the confining stress and is approx. two to three times higher than the E-modulus during initial loading. The results can be summarized with E-modulus value of approx. 500 MPa for a stress level of 5 MPa and approx. 4000 MPa for a stress level of 15 MPa.

It is important to notice, that CU triaxial tests with low stress level and similar cataclasites showed for example an E-modulus of 70 MPa for a confining stresses of 0.5 MPa. This underlines the importance to test the ground material with a stress level of approx. the in situ stress.
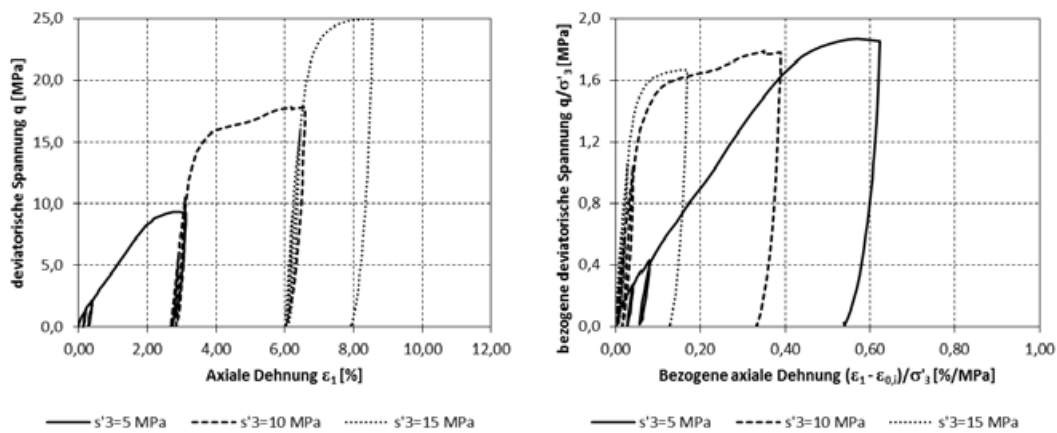
Figure 7: **Stress-strain diagram (left) and normalized diagram (right) for the evaluation of the deformation behaviour.**

4.4. Results – Permeability

The permeability of the cataclasites is calculated form the measured flow through the sample, which is done before the consolidation of the specimen as described in the triaxial testing procedure above. The permeability is in a range of approx. 10^{-10} to $8 \cdot 10^{-9}$ m/s with a mean value of approx. $6 \cdot 10^{-10}$ m/s.

4.5. Hardening soil parameters (HSS)

The test results were additionally evaluated according to the "Hardening Soil Model with Small Strain Stiffness" (HSS), which considers the non-linear behaviour during initial loading, the different behaviour during initial loading and unloading/reloading, the stress dependency of the stiffness and the behaviour due to very small strains (Small Strain Stiffness).

The stress dependent secant modulus E_{50} is evaluated from the lab tests with an assumed R_f value of 0.9 for all stress levels. For example, the E_{50} values of one triaxial test is 450 / 2400 / 4200 MPa for σ_3 stresses of 5 / 10 / 15 MPa. The stress dependent unloading/reloading modulus E_{ur} is evaluated from two unloading/reloading cycles performed at each load stage. For example, the E_{ur} values of one triaxial test 2.0 / 3.9 / 5.2 MPa for σ_3 stresses of 5 / 10 / 15 MPa. Figure 8 shows an example for one load stage with σ_3 = 10 MPa and an example for the unloading/reloading cycle. By evaluating all triaxial tests both, E_{50} and E_{ur} show an almost linear dependency with σ_3. The inclination of the linearity corresponds to a factor m of approx. 0.8 to 1,0 for E_{50}. For very small strains E_0^{ref} is estimated with 3-4 E_{50}^{ref} and the shear strain $\gamma_{0.7}$ is estimated with $1.5 \cdot 10^{-4}$.
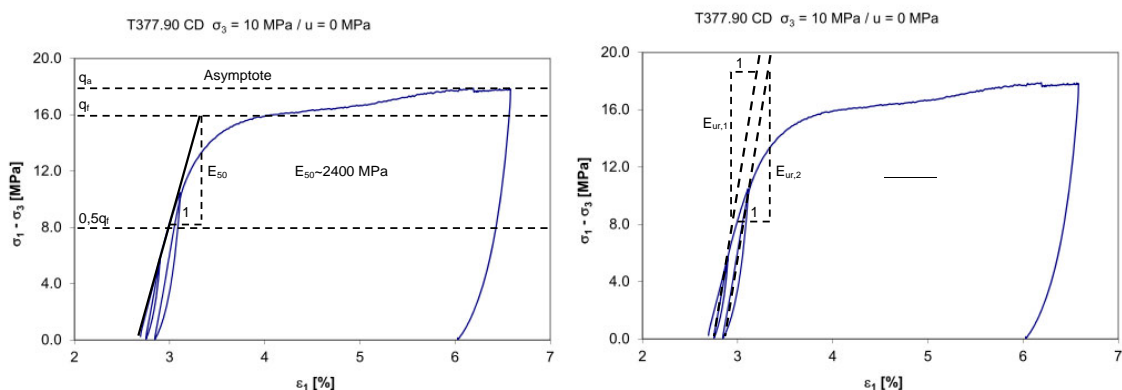
Figure 8: Example for the evaluation of E_{50} (left) and E_{ur} (right) for one load stage.

4.6. Numerical back analysis of the CD triaxial test

The CD triaxial test is back analysed with the finite element code PLAXIS 2D applying the HSS model. The FE model is set up with two rotational symmetry axes and is analysed until occurrence of failure in each load stage.

The back analysis shows a stress-strain diagram with different behaviour of the initial load stage with low confining stress (5 MPa) as observed in the physical test (see Figure 9). The results of the volumetric strains are also quite similar to the lab test results.

1) failure, qf ~ 1.4-1.5 q'/σ_3 2) path after failure
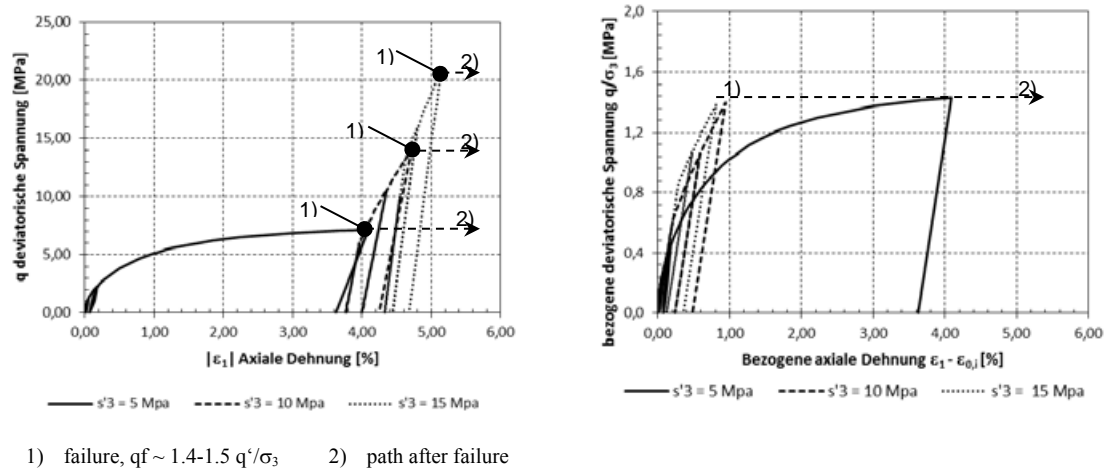
Figure 9: Results of the numerical back analysis with stress-strain diagram (left) and normalized stress-strain diagram (right).

5. CONCLUSION

The triaxial testing of cataclasites with stress levels comparable to the in situ stresses and the control of the pore water pressure leads to reasonable material properties, which can directly be used for geotechnical design of underground structures. With the use of sophistic testing equipment and special testing procedures shear parameters as well as stress depending deformation parameters and permeability can be determined for the usually very critical fault zone section of deep tunnels.

References

[1]   Vogelhuber, M. 2007. *Der Einfluss des Porenwasserdrucks auf das mechanische Verhalten kakiritisierter Gesteine*. Dissertation Nr. 17079, Institut für Geotechnik an der ETH, Zürich.

[2]   Daller, J., Atzl, G. & Blümel, M. 2010. *Bestimmung von Gesteinskennwerten an Störungsmaterial*. Festschrift zum 60. Geburtstag von Wulf Schubert. Institut für Felsmechanik und Tunnelbau, TU Graz.

[3]   Wehnert, M. 2006. *Ein Beitrag zur drainierten und undrainierten Analyse in der Geotechnik*. Mitteilungen des Institutes für Geotechnik, Universität Stuttgart, Vol. 53.

Authors

Dipl.-Ing. Dr. Andreas Goricki
3G Gruppe Geotechnik Graz ZT GmbH
Triester Strasse 478°
8055 Graz-Seiersberg
Austria
goricki@3-g.at

Dipl.-Ing. Dr. Erich Pimentel
ETH Zürich
Institute for Geotechnical Engineering
8093 Zürich
Switzerland
erich.pimentel@igt.baug.ethz.ch

Rückrechnung von Gebirgsparametern in Störzonen – machbare Aussagen, Unsicherheit und Grenzen

P. Schubert [a]

[a] *iC consulenten Ziviltechniker GesmbH, Büro Salzburg Bergheim, Austria*

Das Thema der Rückrechnung von Gebirgsparametern wurde vom Verfasser anlässlich der Auffahrung des Erkundungstunnels Paierdorf in der Zone der Lavanttaler Hauptstörung aufgegriffen und mit einfachen Mitteln (Gebirgskennlinie) zu einem befriedigenden Ergebnis gebracht [1]. Die damals gewählte Vorgangsweise soll hier nochmals dargestellt werden, ebenso wie ein Verweis auf weitere Untersuchungen durch andere Personen zu dieser Störungszone.

Eine Verallgemeinerung der hier gewählten Vorgangsweise stößt vor allem auf 2 Hauptprobleme: a) kurze, inhomogene Störungszonen, wo ein starker 3D Effekt der primären und sekundären Spannungsverhältnisse eintritt, und b) die Wahl der Vorentspannung, welche bei stark druckhaften Gebirgsverhältnissen auch wesentlich von der Steifigkeit des Ausbaus abhängt. In beiden Fällen würde eine Rückrechnung aufwändigere 3D Berechnungen erfordern.

1. LAVANTTALER HAUPTSTÖRUNGSZONE DES EKT PAIERDORF

Der Erkundungstunnel besteht aus der Kalotte des späteren Hauptbauwerkes und wurde in der Lavanttaler Hauptstörung überwiegend mit temporärer Kalottensohle ausgeführt.

Abbildung 1 zeigt eine typisches Stützmittelschema mit Deformationselementen repräsentativ für den Störungsabschnitt ab Station 1180:
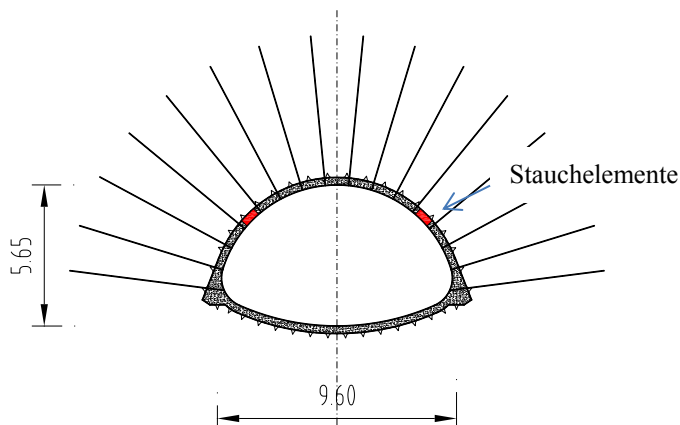
Abbildung 1: Regelquerschnitt im Abschnitt TM 1170 bis TM 1350 mit Deformationselementen.

Im Zuge des Tunnelvortriebs wurden umfangreiche geotechnische Messungen durchgeführt. Neben der üblichen Aufbereitung der Messergebnisse mittels räumlichen Verschiebungsentwicklungen durch Zustandslinien wurden vektororientierte Auswertungen zur Prognose von Steifigkeitskontrasten herangezogen. Diese Methode liefert Hinweise über das Gebirgsverhalten vor der Ortsbrust und ermöglicht zeitnahes Reagieren zur Anpassung der Stützmittel während des Vortriebes.

Als weitere Entscheidungshilfe für den Einsatz von Deformationselementen wurde die Rückrechnung der Spritzbetonauslastung herangezogen. Dabei wurden ab einer Grenzstauchung von ca. 8‰ bzw. einer Auslastung von ca. 80% der Spritzbetonsicherung Deformationselemente zur Anwendung gebracht.

Die Setzungen in der Kalotte zeigen max. ca. 200 mm in den Bereichen mit nachgiebigem Ausbausystem (Abbildung 2). Gegenüber der Erwartung aus der Planungsphase bedeutet dies eine wesentliche Erkenntnis, da wesentlich höhere Verschiebungswerte erwartet wurden.
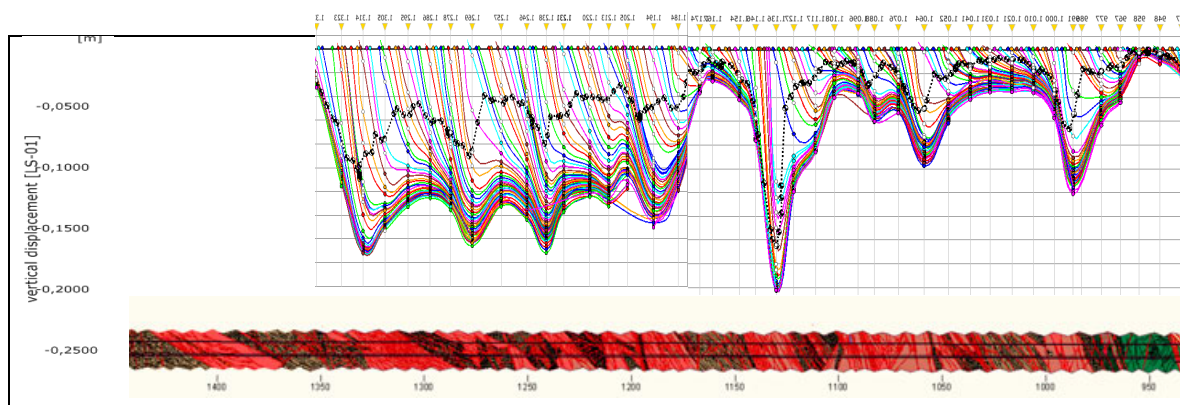
Abbildung 2: Firstsetzung im Abschnitt der Hauptstörung und Sicherungsmittel im Bereich der Ortsbrust.

Für die Rückrechnung der Gebirgskennwerte wurde jener Abschnitt der Hauptstörungszone ausgewählt, welcher mit den Deformationselementen ausgebaut wurde, das ist zwischen TM 1180 und TM 1330. In diesem Abschnitt betrug die Firstsetzung im Mittel ca. 150 mm. Die Ermittlung der Gebirgskennwerte erfolgte mittels Rückrechnung mit dem in der Folge beschriebenen Kennlinienverfahren.

Die Vorverschiebungen in der Natur wurden mit Hilfe der Meßdatenauswertesoftware GeoFit abgeschätzt. Das analytische Modell, welches hinter dem Curve-fitting des GeoFit steht, inkludiert auch die Verschiebungen vor der Ortsbrust, welche natürlich nicht durch die geotechnischen Messungen erfasst werden. Der Ausbauwiderstand, welcher durch die Spritzbetonschale aktiviert wurde, konnte in diesem Fall aus der Charakteristik der Deformationselemente abgeleitet werden. Mit der Annahme dass die Verzahnung zwischen Spritzbeton und Gebirge in der Störung gering ist, wurde mit der aufnehmbaren Normalkraft der Deformationselemente mittels der Kesselformel ein Radialdruck errechnet. Die Komponente der Ankerung wurde durch die Annäherung berücksichtigt, wonach die Tragkraft eines Ankers bezogen auf das Anker-raster bei voller Ausnutzung etwa dem entsprechenden Ausbauwiderstand entspricht.

Das Kennlinienverfahren darf an dieser Stelle als bekannt vorausgesetzt werden. Wegen der einfacheren Handhabung und Möglichkeit der Adaptierung auf die Bedürfnisse der Rückrechnung wurde eine Excel Version verwendet. Das Kennlinienverfahren beruht auf einem zweidimensionalen Modell mit ebenem Dehnungszustand und elasto-plastischem Materialgesetz, in diesem Fall Mohr-Coulomb. Die dritte Dimension wird durch die Wahl einer Vorverschiebung berücksichtigt, nach welcher der Ausbauwiderstand aktiviert wird.

Die Vorgangsweise der Rückrechnung ist wie folgt (Abbildung 3): Für einen gewählten Satz von Gebirgskennwerten E, c und φ ergibt sich eine Gebirgskennlinie und einer maximalen Verschiebung des Ausbruchsrandes im ungestützten Zustand u_{max}. Dem entspricht auch ein relativer plastischer Radius $P_r = r_p/r_o$. Gemäß Hoek et.al [2] leitet sich von P_r ein Verhältnis u_o/u_{max} ab. Bei einem bestimmten u_{max} ergibt sich also eine Vorverschiebung u_o.
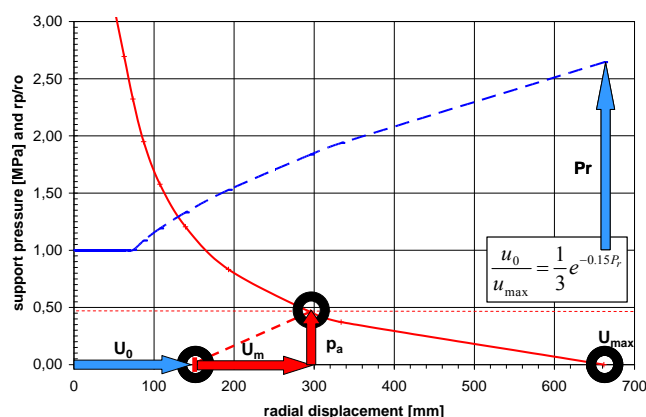
Abbildung 3: Wesentliche Komponenten des Kennlinienverfahrens und der Methodik der Rückrechnung.

Aus den Messdaten sind die gemessenen Verschiebungen, die Abschätzung der Vorverschiebung und die Höhe des Ausbauwiderstandes – wie oben ausgeführt - bekannt. Das analytische Modell muss nun unter Berücksichtigung der Schritte 1 und 2 und dem aus den Messungen ermittelten Verhältnis von uo/um den Gleichgewichtszustand ergeben. Für den charakteristischen Tunnelabschnitt zwischen TM 1200 und TM 1300 wurden folgende Eingabegrößen für die Rückrechnung gewählt:

Tabelle 1: Grunddaten für die Rückrechnung aus der Beobachtung während des Baus.

Charakteristische Firstsetzung [mm]	150
Ausbauwiderstand der Spritzbetonschale [MPa]	0,22
Ausbauwiderstand durch die Ankerung [MPa]	0,24
Summe aktivierter Ausbauwiderstand [MPa]	0,46
Verhältnis Vorverschiebung zu gemessener Verschiebung [-]	ca. 150 : 150

Mit der angeführten Methodik gibt es in der Regel eine relativ große Bandbreite von möglichen Kombinationen zwischen E, C und φ. Die Kombinationen werden eingeschränkt durch das Verhältnis zwischen Vorverschiebung und gemessener Verschiebung (in diesem Fall etwa 1:1) und den plausiblen Bereich für den Reibungswinkel (Abbildung 4). Zu letzterem dienten eine Analyse der Kornverteilung und die Berücksichtigung von Blockanteilen.
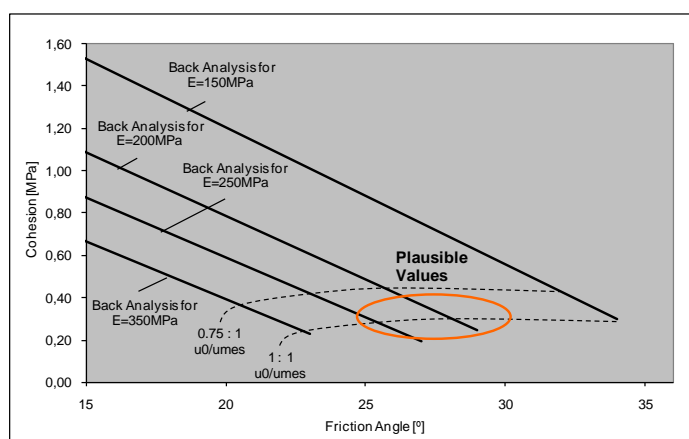
Abbildung 4: Mögliche Parameterkombinationen und Bereich mit plausiblen Werten.

Die für die Autoren plausibelste Kombination ist in Tabelle 2 angeführt.

Tabelle 2: plausible Gebirgskennwerte (aus Rückrechnung).

φ [°]	28
c [MN/m^2]	0,27
E [MN/m^2]	200
γ [kN/m^3]	23

Das gesamte Verschiebungsverhalten repräsentiert in diesem Abschnitt offenbar eine Mischung aus den unterschiedlichen mechanischen Komponenten der Störungskernzone. Einzelne Blöcke oder auch Kataklasitzonen haben sich in dem Bauschnitte mit Deformationselementen nicht sehr ausgeprägt in den Verschiebungen niedergeschlagen. Deshalb ist es sinnvoll, für weitere Projektierungsschritte Mischkennwerte für eine „tektonische Melange" anzunehmen. Eine Einzelbetrachtung der Komponenten feinkörniger, grobkörniger Kataklasit, Zerrüttungszone und Block ist offenbar hier nicht praxisrelevant.

Die Rückrechnungsergebnisse mit der Kennlinienmethode wurden mit einem 2D Flac Modell überprüft. Dabei wurde abweichend vom Kennlinienverfahren die tatsächliche Form des Tunnels gewählt und die Anker explizit modelliert. Das Materialgesetz Mohr-Coulomb, der primäre Spannungszustand und das Ausmaß der Vorentspannung wurde analog zum Kennlinienverfahren gewählt. Dabei konnte gezeigt werden, dass die Ergebnisse sowohl hinsichtlich Spannungs-Verschiebungsverhalten, Ausbaubelastung und plastischer Zone weitgehend identisch sind.

2. ERGEBNISSE AUS DEM VERSUCHSSTOLLEN

Die geomechanischen Eigenschaften der Lavanttaler Hauptstörungszone wurden in einem Versuchsstollen weiter untersucht. Darüber haben Pilgerstorfer et al. [3] ausführlich berichtet. Es ist anzunehmen, dass der Versuchsstollen innerhalb der starken Inhomogenität der Störungszone in einer relativ steifen Zone lag. Hier wurden Verschiebungsmessungen an der Schale, Dehnungsmessungen im Spritzbeton, Ketteninklinometer über der Firste, Ortsbrustextensometer, Doppellastplattenversuche und in-situ Scherversuche an der Kontaktfläche Spritzbeton – Gebirge durchgeführt. Die integrale Interpretation der Daten führte zu folgenden Kennwertempfehlungen (Tabelle 3):

Tabelle 3: empfohlene Gebirgskennwerte aus Versuchsstollen abgeleitet.

Station	φ [°]	c [MPa]	E [MPa]
TM VS 12,79 m	27	0,30	1500 – 2100
TM VS 15,36 m	27	0,20	800 – 2500
TM VS 19,29 m	30	0,25	1000 – 1800

Man sieht, dass die Einschätzung der Scherfestigkeit (Reibung und Kohäsion) sehr ähnlich den Rückrechnungswerten sind, der E-Modul jedoch deutlich höher. Wie stark dieser Befund durch die lokalen Verhältnisse beeinflusst ist, ist meines Erachtens nicht eindeutig zu sagen. Jedenfalls scheint aber bestätigt, dass tiefliegende Störungszonen durch die hohe Verspannung der Überlagerung eine sehr hohe Steifigkeit aufweisen können. Der Einfluss der Überlagerungsspannung auf die Gebirgssteifigkeit muss deshalb bei der Festlegung von Kennwerten unbedingt beachtet werden.

3. PROBLEM VORENTSPANNUNG

Die hier gezeigte, offenbar durchaus erfolgreiche Rückrechnung bezieht ihre Vorverschiebungswerte aus den 3D Modellrechnungen von Hoek et al. [2]. Diese Rechnungen wurden allerdings ohne Ausbau gemacht. Cantieni und Anagnostou [4] haben uns allerdings drastisch vorgeführt, dass die Vorentspannung bei stark druckhaften Verhältnissen und steifem Ausbau erheblich anders zu bewerten ist. Ein steifer Ausbau reduziert dann die vorauseilende Entspannung ganz erheblich und erhöht damit die Lasten des Ausbaus.

In unserem Fall ist der Ausbau durch die Deformationselemente sehr weich, wodurch dieser Effekt stark reduziert wird. Andernfalls scheint aber auch aus diesem Aspekt eine 3D Simulation unausweichlich.

4. PROBLEM 3D EFFEKTE

Die oben angeführte Rückrechnung für die Lavanttaler Hauptstörungszone beruht auf einem ebenen 2D Modell. Das ist bei der 450 Meter langen Störungszone berechtigt. Bei kurzen Störungszonen treten jedoch erhebliche Randeffekte durch die benachbarten kompetenteren Gebirgsbereiche auf, wodurch die Spannungs- und Verschiebungsprognose eines ebenen Modells zunehmend falsch wird. Zum Beispiel hat Graziani [5] gezeigt, dass bei den in seiner Studie gewählten Parametern ab einer Störungslänge von etwa 50 m die Randeffekte weitgehend verschwinden, und unter 20 m Störungslänge sehr erheblich werden (Lasten sinken auf unter 50%). Eine Verallgemeinerung ist hier sicher nicht zulässig und kurze Störungen würden jedenfalls ein 3D Modell für eine Rückrechnung erfordern.

5. SCHLUSSFOLGERUNG

Es ist hinreichend erwiesen, dass Tunnelstatik mit vielen Fragezeichen behaftet ist. Dasselbe gilt natürlich für Rückrechnungen jeder Art. Der Verfasser ist jedoch überzeugt, dass die einfache Methode der Rückrechnung mittels Kennlinie am ebenen Modell im Vergleich zur Ableitung von Kennwerten aus Bohrkernen und Laborversuchen zu erheblich wirklichkeitsnäheren Ergebnissen führt und deshalb in jedem Fall lohnend ist. Bei komplexen geometrischen Verhältnissen ist allerdings eine aufwändige 3D Modellierung nicht zu vermeiden.

Referenzen

[1]   Schubert, P., Hölzl, H., Sellner, P. & Fasching, F. 2010. Geomechanical knowledge gained from the Paierdorf investigation tunnel in the section through the Lavanttal main fault zone, *Geomechanics and Tunnelling* 3 (2), pp. 163-173, Berlin: Ernst & Sohn.

[2]   Hoek, E. 1999. Support of very weak rocks associated with faults and shear zones. In: *International Symposium on Rock Support and Reinforcement Practice in Mining*. Kalgoorlie, Australia.

[3]   Pilgerstorfer, T., Radoncic, N., Moritz, B. & Goricki, A. 2011. A Evaluation and interpretation of monitoring data in the test adit EKT Paierdorf. *Geomechanics and Tunnelling* 4 (5), pp. 423-434, Berlin: Ernst & Sohn.

[4]   Cantieni, L. & Anagnostou, G. 2009. The Effect of the Stress Path on Squeezing Behavior in Tunneling. *Rock Mech Rock Eng* 42, pp. 289-318, Wien: Springer.

[5]   Graziani, A., Capata, A. & Romualdi, P. 2007. Analysis of Rock-TBM-Lining Interaction in Squeezing Rock, *Felsbaumagazin* 25 (2007), Vol. 6, pp. 22-31, Essen: VGE.

Autor

Dipl.-Ing. Dr.mont. Peter Schubert

iC consulenten Ziviltechniker GesmbH

Zollhausweg 1

5101 Bergheim

Austria

p.schubert@ic-group.org

Tunnelling through a Major Fault: Considerable Overburden, Squeezing and Flowing Ground; At-Face Selection of Support

U. Glawe [a]

[a] Freelance Consultant in Geomechanics & Rock Engineering

Unexpected occurence of large faults in tunnelling is common in hydropower and infrastructure projects located in remote areas. It requires adequate geological and geomechanical characterisation of the fault and of the encountered materials. Tailoring appropriately the available engineering tools to the prevailing ground conditions is essential for doing well in the construction of the tunnel. This case study directly addresses such circumstances, where the top heading of a tunnel was driven through an unpredicted fault and the obtainable construction utensils were modified to deal with the extraordinarily difficult ground conditions, successfully. The fault is getting characterised by its geometry, the fault structure, the geological units in the fault as well as by the hydrogeological conditions. Implemented adjustments of the support and of auxiliary measures to tunnel through squeezing and flowing ground of the fault are addressed and typical monitoring results are presented.

1. INTRODUCTION AND PROJECT SETTINGS

This contribution to the workshop refers to the construction of the top heading of a 1.175 km long tailrace tunnel of a hydropower project in tropical SE-Asia. The project is located on the Malaysian Peninsula 150 km south of the Thai/Malay border 50 km west of the coastline.

After tendering and commencement of the initial construction works (river diversion) additional geological investigations at the tailrace were conducted. They revealed a zone of deteriorated rock at the tunnel level at a depth of 100 m. The detail design incorporated these adverse ground conditions and provided relevant assistance to tunnel through the anticipated conditions – within the contractual outline of the awarded project.

The tunnel has an excavation diameter of 9.70 m (for the heaviest support type). After 400 m in reasonably good rock the top heading entered the zone of deteriorated rock. The following 100 m revealed severe ground conditions. In addition groundwater was encountered, which led to erosion and squeezing and flowing ground in the central zone of this tunnelling section. During construction this 100 m wide zone was identified as a fault of very large scale with outer damage zones and a central fault core.

The contractual available ground reinforcement and support had to be modified to address the prevailing conditions: there were only basic and conventional methods available that were adjusted to meet the requirements to build the tunnel, safely.

2. REGIONAL GEOLOGY AND ENCOUNTERED ROCK TYPES

The project region is geologically characterised by low seismic activity and by N-S trending large scale folds of Permo-Triassic Age.

In the project area the following lithological units are prevailing (Figure 1):

- sedimentary rock (low grade metamorphic); graphitic shale, siltstone, fine-grained sandstone
- volcanic rock (andesite)
- interlocking strata (sedimentary/volcanic), which was defined (thickness, mechanical characteristics) during construction of the diversion works
- granite (4 km away, bee-line distance)

The area is covered by dense jungle and exhibits a hilly topography (elevation 150 m to 400 m asl.). The depth of weathering depends on rock type and other factors, but reaches for the volcanic rock typically

down to 40 m below ground level at a maximum, where the boundary of moderately to slightly weathered rock is located. The actual soil thickness (= ISRM weathering grade V and VI) is around 20 m in general.
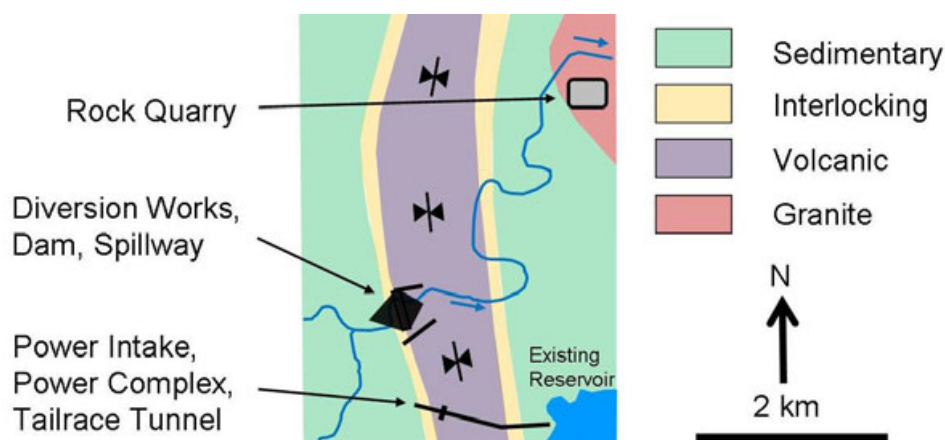
Figure 1: Schematic sketch showing the project arrangement and the tunnel with respect to the major geological structures and encountered lithological units.

3. FAULTS AND DISCONTINUITY PATTERN

During previous stages of the project (feasibility study to tender design) focus was predominantly on identifying faults at the actual dam site. A few faults of minor extend (several tens of metres) with small off-set were identified through evaluation of aerial photos and field investigations. There was no indication of the existence of a large scale fault anywhere in the project area.

Beside bedding joints in the sedimentary and the interlocking sequences a discontinuity pattern typical for a rock mass folded at large-scale is prevailing with well developed extensional joints (ac-jointing) and conjugated shear jointing (hk0-jointing).

4. TUNNEL GEOLOGY AND EXCAVATION CLASSES

4.1 Tender Stage

For tendering the geological model shown in Figure 2 was used. It describes in sufficient detail the general ground conditions known at that stage of the project. Four excavation classes were specified for different rock classes (Q – values), which included shotcrete and rock bolts. Two heavier classes were assumed to be necessary for the portal section and for crossing potential minor faults. Hence, typical support and reinforcement used for such conditions - steel sets, canopy tubes and face nails – were added in the design and the head & bench method was suggested for excavation.
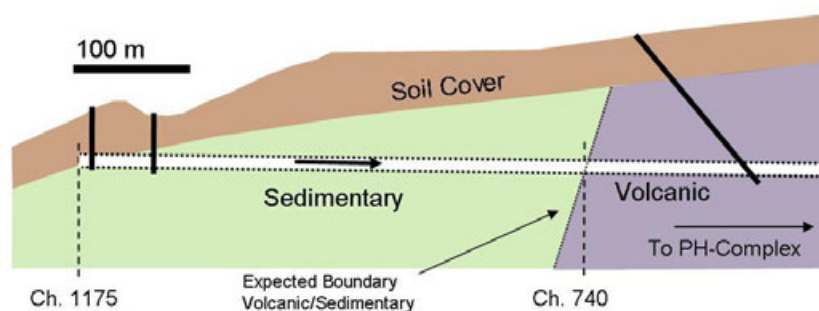
Figure 2: Sketch showing the geological model for the tunnel at tender design stage. (Ch. = chainage or tunnel meter).

The construction schedule required that the 1.175 km long tunnel will be driven towards the powerhouse complex from downstream and down-hill at a gradient of 1%. At the downstream portal the tunnel will discharge into an exiting reservoir. The full supply level of this reservoir is close to the tunnel roof at the portal. The respective water level is indicated in Figure 3.

4.2 Detail Design Stage

During detail design further geological investigations were conducted along the alignment with focus on the portal excavation. Furthermore a 120 m deep inclined borehole was drilled (HTS5 in Figure 3) to better characterise the expected contact of the volcanic rock with the sedimentary rock.
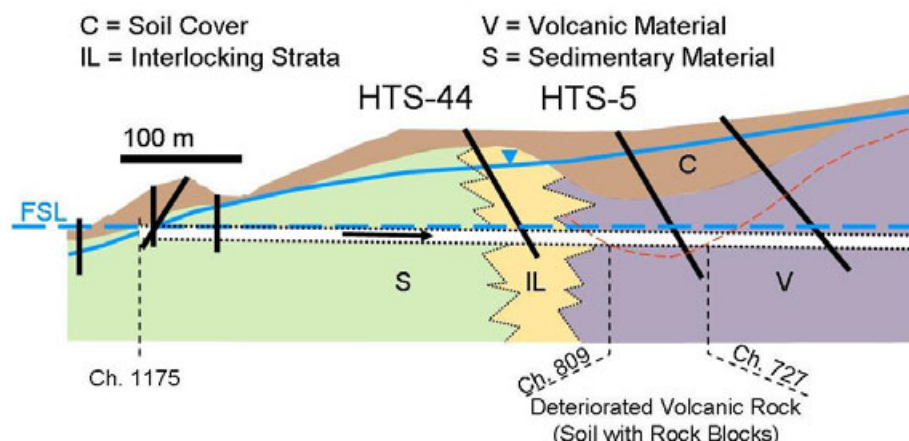
Figure 3: Sketch showing the geological model during detail design prior to construction. FSL stands for Full Supply Level of the existing downstream reservoir. The dashed red line represents the assumed "rock line". The direction of the tunnel drive is indicated with the black arrow.

Surprisingly, down to an elevation of 10 m below the tunnel invert the entire drilling showed soil like material with a few small blocks of volcanic rock. The soil in the drilling was visually and from its estimated grain size distribution similar to residual soil produced by weathering of the volcanic rock. However, deep-seated weathering was soon excluded from potential sources as the soil was found down to a depth of more than 100 m and the surface of slightly weathered rock is located generally not deeper than 40 m below ground level. The surfaces of the few blocks in the drilling block showed coatings and signs of cauterisation. Hence, hydro-thermal alteration along a minor fault or similar genesis was considered to be a reasonable geological explanation.

Figure 4: Drill cores obtained from borehole HTS-5 (see Figure 3) from the tunnel level with a triple-tube core barrel. The borehole penetrated the tunnel at around Ch. 750 (compare Fig. 5 and Table 1 for actual geology at Ch. 750).

As the location and geomechanical characteristics of the contact sedimentary/volcanic rock was still unidentified, in-depth geological mapping was performed at the morphological ridge along the tunnel alignment. Quartz pebbles in the residual soil were used as indicator of sedimentary strata. Based on the results of mapping another borehole was drilled (HTS44 in Figure 3). It revealed that the contact is not sharp, but it is characterised by interlocking of the individual strata. This interlocking was irrelevant for the design and for the construction of the tunnel as both rock types are of good quality when fresh.

A newly developed geological model was set up as presented in Figure 3. It shows a zone of "deteriorated rock, soil with rock blocks" from Ch. 727 to Ch. 809. A "rock line" was introduced that separates the soil type material from the material with rock properties. At that stage of the project it was still unknown that the tunnel would cross a wide major fault at a cover thickness of approximately 100 m.

The designed tunnel support for the zone of "deteriorated rock" is characterised by the following components:

- Steel sets HB 200 x 200 x 49.9 kg/m, grade 275, 1 m c/c; on top heading arch outer rib with footing (steel plate) and inner rib with connecting plate, only
- Canopy tubes for forepole umbrella,114.3 x 6.3, grade 275, 0.5 m c/c, 9 m, 3 m overlap, outward directed at 6.5° to the tunnel centre line
- Fibreglass face dowels, 12 m long, 1.5 m c/c staggered, 3 m overlap (= 30% of excavation diameter)
- 250 mm shotcrete SFR 40, crown and side walls
- 50 mm SFR 40 at the face
- Central exploratory drill hole

In addition to these measures there were provisions for cement grouting and drainage measures provided in the contract. It is pointed out that the listed support and auxiliary measures were basically the only available engineering tools to use in tunnelling through the squeezing and flowing ground in the fault core. Fortunately, the designer has addressed uncertainties in the tunnel geology through permission of directives of the engineer at the spot as some of the above listed engineering measures had to be significantly modified, reinforced and tailored to engineering requirements to deal with the prevailing ground conditions. This is further detailed in chapter 6.

In early 2012 the tunnel was driven from the portal (Ch. 1+176) towards the powerhouse complex. It entered the damage zone of the fault at Ch. 828.

5. GEOLOGICAL CHARACTERISTICS OF THE FAULT

5.1 Fault Geometry

There were no morphological signs of the fault and of its orientation prior to the construction of the tunnel. Even now, after driving the tunnel through the fault, the exact orientation of the fault is not entirely clear. There are several geological indications, such as lithological boundaries found in horizontal probe holes (drilled at Ch. 765 and Ch. 741, see Figure 5), or the discontinuity pattern in the host rock next to the fault, which point to a steep dip angle of the fault and an obtuse angle between the tunnel axis and the fault plane.

Further indication referring to the fault orientation is a sharp contact in the fault damage zone at Ch. 721, which is sub-vertically dipping and orientated perpendicular to the tunnel axis. Based on these observations it is considered that the fault is dipping at steep angle and is striking in N-S direction (= orthogonal to the tunnel axis). This statement refers to the location where the tunnel passed through the 100 m fault. The extension of the fault away from the tunnel is unknown.

One may question why such major fault could not be identified by the geologist prior to driving the tunnel into the fault. A possible explanation is: both soil types, the completely weathered/residual volcanic material (ISRM weathering grade V and VI) and the fault material exhibit very similar geological characteristics. This refers in particular to inspected drill cores as well as to the grain-size distribution (high fine content with some sand, gravel and blocks). Such resemblance indicates similar proneness to erosion. This fact and the 20 m thick soil cover of the volcanic material adjacent to the fault does not allow the development of topographic features typical for large faults in moderate or arid climate.

5.2 Fault Structure and Fault Geological Units

The structure of a fault is shown schematically in Figure 5 and the actual geology exhibited in the tunnel is detailed in Table 1.

During tunnelling both damage zones were identified and a 39 m wide central fault core could be designated. Most of the boundaries between zones were clear, but there is also a 12 m wide transition zone between damage zone and fault core at one side of the fault core.

From Ch. 735 to Ch. 724 strong marble blocks were encountered in the matrix material of the fault core (light blue blocks in Figure 5). This was entirely unexpected as there are no limestone or marble outcrops known in the nearby area (for at least several kilometres away from the tunnel). The metamorphic marble blocks are embedded in a soil matrix that showed no signs of lithification or metamorphism. The block surfaces showed karstic features. The origin and the genesis of the marble blocks remain mysterious.
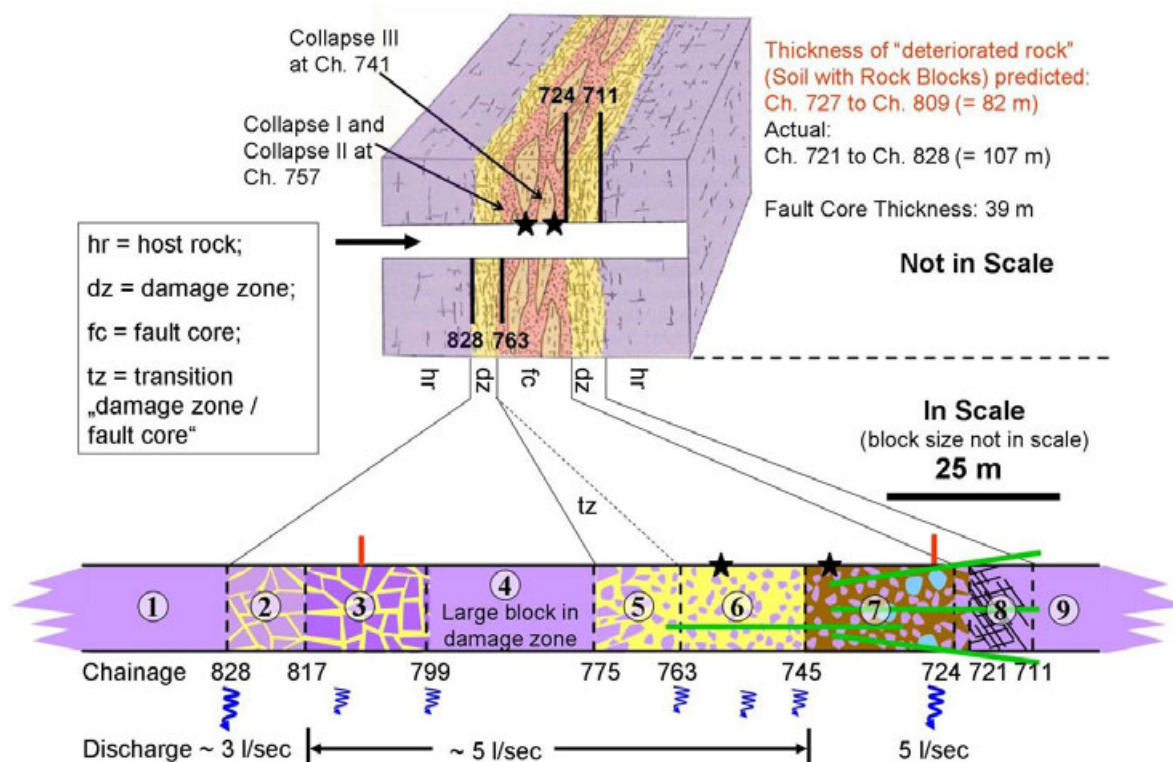
Figure 5: The upper block diagram shows the schematised structure of a fault (block diagram modified after [1]). The actual fault geology and thickness of individual zones observed in the tunnel is presented in the geological profile below including discharge into the tunnel. The numbers in the geological profile refer to those used in Table 1. The red bars in top of the profile indicate the extent of "deteriorated rock" predicted for detail design. The green lines indicate schematically the probe drillings ahead of the respective tunnel face.

Table 1: Fault geology, fault zoning and respective tunnel support. The numbers of the zones refers to the numbers in Figure 5.

#	Chainage	Geology	Zone in Fault	Support (schematic)
1	To 828	Andesite (Q > 50)	Host Rock	Spot Bolting
2	828 - 817	Blocky andesite with randomly shaped large angular blocks (edge length up to 3 m). No direct block/block contacts, but blocks are separated by thin (< 3 cm) yellowish fine-grained soil material.	Damage Zone	Ribs & Shotcrete
3	817 - 799	As from Ch. 817 to 799 with long (< 1.5 m) and thick (< 0.3 m) lenses of fine material between blocks	Damage Zone	Canopy Tubes & Ribs & Shotcrete & Face Support
4	799 - 775	Andesite (2 < Q < 50)	Large Block in Damage Zone	Syst. bolting & Shotcrete
5	775 - 763	Gradual transition from the andesite (as at Ch. 799 - 775) to fault core material (as at Ch. 763 - 745).	Transition Damage Zone / Fault Core	Ribs & Shotcrete
6	763 – 745	Yellowish-brownish soil material (see Figure 6): intermittent grain size distribution, rounded, rounded/angular and angular andesite blocks (block edges always rounded) with a max. diameter of 0.5 m embedded in soft to medium stiff fine-grained matrix (see Table 2). Volumetric block content < 25%. Unit weight of blocks ranging from 18 kN/m^3 to 26 kN/m^3 indicating (hydro-thermal?) alteration. Cohesive BiM-rock fc 25 (after [1]).	Fault Core	Canopy Tubes & Ribs & Shotcrete & Face Support & Auxiliary Measures
7	745 - 724	Brownish-blackish soil material (Figure 7) with physical characteristics similar to the fault core material described above (Ch. 763 to 745), but softer. Locally internal layering in the matrix material and slickensides (Figure 8). Volumetric block content << 25%, blocks are more angular than in previous section. Cohesive BiM-rock fc 25. Rounded marble blocks with a diameter of up to 2 m encountered from Ch. 735 to 724.		
8	724 – 711	Transition from fault core material to damage zone material (here fractured andesite) from Ch. 724 – 721. Sub-vertical persistent few centimetres thick "fault" at Ch. 721. Rapid decrease of jointing from Ch. 721 to Ch. 711 where Q > 10.	Damage Zone	Initially Ribs and Shotcrete, then Shotcrete and Syst. Bolting
9	from 711 onward	Andesite (Q > 10, generally >> 50)	Host Rock	Bolting, Spot Bolting

Table 2: Grain size distribution and natural moisture content (NMC) determined for the brownish-blackish and the yellowish-brownish matrix material.

Sieve Size [mm]	Brownish-blackish Matrix	Yellow-brownish Matrix
	Passing	
2	88%	98%
0.212	77%	86%
0.075	75%	71%
NMC	28%	30%

Figure 6: Tunnel face at Ch. 760 prior to shotcreting and placing of steel set. Cohesive yellowish-brownish matrix material and dark-grey andesite blocks (BiM-rock fc25).

Figure 7: Lump of brownish-blackish undisturbed matrix soil of the fault core (Ch. 730). The material feels similar to damp compacted peat. For grain size distribution and NMC see Table 2.

Figure 8: Brownish-blackish matrix material with slickensides (left) and layering (right). The slickensides were presumably generated by deformations ahead of the face (Ch. 735) and not by tectonic processes. The layering may indicate previous internal tectonic deformation of shear lenses in the fault core.

5.3 Groundwater and "Soil Sweating"

The groundwater table observed in borehole HTS5 and other drill holes is indicated in Figure 3. Maximum discharge into the tunnel occurred at the outer boundaries of the individual damage zones: once the tunnel entered the damage zone at Ch. 828 local discharge of approximately 3 l/sec. was observed (Figure 5).

From Ch. 817 to Ch. 735 discharge occurred locally, generally from the tunnel side walls. In addition, where the fine-grained matrix was exposed, "sweating" was observed. This superficial pore water pressure release was presumably caused by the increased tangential stresses in the face or side walls, unconfined conditions and due to the high natural moisture content of around 30% for both matrix types. The "beads of water" that developed soon after exposure changed rapidly into a thin "mud coating" of the exposed soil surfaces and led to serious problems during shotcrete application.

Water discharge increased significantly from Ch. 745 onward when the tunnel approached the other boundary fault core / damage zone. Over the last 12 metres in the fault core, discharge was entering the tunnel along a few distinct flow paths in the tunnel face with a total of about 5 l/sec.. Some of the few flow channels discharged dark-brown muddy suspension (dissolved brownish-blackish matrix material), which indicated the development of erosional cavities ahead of the face.

6. TUNNELLING THROUGH THE FAULT

6.1 Tunnelling from the Damage Zone into the Fault Core

Due to reasonable stability of the face and limited water discharge in Zone 5 of the fault (see Figure 5 and Table 1), the top heading was driven "full face" with all available support and auxiliary measures described in section 4.2 with a round length of 1 m.

The tunnel drive encountered no worth mentioning problems until it reached Ch. 757, where a combined face-crown collapse occurred (Collapse I in Figure 5). As with most tunnel collapses there are several reasons for such failures [2], adverse ground conditions were in this case one of them.

A more than 8 m high chimney-like cavity was back-filled in three stages with a total of more than 80 m^3 of light-weight concrete and some cubic metres of mortar. Light-weight concrete (or "foam concrete") was selected as back-fill material due to its good workability and excavatability – not due to its light weight, only. The design mix of

160 kg sand, 650 kg OPC, 150 l water, 6.5 kg superplasticiser and 11 kg poly-beads per m^3

resulted in a unit weight close to 10 kN/m^3 and a 28 days cube strength of 6 MPa. This strength allows that the material can be excavated easily with a standard excavator or even with a pick with difficulty.

After re-establishment of the tunnel a crown failure (= Collapse II in Figure 5) occurred at the same location as Collapse I (Ch. 757). This happened just before the next rib could be placed underneath the newly installed canopy tubes. As with the previous collapse, adverse ground conditions were one of the reasons of the failure. The situation was re-established after only a few days: more than 40 m^3 of light-weight concrete and some mortar were pumped into the collapse cavity.

6.2 Tunnelling in the Fault Core

After the second re-establishment, the tunnel was progressively driven through the fault core. The tunnel instabilities experienced called for adjustments of the support and change of the excavation system. The heaviest support type was already in place and there was only the option to utilise available tools, which required on-the-spot modification as described in the following sections, and step-by-step implementation. The tunnel advanced from Ch. 757 to Ch. 745 with the support and auxiliary measures detailed below at a rate of less than 0.2 m/day.

6.2.1   Additional fibreglass dowels

To increase face stability in the tunnel the overlap of the face dowels was increased to more than 50% of the tunnel diameter. This was in line with experience reported by others, e.g. [3] that such overlap is required to significantly increase face stability in cohesive ground. Increasing the overlap to more than 50% of the tunnel diameter (= more than 5 m) means for this case effectively reducing the spacing of the 12 m long dowels by approximately 50% to 0.75 m c/c.

6.2.2   Partial and Sequential Excavation

The excavation was subdivided into three sections and a face buttress was developed. Further along the tunnel the face was subdivided into five and more excavation and shotcrete sectors. This allowed better control the face (stability) and eventually created a thick shotcrete shell.

6.2.3   Drainage Canopy

A de-watering shield consisting of 9 m long perforated PVC-pipes wrapped with geotextile and drilled in-between individual canopy tubes at steeper angle than the tubes was installed to drain water away from the soil ahead of the face. However, as the ground water followed distinct flow channels in the cohesive soil of the fault core, very few of the tubes were productive and therefore this measure was no longer implemented in the tunnel drive.

6.2.4   Temporary Invert Liner

The design provided provisions for a thin temporary shotcrete lining of the invert in the top heading. As the ground was so soft and could not withstand mechanical impact such as excavator tracks and for other practical reasons, the shotcrete liner was replaced by a 200 mm mesh reinforced concrete slab.

6.2.5   Change of Excavation Techniques

To separate individual excavation sections in the face, line drilling through the shotcrete was implemented with a drilling bit of small diameter (2 inches). To avoid overbreak and disturbance of the face during excavation, the excavator was replaced by a pneumatic percussion drilling rig with a 150 mm drilling bit. The so easily excavated material was later removed with an excavator.

6.2.6   Improvement of Steel Set Foundations with Cement Grouting

Bearing capacity of the steel set foundations was considered to be crucial for distributing forces from the stiff mechanical unit "forepoles - steel sets - shotcrete vault" into the ground. Softening of the foundations would seriously call into question the entire engineering approach in this regard. Pressure cement grouting was conducted from the face into the up-coming foundation material, but soon abolished due to the required effort and questionable success to very locally achieve ground improvement.

6.2.7   Improvement of Steel Set Foundations through Grouted Rib Footings and Ring Drains

Softening of the material in the small excavated pits for the steel set footing due to accumulation of water from "sweating" and from local water ways was addressed by the following approach: the readily excavated pits were cleaned shortly before shotcreting. The gap between ribs and the ground was filled with aggregates and shortly after with grout to create a load bearing connection between the steel set and the soil foundation material (Figure 9).

A wound roll of geotextile was fixed onto the walls with nails to prevent water flowing from the walls and from the tunnel face into the pit. The geotextile roll was extended further into the tunnel profile with a ribbed PVC-pipe (Figure 9) and simply covered with shotcrete. This simple drain worked well prior and after shotcreting.

Figure 9: Details of rib footings prior to shotcrete application. The footing of the outer ribs (highlighted with the dashed white line) stands on aggregate and a wooden formwork was installed before the rib footing pit is filled with grout. A ring drain of wound geotextile is nailed onto the soil to prevent water from the walls entering the excavation pit of the footing. A steel plate is welded on the inner rib in preparation for the installation of micro-piles.

6.2.8   Provisions for Micro-pile Foundations for Steel Sets

In the soft ground micro-piles can act as auxiliary foundation of ribs. Hence, there were an option. To connect possible micro-piles to the ribs, rectangular steel plates (940 mm x 370 mm x 20 mm) were welded onto the inner flange of the inner rib (Figure 9).

6.2.9   Strengthening of Vault through dense Steel Sets and increased Shotcrete Thickness

Steel rib spacing was gradually decreased from 1.0 m to 0.5 m and the thickness of shotcrete could be increased only by increasing the excavation diameter to assure the shotcrete does not penetrate the specified B-Line (here defined as outer boundary of reinforced concrete liner).

6.2.10   Modification of Canopy Tubes for Pressure Grouting

The canopy tubes were initially designed as un-perforated steel tubes filled with grout followed by annulus grouting. To modify the tubes for pressure grouting a simple system was implemented as shown in Figure 10.

Non - perforated section (300 cm)   Perforated section (600 cm)
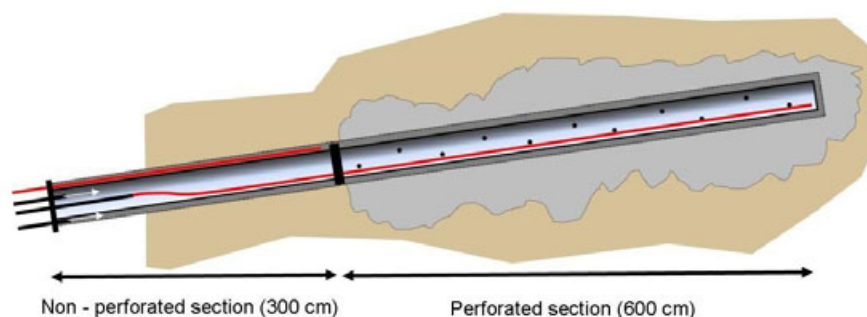
Figure 10: Modified canopy tube for pressure grouting. The non-perforated and perforated sections are divided by a sleeve of mild steel of the diameter of the borehole and welded onto the tube. In a first stage the annulus of the none-perforated section was filled with grout at low pressure (red = return pipe). In a second stage the steel tube was filled with grout until return occurred through the red pipe. This pipe was then closed and pressure grouting was conducted.

6.3 Tunnelling in Squeezing and Flowing Ground of the Fault Core

Due to the low advance rate, which was caused by the necessity to apply required support and implement auxiliary measures as described above, it could not be avoided that the soil was getting longer in contact with water and got increasingly soft. From Ch. 745 onward discharge was observed in the face. Erosion of the soil material ahead of the face was indicated by brown soil suspension flowing into the tunnel.

Once the tunnel entered Zone 7 of the fault at Ch. 745 (see Figure 5), which comprises material that is even softer than the previous material, squeezing phenomenon were evident and the situation in the tunnel got increasingly serious. The main concern was possible sudden and brittle failure of the entire shotcrete-rib-vault due to bearing capacity failure of the rib foundations.

Figure 11: Spalling of shotcrete at the tunnel perimeter in-between canopy tubes. Radial cracking of the shotcrete at the face and buttress further demonstrated ongoing instability in the face.

Spalling of shotcrete as well as radial cracking of the shotcrete in the face and face buttress indicated that the canopy tubes were failing ahead of the face and getting bent down due to squeezing ground (Figure 11). The tunnel face was getting pushed into the tunnel. Despite all efforts, eventually at Ch. 741 the face gave way and face collapse of a few cubic metres occurred (Figure 12).

Figure 12: Collapse III at Ch. 741. This face collapse of a few cubic metres only, occurred after observation of significant squeezing of the tunnel face and the adjacent roof and the side-walls. The blocks in front of the debris are blocks of matrix soil including smaller rock blocks that were separated from the face. Note the bent-down canopy tubes in the crown and the discharge of muddy suspension from the face. The latter was creating large erosional cavities with a total volume of several tens of cubic metres ahead of the face.

After establishing reasonably safe conditions in the tunnel, three exploratory bore holes were drilled which indicated far better ground conditions approximately 20 m ahead of the face (for location of drillings and orientation see Figure 5).

During drilling of the canopy tubes large cavities generated by soil erosion ahead of the face were discovered. They required filling with more than 40 m³ of light-weight concrete. In addition cement grouting was conducted along the tunnel perimeter prior to placing the next canopy tubes. At Ch. 741 more than 30 tons of cement was pumped into the perimeter before the works advanced.

It was evident that the so far implemented measures were insufficient for tunnelling in such poor and unpredictable ground. To deal with these conditions further support and auxiliary measures were implemented step by step when the tunnel progressed.

6.3.1 Perimeter and Face Grouting

Perimeter and face grouting was considered necessary for the upcoming 20 m in adverse ground as an auxiliary measure to contribute to stabilize the face: 9 m long holes were drilled in-between canopy tubes and grouted at a low water cement ratio with a maximum pressure of 10 bars. The holes were left open and unsupported prior to grouting; only a 1.5 m steel tube was inserted and the hole was sealed.

Grouting pressure and w/c ratio were consistently adjusted. Grout takes varied significantly, from nil in some holes to several hundreds of kilograms of cement per hole. In some of the holes that had high grout takes, grouting was stopped when no pressure changes but continuous takes were recorded. Grouting was started along the perimeter to radially confine the soil ahead of the face. This was followed by systematically grouting of the face towards the centreline.

A few grout holes penetrated distinct water paths. These holes were used as drain holes after a 9 m long geotextile-wrapped PVC-pipe was inserted (where possible).

6.3.2 Reinforcing Canopy Tubes and Canopy Grouting at significant Discharge

The canopy tubes drill holes intercepted distinct groundwater flow paths with increasing discharge and the previously introduced tube pressure grouting system (shown in Figure 10) became ineffective. The canopy tubes were reinforced with three centrally placed 26 mm steel bars of grade 460 and modified as shown in Figure 13.
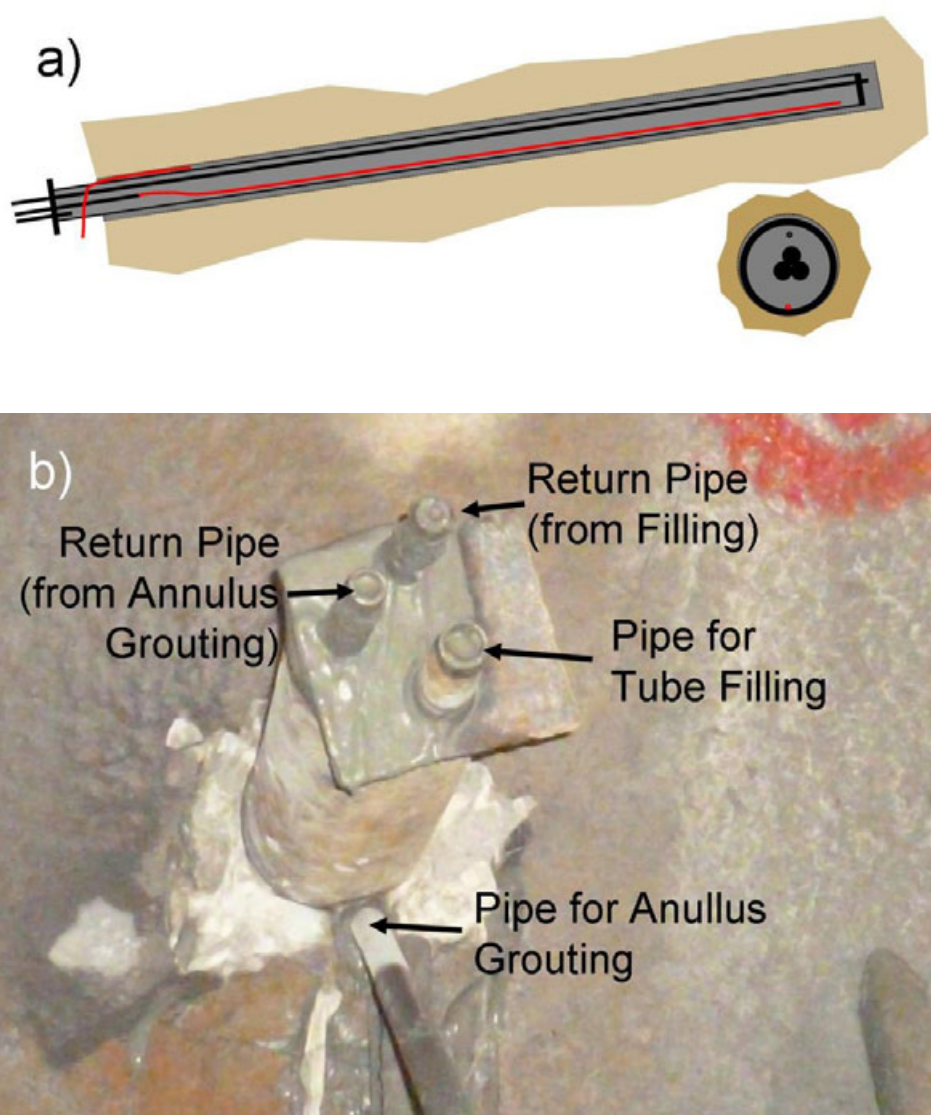
Figure 13 a and b: Modified canopy tube for grouting in ground with high water discharge. The tube is closed at both ends. After installation of the tube the annulus is closed at the face. This is followed by grouting the canopy tube. This procedure guarantees that the entire tube is filled with grout and no grout is washed away. Together with the three centrally placed steel rebar it can act as stiff and strong cantilever. In a second stage the annulus is (pressure) grouted.

6.3.3 Dense and Double Forepole Umbrella

The spacing of canopy tubes was further reduced to 0.4 m and where the space allowed, a second row of canopy tubes was installed. The latter procedure was only possible at Ch. 741 (Figure 14).

Figure 14: Upper section of the face at Ch. 741 with double forepole umbrella on the right side of the roof and side wall. Note that there is a third row of tubes of the previously installed canopy tube set above the steel set which reaches 3 m ahead of the last installed steel set. The tubes were installed with protruding ends to minimise the excavation required for the installation of the next steel set. The yellow circles indicate optical targets placed strategically onto the last steel rib and in the tunnel face and buttress. This allowed monitoring displacements during canopy installation and during the excavation.

6.3.4 Reinforced Micro-Piles as Steel Set Foundations

As previously noted, bearing capacity failure of the foundation soil beneath rib footings was a very serious concern of the engineer in charge. The results of tunnel monitoring indicated continuous and differential settlements of the shotcrete-rib vault (Figure 15 and Figure 17). Radial cracking of the shotcrete between steel ribs at Ch. 746 occurred.

Section 6.2.8 describes the preparation of the ribs to connect them to micro-piles and hence immediate installation was possible. Material available at the site (= canopy tubes) was used as micro-piles: 6 m long steel tubes, 114.3 x 6.3, grade 275, one pile at each side of a rib (= four piles per steel rib). The principle for fixing the piles to the ribs is detailed in Fig. 16. It leads to immediate mobilisation of the piles at any settlements of the ribs.

Due to restriction in space (drilling rig and location of foot plate of the outer rib) the micro-piles could only be drilled at a maximum inclination of about 30° to the horizontal. Hence, they are acting primarily through bending rather than skin friction and end bearing. Therefore, the piles were reinforced with a centrally spaced steel bar of 26 mm diameter (grade 460).

Initially it was not clear whether the micro-piles could substantially support the steel set foundations and take the loads transferred from the reinforced forepole umbrella onto the ribs. Tunnel monitoring was an essential tool to observe functioning of the micro-piles and to identify their role in tunnel stabilisation. The monitoring results presented in Figure 17 indicate that the micro-piles required more than 20 mm of displacements until they were significantly contributing to stabilise the tunnel, which is considered to be small bearing in mind the poor ground conditions.
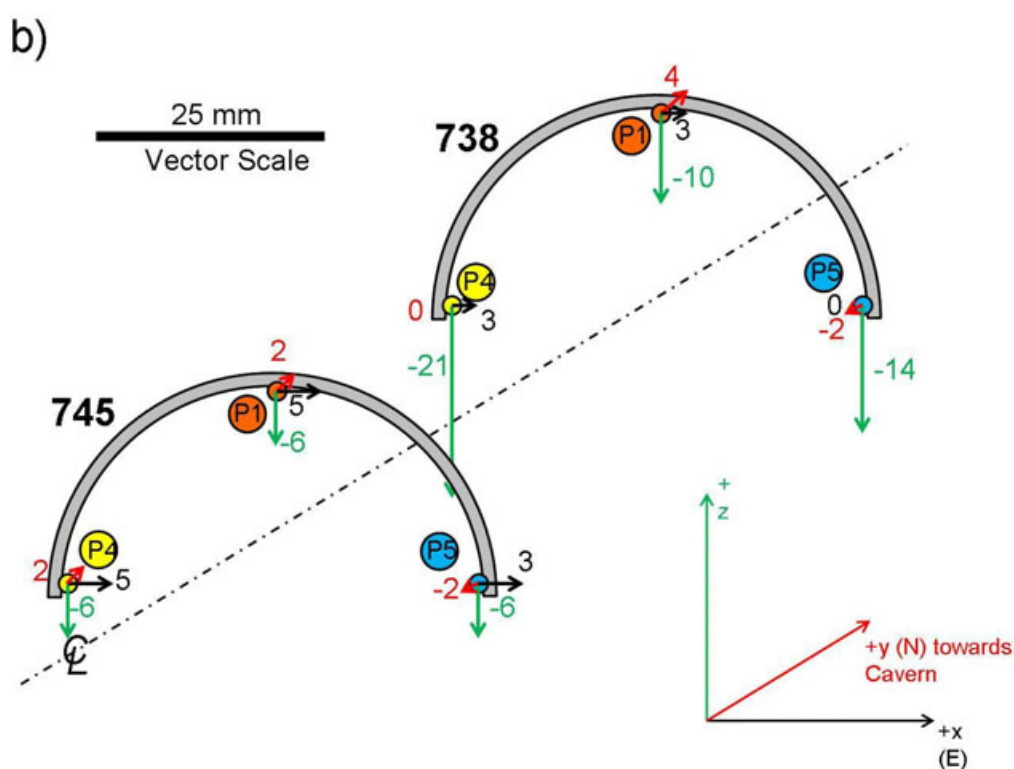
Figure 15 a and b: Displacement monitoring results for sections at Ch. 738 and 745 for a period of 27 days in early 2013 (Feb 23 until March 22, 2013). The results indicate differential settlements between the two sections as well as differential settlements within the section at Ch. 738.
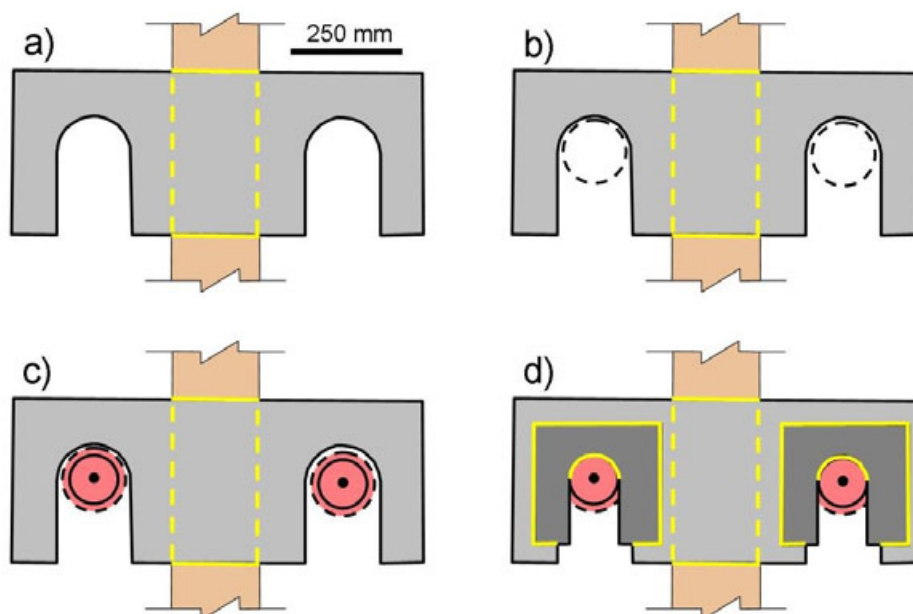
Figure 16: Construction principle for fixing the micro-pile steel tubes onto the steel sets leading to immediate mobilisation of the piles (frontal view): a) A steel plate (940 mm x 370 mm x 20 mm) is welded onto the inner rib. U-shaped openings "upside down" are cut into the plate; the yellow lines represent welded seams. b) Holes are drilled for the piles (into the drawing plane and downward). c) Holes are filled with grout (red) and the micro-piles with a centralized 26 mm steel rebar are inserted. d) Small steel plates of 20 mm thickness with "upside down" U shaped openings are welded onto the larger plate and connected to the steel tube (yellow lines are welding seams).
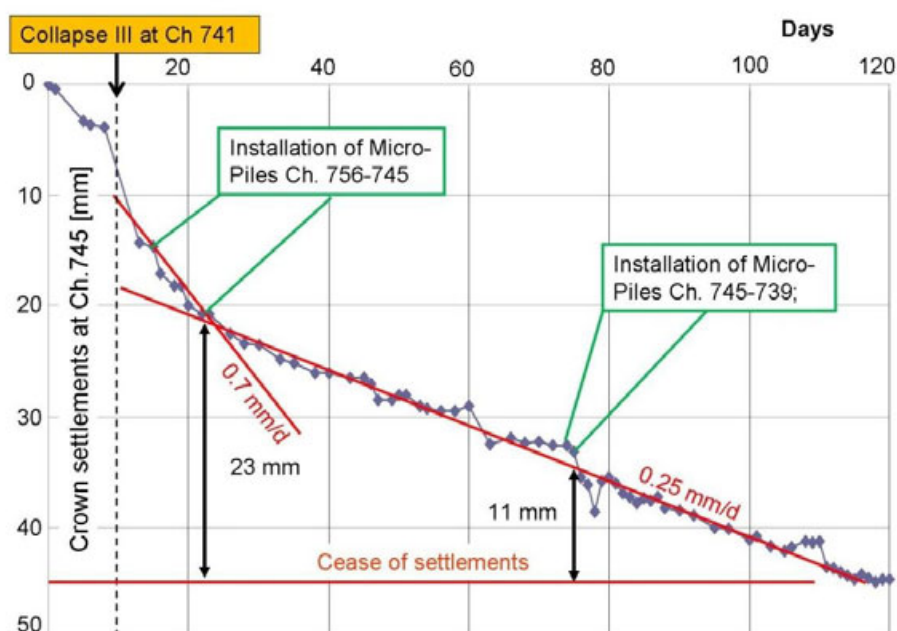
Figure 17: Results of monitoring the crown settlements at Ch. 745 for the period Dec 07, 2012 until April 05, 2013. After the collapse at Ch. 741 the micro-piles were soon installed at Ch. 756 to Ch. 745 and settlements continued. It took 23 mm and 11 mm of settlements, respectively, after the piles were installed to stabilise the tunnel (= cease of settlements).

6.4 Tunnelling out of the Fault Core into better Ground

The anticipated ground ahead of the face (Ch. 741 to Ch. 724) consisted of

- Soft matrix with few small andesite blocks and completely saturated soil (= mud)
- Few strong marble blocks ($\sigma_c \gg 150$ MPa) with a diameter of up to 2 m (Ch. 735 to Ch. 724)
- Water in distinct flow paths
- Light-weight concrete and grout
- Unexpected cavities of unknown volume and location

Hence, all necessary support and auxiliary measures were put in place and the tunnel advanced at low rate.

Figure 18: Canopy tube grouting at Ch.735 after pneumatic (dry) drilling and tube installation. The photograph shows the release of liquefied *in-situ* mud of the brownish-blackish matrix material from the holes, which is flowing down the face.

Figure 19: The geological conditions got rapidly better once the damage zone was reached. Fractured andesite and lenses or bands of clayey-silty soil at Ch. 722 are exhibited in the tunnel face. The lenses of soil are marked with dashed yellow lines. Some of the lenses were connected with long shear fractures (dashed white lines).

The material was at some locations so soft that it was flowing into the tunnel when the face was opened or during drilling of holes for canopy tubes (Figure 18). Surprisingly, out of the 40 m^3 of light-weight concrete and 30 tons of cement pumped into the face at Ch. 741, only a few cubic metres were found in the mucked material.

As shotcrete shell settlements and squeezing were still ongoing extreme care was taken. At one location one could visually observe opening of radial cracks in the face. The situation was controlled by immediately placing a stabilising buttress/ramp of rock fill against the face and spraying additional 250 mm SFR 40 onto the face, starting from the crown perimeter and continuing downward.

Simultaneously with the cease of the rib settlements (Figure 17) the last canopy tube set in the fault core was installed at Ch. 729. These canopy tubes reached into better ground (= damage zone) and squeezing stopped promptly. From Chainage 724 onward the ground conditions improved rapidly (Figure 19).

Break-through of the top heading of this tunnel was in mid July 2013 and it was in schedule of the project. Finally it is noted that despite the three collapses and frequent and unavoidable very dangerous working conditions at the face and in the tunnel no one was injured and no equipment was lost in this operation.

7. FINAL REMARKS

The top heading of a 9.7 m excavation diameter tunnel has been driven successfully through a 40 m wide core of a major fault at 100 m overburden thickness. The material consisted predominantly of soft soil and water was encountered leading to squeezing and flowing ground conditions. This required modification of the initially designed support and auxiliary measures.

The geology of the fault is considered to be reasonably well understood and characterised, but there are many open geological questions. These inquiries refer to the genesis of the fault, the materials in the fault (e.g. the origin of the marble blocks) and several other geological issues.

The adjustment of the measures to deal with the prevailing ground conditions was essentially based upon "engineering and experienced-based judgement". The approach selected by the authorised engineer in charge avoided lengthy academic discussions, but crucial decisions were made pragmatically and promptly at the tunnel face, and they were instantly directed.

This case study is contributed due to its high relevancy to the subject of the workshop. It is envisaged to publish this data as part of a more comprehensive paper that will include reference to and acknowledgement of all participatory stakeholders.

References

[1] Fasching, F. & Vanek, R. 2011. Engineering geological characterization of faults. *Geomechanics and Tunnelling* 4 (3), pp. 181-194, Berlin: Ernst & Sohn.

[2] Seidenfuss, T. 2006. Collapses in Tunnelling. Master Thesis, Technical College Stuttgart, Stuttgart.

[3] Cassani, G. 2013. Excavation of tunnels in structurally complex formations. *Geomechanics and Tunnelling* 6 (3), pp. 197-214, Berlin: Ernst & Sohn.

Author

Ulrich Glawe
PhD. Eng Geol.
MSc. Eng Rock Mech., DIC.,
MSc. Eng Geol.
enggeoconsult@googlemail.com
LinkedIn: Ulrich Glawe

A Fault Zone Management for Deep Seated Tunnels

U. Burger [a], T. Marcher [b], E. Saurer [b] & L. Soldo [c]

[a] *Galleria di Base del Brennero · Brenner Basistunnel BBT SE, Innsbruck, Austria*

[b] *ILF Consulting Engineers Ltd., Rum/Innsbruck, Austria*

[c] *GEODATA Engineering S.p.A., Milan, Italy*

1. INTRODUCTION

Geological uncertainties and the ensuing risks in the construction of long tunnels at great depth has been described in the ITA Report no. 4 - Long tunnels at great depth (ITA) [1]: *".... the deeper the tunnel, the larger the uncertainties; the higher the probability of encountering adverse or unforeseen conditions for tunnelling, the greater the effort and the cost for site investigations to reduce the uncertainties"*.

Among the identified hazard sources, faults play a dominant role, due to their squeezing potential, swelling and creep, possible inflow of water (and/or gases) and debris, or eventual displacements along active shear zones.

Tunnelling through fault zones may therefore lead to critical events for both the construction process and the safety of the personnel. In order to minimise the risk, to be prepared in the case of an event or to overcome fault zones efficiently, a Fault Zone Management Plan has been developed. This Fault Zone Management Plan provides a systematic process developed for the cross-border BBT (Brenner Base Tunnel) railway tunnel at great depth between Italy and Austria (Bergmeister [2]).

Information from other base tunnels, the existing BBT geomechanical project and the knowledge from currently driven BBT exploratory and main tunnels will be taken into account in order to optimise the fault zone management process.

2. SPECIFICS FOR A TUNNEL AT GREAT DEPTH

2.1. General

Examining the design projects of tunnels at great depth, the experience gained from the first BBT exploration tunnels crossing different fault zones and from international tunnel projects served to define several specifics for tunnels at great depth. These specifics have to be considered in the fault zone management plan.

Experience in the BBT project include the following:

- Perpendicular main fault in granite crossed by the Aica-Mules exploration tunnel with a instationary inflow of 160 l/s (Perello et al. [3]).
- A fault zone in granite striking sharply to the tunnel axis of the Aica-Mules exploration tunnel: due to the deformation a four month stop of TBM followed (Barla et al. [4]).
- A fault zone striking perpendicular to the tunnel axis of the shallow tunnel "Saxen": the tunnel crossed a principal nappe fault with approx. 20 l/s instationary inflow.
- Main fault zones in the phyllite, striking parallel to the exploration tunnel Innsbruck-Ahrental and flat lying fault zones as crossed by the access tunnel Ahrental with approximately 15 l/s instationary inflow.

2.2. Specifics for tunnels at great depth derived from design projects and experiences in fault zone crossing

Specifics for tunnels at great depth, which have to be considered in the Fault Zone Management Plan:

Regional character of tunnel projects at great depth:

- Due to the depth of the tunnels, the involved volume of the rock mass is large; this means that regional knowledge of the geology and hydrogeology is required.
- Long tunnels at great depth usually cross multiple tectonic units, therefore tunnels at great depth usually cross regional fault zone systems. Additional literature on this topic see e.g. Damiano et al. [8] and Eusebio et al. [9].
- Due to the regional character of the fault zone systems, similar faults may be crossed several times and even by different lots (e.g. NE-SW and N-S striking faults in the BBT project).
- Events may have a regional impact, larger than the actual construction lot limits.

Complex shear zones:

- Deformation along shear zones leads to the characteristics of the rock mass, including the fabrics and mineral assemblages.
- Major shear zones that cross the crust down into the upper mantle show both brittle and ductile sectors. Brittle fault related rock masses, such as breccias or gouges, are obviously related to most of the critical conditions for tunnels, both during excavation and operation.

Complex project:

- Tunnels at great depth have more construction lots.
- Tunnels at great depth have huge project teams, often situated in different places and even in different nations.

2.3. Risk management

The Risk Management paper published by the International Tunnelling Association (ITA) [5] is widely considered as a guideline. The AFTES Recommendations [6] follows this conceptual approach.

The insurance and re-insurance groups are very actively promoting the use of Risk Management at all stages of a project in order to minimize insurance losses. An International Code of Practice, (german version: Richtlinien zum Risikomanagement von Tunnelprojekten) which follows the ITA guidelines closely, has been published by the International Tunnelling Insurance Group (ITIG) [7].

In simple terms, the risk management approach consists in identifying and listing the potential hazards associated with the tunnelling activities, assigning a probability of occurrence to each hazard, and allocating an index of severity to the consequence. The next steps involves a definition of the measures to reduce the probability of occurrence of an event and to reduce the severity of the consequence (the so called "mitigation measures").

The analysis process prosecutes reassessing the remaining risk level after the application of the mitigation measures, obtaining an updated risk level, a "residual risk level". This "residual risk level" should be examined for acceptance (and then shared among the parties involved in the project) considering the "global cost" necessary for reducing or completely eliminate the source of risk.

The adoption of a RMP enhances the conceptual framework given by the "observational method" establishing a previously planned, sound and rational, framework for the design changes during construction that finally creates a favourable environment for cost or time savings and avoid unnecessary claims.

The proposed BBT approach for the risk management related with fault zones gives a comprehensive map of actions that shall be followed to avoid accidents together with the necessary countermeasures in presence of unfavourable conditions. But also it introduces a procedure for their continuous updating during construction, based on the registered evidences and feedbacks implementing appropriate amelioration if necessary.

3. FAULT ZONE MANAGEMENT - WORK PROCESS

3.1. Flow chart

The general structure of fault zone management in terms of working steps, necessary decisions and additional input is illustrated in the BBT Fault Zone Management Flow Chart (see Figure 1).
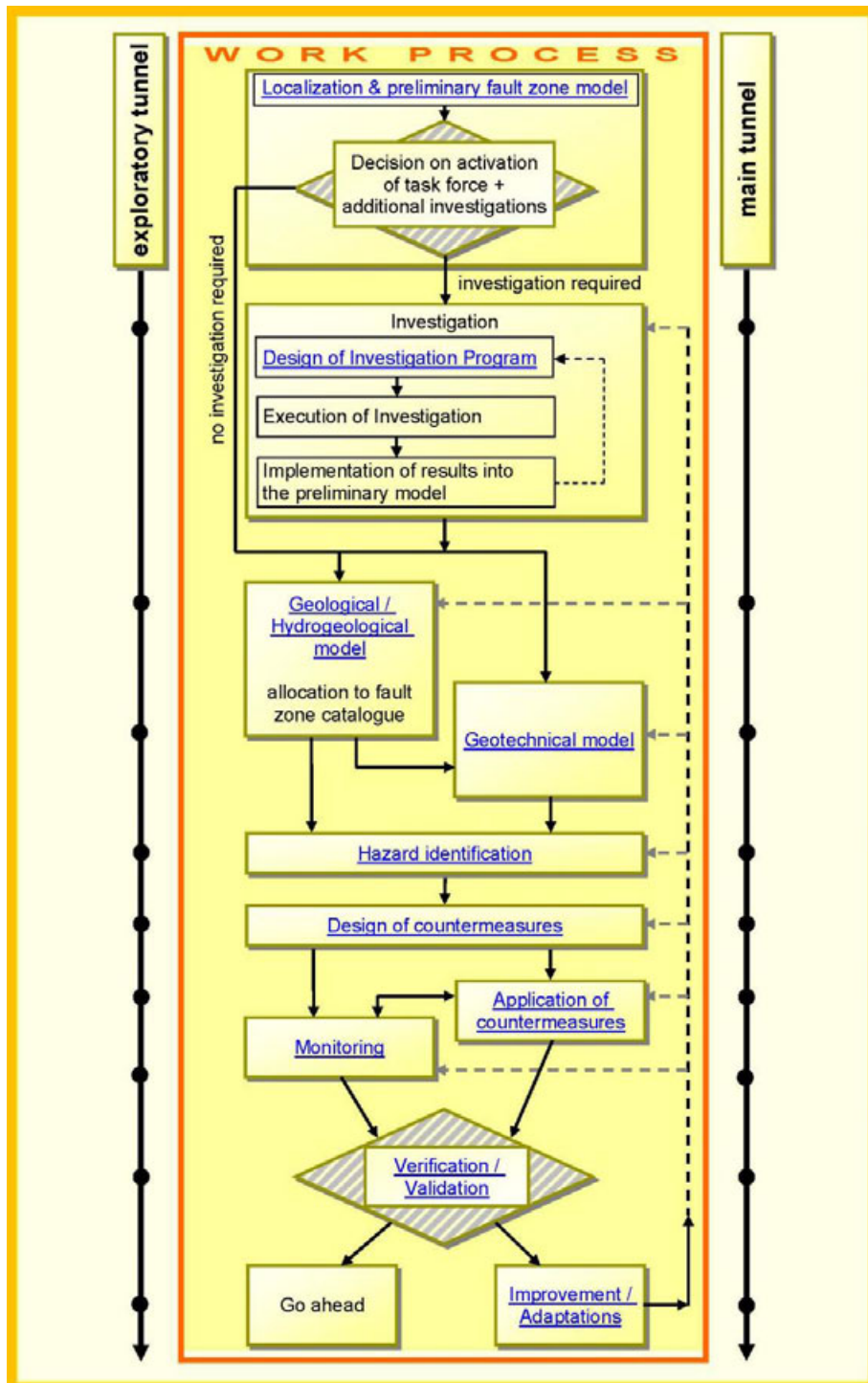
Figure 1: Fault Zone Management Plan – flow chart with main packages of the working process in the case of an event.

As can be seen from the flow chart, the Fault Zone Management Plan can be applied during the construction of the exploratory tunnel (see left black line on the flow chart) and the main tunnels (see right black line on the flowchart). The major steps (boxes) are described in the following chapters.

3.2. Localisation and preliminary fault zone model

On account to the large size of the project team it becomes necessary to provide a first characterization of the fault zone. The first fault zone model has to be distributed to all members of the project. Therefore a simple template has to be filled out by the site geologist, the site geotechnical engineer and the responsible person for the construction lot.

Main contents of the template are:

- Localization of the fault zone in relation to the tunnel
- Preliminary geological fault zone model including graphic illustration
- Decision whether or not the fault is situated in a zone with applicable authority requirements
- Decision about necessary additional investigations from a geological and / or geotechnical point of view
- Definition of the event class (minor, critical, major)
- Activation of required members

3.3. Investigation

If the first characterisation shows that an investigation programme is recommended for preparing the final geological and geotechnical model, a detailed investigation programme including the aim of the investigations has to be drawn up. The purpose of the investigation programme is to characterise in detail the fault zone with respect to:

- Localisation, orientation and geometry
- Material
- Hydraulics

A tool box with investigation methods and the related investigation interests is included in the fault zone management plan.

3.4. Geological, hydrogeological and geotechnical model

The geological / hydrogeological model shall contain at least all parameters included in the template of the fault zone catalogue (see Figure 2).
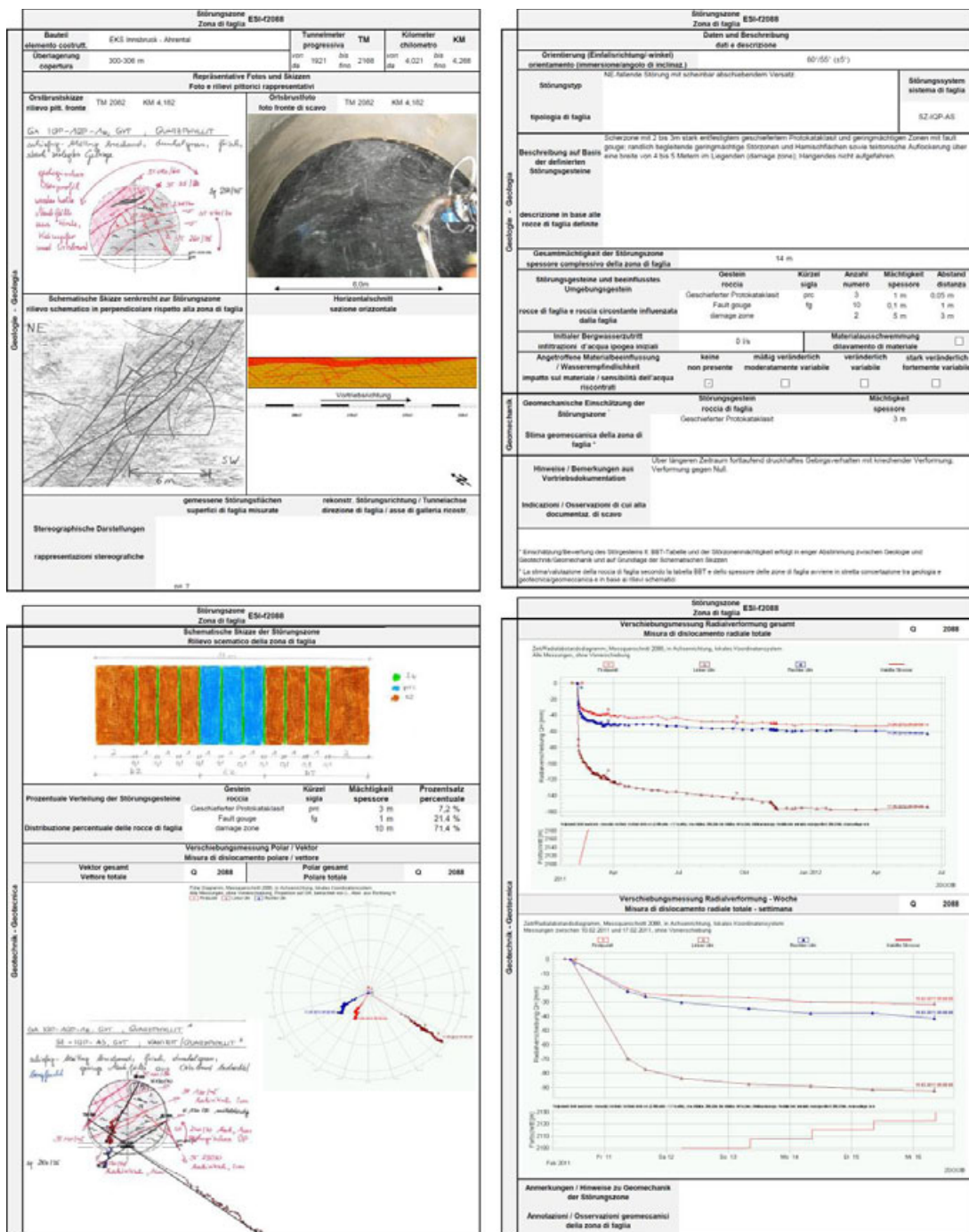
Figure 2: Template for the fault zone characterisation. The upper 2 sheets include a description, illustration and characterisation of the geology and geotechnics of the fault zone. The lower 2 sheets of the template contain information on the deformation behaviour in the case of available data from exploration tunnels. The example shows the information for a fault zone inside the Quartz phyllite striking parallel to the Innsbruck-Ahrental exploration tunnel and dipping east.

3.5. Hazard identification and definition of countermeasures

With the information obtained from the geological/hydrogeological and geotechnical model, the dominant hazard has to be identified and defined (hazard identification).

A table shall be used for the definition of the hazards (type) and their description (in columns). An excerpt of such a table is provided in the tool box (see Table 1). In the column labelled "indicators", parameters which could give an indication of the type of hazard are provided.

Table 1: Definition of possible hazards (excerpt).

Hazard Scenario for both Cyclic and Continuous Excavation		
Type	**Description**	**Indicators**
Tunnel face instability	Due to high primary stresses, favored by interfaces, jointed rock bodies and insufficient strength, blocks may detach themselves from the face thus rendering the face instable (see also instability ahead of TBM).	– Results from investigations ahead of the face provide information on the degree of fracturing – Observation of the unsupported tunnel face
Caving behind the shield / tunnel face	Uncontrolled rock fall of a large volume of rock mass behind the shield due to the retrograde process of a collapse ahead or above the TBM or due to insufficient support measures.	– In particular in areas consisting of brittle tectonic, cohesionless rock and materials similar to loose rock. – Sometimes announced by the occurrence of fissures in shotcrete and audible cracking in the rock mass.
Unacceptable deformations of tunnel	Squeezing rock can lead to inacceptable deformations at the edge of the excavation or of the applied support measures which may cause the need for a reconstruction of the lining or support measures.	– High primary stresses and low strength of the rock mass
Ingress and flooding (water / mud)	Intersecting water-bearing fault zones may cause significant water ingress. If the joints are filled with loose material or if a zone with hydrothermally altered rock is intersected, this may lead to an ingress of mud.	– Results from investigations ahead of the face – Progress of water pressure and of water flow – Progress of rock temperature
Rock bursts	Rock bursts describe a spontaneous process of stress redistribution in compact, brittle rock under high overburden. Rock bursts lead to audible shocks in the rock and to explosive separations at the surface.	– Warning signs: crackling and cracking – Peeling and flaking due to stress
Unacceptable deformation of above-ground surface	Tunneling has a drainage effect on the surrounding rock mass. This causes a change in the effective water pressures in the rock mass which may lead to above-ground surface settlements	– Continuous recording of the water leakages during the excavation facilitates early detection. – Monitoring of above-ground surface settlements.

For the design, a distinction is made between preventive countermeasures and those applicable in the case of the occurrence of an event.

- Preventive countermeasures
- Event-related countermeasures and equipment

A list with fault zone phenomena and proposed countermeasures from experience made during tunnel construction under comparable boundary conditions and corresponding references is given in a tool box (see Table 2).

The definition of possible hazards and preventive countermeasures are based on experience and on literature, e.g. Amberg [10], Bonzanigo et al. [11], Daller et al. [12], Fellner et al. [13], Ferrari et al. [14], Röthlisberger et al. [15], Sausbriber et al. [16], Stadelmann et al. [17], Weh et al. [18], Wildbolz [19], Ziegler [19].

Table 2: Fault zone phenomena and proposed countermeasures (excerpt). Cases A to D are referred to the knowledge of a fault zone: Case A = assumed fault zone; Case B = fault zone localized with investigations ahead of the tunnel; Case C = close to the tunnel lying fault zone localized by interpretation of monitoring data; Case D = intercepted fault zone.

Hazard Scenario for both Conventional and Continuous Excavation		
Type	**Preventative measure (Case A/D)**	**Countermeasures in the case of an event (Case B/C)**
Tunnel face instability	– Visual observation of material flow on conveyor belt – Maintain cutter head under permanent thrust – Limit the number and size of openings in the cutting wheel – Inclined Tunnel face / wedge	– Excavation with reduced thrust – Blasting or manually breaking up of blocks – Enhanced investigation ahead of the face and in case of possible cave-in, see Collapse ahead of TBM.
Caving behind the shield / tunnel face	– Installation of spiles – Provision of support measures – Strengthening of support measures – Drainage drilling – Grouting / injections	– Immediate installation of support – Installation of more support elements if needed – Installation of spiles – Grouting / injections
Unacceptable deformations of tunnel	– Systematic investigation ahead of the face – Strengthening of support elements – installation of provisional runway	– Systematic investigation ahead of the face – Strengthening of support elements – installation of provisional runway
Ingress and flooding (water / mud)	– Monitoring and interpreting water ingress in tunnel – Drilling using a preventer in case of mud – Provision of pumps and tubes – Controlled drainage of the rock in case of clear water – Grouting / injections in case of mud	– Controlled drainage of the rock in case of clear water – Grouting / injections in case of muddy water / mud – In case of ingress of hot water: additionally check tunnel climate

3.6. Application of countermeasures and monitoring

The designed countermeasures are applied in order to overcome the construction difficulties in the fault zone. Main steps are:

- The countermeasures have to be applied according to the design.
- During the application, the behaviour of the fault zone has to be observed and monitored intensively in order to be able to validate the design.
- A report on the application of countermeasures and the excavation has to be prepared (e.g. as-built reports from ÖBA/DL).

4. CONCLUSIONS

The proposed BBT fault zone management plan provides a comprehensive action plan that shall be followed in the case of an event. The plan includes different tool boxes such as proposals for required countermeasures in presence of unfavourable fault zone conditions during the excavation process.

The presence of a permanent team of specialists, specifically working within the framework of the "fault zone management approach", facilitates transferring the continuously identified design and construction "best procedures and solutions" into the subsequent design and tunnel construction packages.

The advantages derived from this ongoing "learning, test, apply and transfer" sequence will provide a wealth of experience to the whole project team.

Experience in the next BBT construction lots may provide the opportunity to validate and verify the action plan and to improve and adapt it.

References

[1] ITA WG 17. 2010. *Long Tunnels at great depth*. `http://www.ita-aites.org/en/wg-committees/committees/itatech/downloads/content/22/working-group-17-long-tunnels-at-great-depth`. (last access 08/2013).

[2] Bergmeister, K. 2011. *Brenner Basistunnel – der Tunnel kommt*. pp. 263, Lana: Tappeiner.

[3] Perello, P., Baietto, A., Burger, U. & Skuk, S. 2013. Excavation of the Aica-Mules pilot tunnel for the Brenner base tunnel: experience gained on water inflows in tunnels in granitic massifs. *Rock Mechanics and Rock Engineering*. In press.

[4] Barla, G., Ceriani, S., Fasanella, M., Lombardi, A., Malucelli, G., Martinotti, G., Oliva, F., Perello, P., Pizzarotti, E.M., Polazzo, F., Rabagliati, U., Skuk, S. & Zurlo, R. 2010. Problemi di stabilità al fronte durante lo scavo del cunicolo esplorativo Aica - Mules della Galleria di base del Brennero. In: Barla, G. & Barla, M., Proc. *XIII ciclo di conferenze di meccanica e ingegneria delle rocce MIR 2010, Torino.*

[5] ITA Working Group No. 2. 2004. Guidelines for tunnelling risk management. *Tunnelling and Underground Space Technology* 19, pp. 217-237.

[6] AFTES Recommendation GT32.R2A1. 2012. Recommendations on the characterisation of geological, hydrogeological and geotechnical uncertainties and risks.

[7] International Tunnelling Insurance Group (ITIG). 2006. Richtlinien zum Risikomanagement von Tunnelprojekten ("*A Code of Practice for Risk Management of Tunnel Works*").

[8] Damiano, A., Venturini, G., Alzate, M., Mancari, G., Dematteis, A., Soldo, L. & Vendramini, M. 2011. The Reference Geological Model for the Corredor Bioceanico Aconcagua project. In: *Congrés International AFTES*: Lyon.

[9] Eusebio, A., Soldo, L., Pelizza, S. & Pettinau, D. 2005. Preliminary geological studies for the design of Mercantour base tunnel. *AFTES Tunnelling for a sustainable Europe*: Chambery.

[10] Amberg, F. 2006. Geologie, Vortriebsmethoden und Bauhilfsmassnahmen in der Multifunktions-stelle Faido. *Geologie und Geotechnik der Basistunnels*, pp. 225-237, Zürich: Löw Hochschulverlag.

[11] Bonzanigo, L. & Oppizzi, P. 2006. Low Angle fault zones and TBM excavation in Bodio section of Gotthard Base Tunnel. *Geologie und Geotechnik der Basistunnels*, pp. 156-184, Zürich: Löw Hochschulverlag.

[12] Daller, J., Atzl, G. & Weigl, J. 2011. The new Semmering base tunnel – tunnel design in the fault zone. *Geomechanics and Tunnelling* 4 (3), pp.237-253, Berlin: Ernst & Sohn.

[13] Fellner, D., Bachmann, M. & Bönsch, W. 2007. DS-TBM over its Limits" / Schwierigkeiten mit Zuckerkörnigem Dolomit beim Bau des Shanggongtunnels in Südwestchina. In: *Internationales Symposium BBT*: Innsbruck.

[14] Ferrari, A., Fabbri, D. & Sidler, M. 2007. Bewältigung von unerwarteten Störzonen beim TBM-Vortrieb im Gotthard-Basistunnel Baulos Bodio. In: *Internationales Symposium BBT*, pp. 56-62: Innsbruck.

[15] Röthlisberger, B., Stadelmann, R. & Wei, Z.Q. 2007. Bewältigung der Herausforderungen im Bauabschnitt Faido des Gotthard Basistunnels. In. *International Symposium BBT*: Innsbruck.

[16] Sausbriber, T. & Brandner, R. 2001. The relevance of brittle fault zones in tunnel construction. Lower Inn Valley Feeder Line North of the Brenner Base Tunnel, Tyrol, Austria. *Mitt. Osterr.Geol. Ges.* 94, pp. 157-172.

[17] Stadelmann, R., Rehbock-Sander, M. & Rausch, M. 2007. Crossing of fault zones in the MFS Faido by using the observational method. *Underground Works under Special Conditions*. Romana, Perucho, Olalla (eds). London: Taylor & Francis.

[18] Weh, M. & Bertholet, F. 2011. TBM advance in the main adit to the Nant de Drance pumped storage power plant. *Geomechanics and Tunnelling* 4 (5), pp. 284-591, Berlin: Ernst & Sohn.

[19] Wildbolz, A. 2006. Befreiung der Tunnelbohrmaschine Gabi II in Amsteg. *Schweizer Baujournal*.

[20] Ziegler, H.-J. 2011. 150 km Vortrieb durch die Alpen – Ingenieurgeologische Erfahrungen. In: *Swiss Tunnel Congress 2011*.

Authors

Mag. MSc. Ulrich Burger
Brenner Basistunnel BBT SE
Amraser Strasse 8
6020 Innsbruck
Austria
ulrich.burger@bbt-se.com

Dipl.-Ing. Dr. Ing. Thomas Marcher
ILF Consulting Engineers Ltd.
Feldkreuzstrasse 3
6063 Rum/Innsbruck
Austria
Thomas.Marcher@ilf.com

Dipl. Bau-Ing. Dr. sc. ETH Erich Saurer
ILF Consulting Engineers Ltd.
Feldkreuzstrasse 3
6063 Rum/Innsbruck
Austria
Erich.Saurer@ilf.com

Geol. MSc Ph.D. Luca Soldo
GEODATA Engineering S.p.A.
Via Leopardi 1
20123 Milan
Italy
lso@geodata.it

Numerical Analysis of Fault Zones - Coming Closer to a Solution

M. Brandtner [a]

[a] *IGT Ziviltechniker GmbH, Salzburg, Austria*

Numerische Modellierung von Störungszonen - Eine Annäherung: In der ÖGG Richtlinie für die geotechnische Planung von Untertagebauten [1] ist ein wichtiger Entwurfsschritt die Überprüfung, ob das ermittelte Systemverhalten mit den Anforderungen übereinstimmt. Für heterogene Bereiche bzw. Störungszonen reichen analytische Methoden wie z.B. das Kennlinienverfahren bzw. numerische 2D Modelle wegen der unzutreffenden Randbedingungen bezüglich räumlichen Spannungszustand und Porenwasserdruck im Falle eines Bergwassers nicht mehr aus. In manchen Fällen sind axialsymmetrische Modelle noch vertretbar. Die Inkaufnahme etwaiger Ungenauigkeit muss in jedem Fall gesondert beurteilt werden. Bezüglich der Modellierung des primären Spannungszustandes und des Porenwasserdrucks können diese Modelle in den meisten Fällen eine 3D Anylyse nicht ersetzen.

According to the Guidline for the Geotechnical Design of Underground Structures published by the Austrian Society for Geomechanics [1], the assessment of the system behaviour is an essential step in the design process. For heterogeneous ground conditions and fault zones methods with closed solutions based on the Ground Reaction Curve (GRC) and numerical 2D analyses are inapplicable due to unrealistic boundary conditions concerning the stress state and pore water pressure in case of groundwater. In rare cases axisymmetric models can do the job. The acceptance of this mismatch has to be judged in each individual case seperately. However in terms of initial stress conditions and pore water pressure these models cannnot fully replace 3D models.

1. CHARACTERISTICS OF THE 3D MODEL

In most cases the normal vector of the fault zones orientation plane is not parallel to the tunnel axis and therefore an axisymmetric model cannot reflect the real situation. For the sake of reduced model size a symmetry plane can be utilized if the fault zone strikes perpendicular to the tunnel axis and the initial stress state is homogeneous (Figure 1), a full 3D model has to be chosen otherwise.
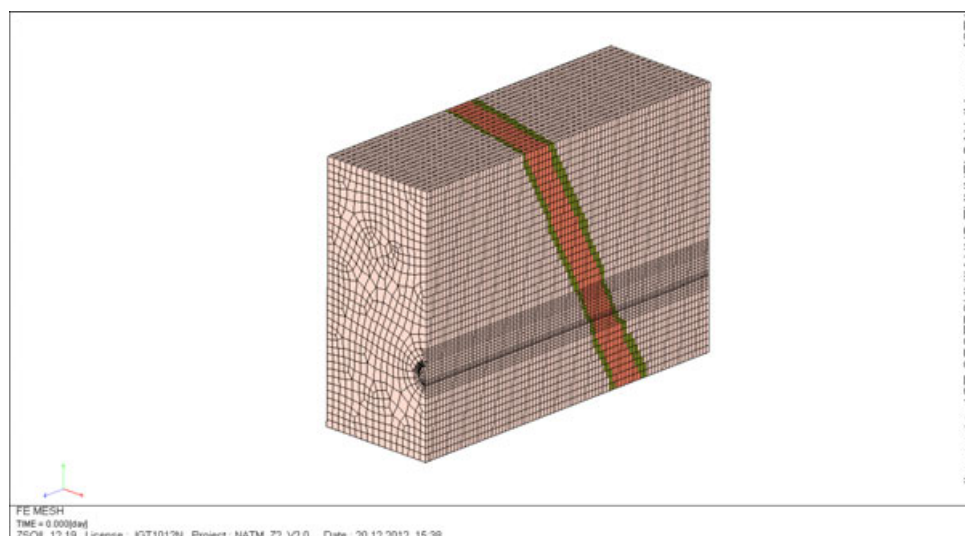
Figure 1: Typical 3D model for fault zone with transition zones adjacent to unfaulted regions.

The determination of suitable model boundaries is essential. One should bear in mind that each plane on the boundary is a symmetry plane anyway and the influence to the region where the tunnel is driven through the fault zone should not be influenced by model boundaries.

2. MATERIAL MODEL FOR ROCK MASS

Since the area of interest is rather in the zone of the intersection between tunnel and fault zone, the Mohr Coulomb criterion in unfaulted regions is sufficient. This might have some disadvantages concerning the undrained behaviour of the rock mass, but in order to reduce computational costs it can be accepted. In the faulted region an advanced model has to be employed for several reasons:

- Different stiffness for unloading and reloading (excavation)
- Realistic stress path in combination with pore water pressure (strength)
- Double hardening constitutive model (shear and compression hardening)
- Stress dependent stiffness (yield surface expands with increase of plastic straining)

The Hardening Soil Model was originally developed for soils, but for cataclastic rocks it seems to be suitable as well.
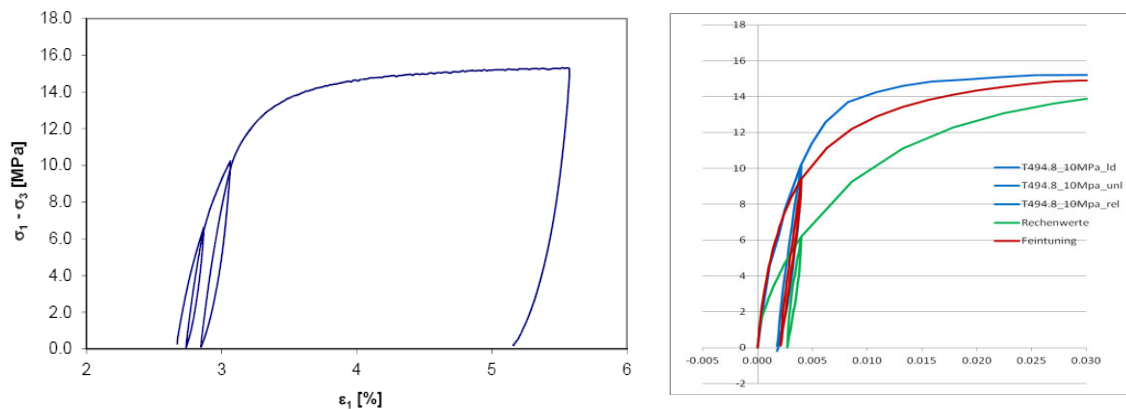
Figure 2: Determination of parameters from laboratory tests.

The comparison of stress strain relations gained from laboratory tests (Figure 2 left side) with calibrated parameters for the constitutive model (Figure 2 right side) shows a good compliance and justifies the deployment of the HSS-Model. The consideration of groundwater needs a special treatment but different to soil mechanics. The thesis by Wehnert [2] gives an excellent overview concerning drained vs. undrained analysis, but deals only with soils, where the bulk modulus of the skeleton material (Ks) is much higher than that one of bulk material itself (Ks >> K). In soil mechanics it may be accepted that saturated ground is assumed to be incompressible, but deep rock tunnels are exposed to a higher stress level. Water has a bulk modulus of approx. 2.3 GPa and cannot be treated as incompressible anymore. A starting point to find an adequate theoretical basis for the treatment of water under such conditions is the theory of porous rocks. It should be emphasized that the debates on the applicability of the principle of effective stresses for rocks seem to be a never ending story, but it is accepted that Terzaghi's approach has to be adapted for a rock mass [3] [4]. A different approach, which was applied successfully in several pressure tunnels, is provided by Innerhofer [5]. In addition attention should be paid to the contact zone between fault and unfaulted rock mass. Whilst the material in the fault zone may have very low permeability, the adjacent rock mass can even be nearly dry. In [6] some situations are sketched.

'Open' contact;
Equal pore pressure p on both sides;
Possible difference in porosity Φ causes
'jump' in skeletal stress:

$$| \sigma^S{}_{(1)} | - | \sigma^S{}_{(2)} | = (\Phi(2) - \Phi(1)) \cdot p$$

Sealed contact;
Possible difference in pore pressure
causes 'jump' in effective normal stress:

$$| \sigma'_{(1)} | - | \sigma'_{(2)} | = p(2) - p(1)$$

Low-permeability interlayer;
Possible difference in pore pressure causes flow
and 'jump' in effective normal stress:

$$| \sigma'_{(1)} | - | \sigma'_{(2)} | = p(2) - p(1)$$
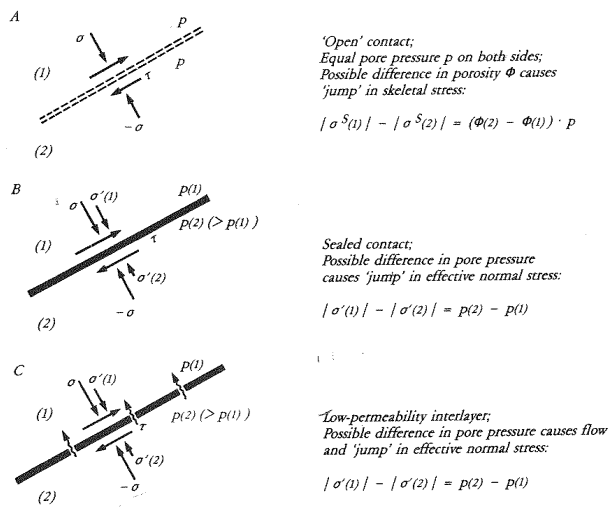
Figure 3: Contact between porous rocks according to [6].

3. STRUCTURAL ELEMENTS

The shotcrete lining in reality behaves highly non linear, but for the sake of simplicity on this scale of models a pragmatic approach has been chosen. An average stiffness of 5 GPa regardless of age or time dependent creep effects is accounted for the support resistance of the primary lining, which is modelled with linear shell elements. Rock bolts have been completely omitted. The resistance is taken into account by increase of the cohesion. Special attention was paid to the effects of damping elements. The dissipation of displacement energy results from LSC elements (lining stress controllers) with a given stress strain relation. These elements are modelled with nonlinear beams showing a characteristic working curve depicted in the diagram below.
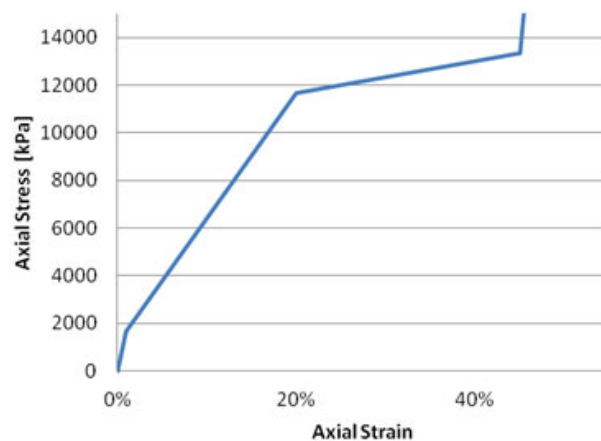
Figure 4: Working curve for damping elements.

After a shortening of approx. 50% of the total element length (0.4m) absorption of energy is no longer possible and the axial load is transferred directly to the primary lining.

4. RESULTS

If dealing with the development of pore pressure the analysis has to be made in real time scale and post processing the results is another challenging task. One should bear in mind that the job is not done when the computation is finished, most of the times the effort for looking through and visualizing the results is underestimated. Exemplarily some results are show in the following figures.
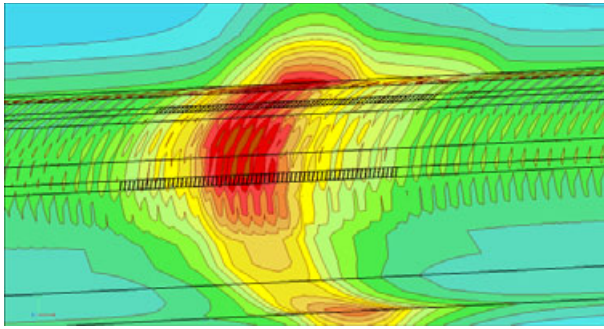
Figure 5: Absolute displacements after the tunnel has been driven through the fault zone.
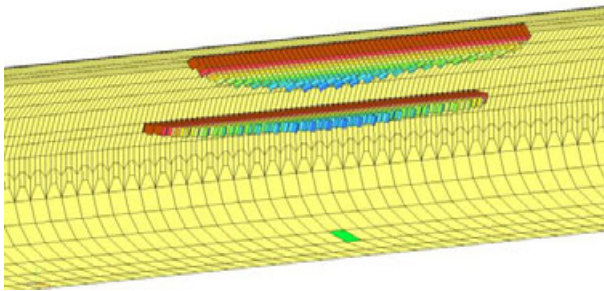
Figure 6: Axial forces in the damping elements (Lining Stress Controllers).

The elapsed computation time for typical models containing features described above is between one day and half a week. It is obvious that performing parameter studies ends up in excessive computational costs. However we should keep in mind that such analyses have the objective to assess the system behaviour and cannot be seen as a detailed stress analysis.

References

[1]   Austrian Society for Geomechanics. 2010. *Guideline for the Geotechnical Design of Underground Structures with Conventional Excavation.*

[2]   Wehnert, M. 2006. Ein Beitrag Zur Drainierten Und Undrainierten Analyse in der Geotechnik. *Mitt. Inst. für Geotechnik*.

[3]   Nur, A. & Byerlee, J.D. 1971. An Exact Effective Stress Law for Elastic Deformation of Rock with Fluids. *Journal of Geophysical Research* Vol. 76, pp. 6414–6419.

[4]   De Boer, R. & Lade, P.V. 1997. The Concept of Effective Stress for Soil, Concrete and Rock. *Géotechnique* 47, pp. 61–78.

[5]   Innerhofer, G. 2008. Action of Force on Rock Mass by Crack Water Pressure. *Geomechanik und Tunnelbau* Vol. 1, pp. 583–589.

[6]   Mandl, G. 1988. *Mechanics of Tectonic Faulting.* Amsterdam: Elsevier.

Author

Ing. Markus Brandtner
IGT Ziviltechniker GmbH
Mauracherstraße 9
5020 Salzburg
Austria
m.brandtner@igt-engineering.com

Design of Ductile Supports

W. Schubert [a], N. Radončić [b]

[a] *Graz University of Technology, Institute for Rock Mechanics and Tunnelling, Graz, Austria*

[b] *Geoconsult ZT GmbH, GTU Koralmtunnel, Wals bei Salzburg, Austria*

1. INTRODUCTION

The combination of high stresses and poor ground quality frequently leads to large displacements, unsustainable by conventional tunnel supports. Ideas for ductile supports have been around for many decades, but systematic application has started on a larger scale only in the nineteen nineties. Over the past decades, various ductile elements have been proposed and sometimes successfully applied. The successful applications showed to increase safety, as well as considerably reduce displacements. While most systems fulfilled their role as "deforming element", costs and operational feasibility, as well as their interaction with shotcrete and deforming ground are seldom discussed. This paper focuses on important issues in design and implementation of ductile elements in combination with shotcrete linings.

2. REQUIREMENTS

The requirements on the ductile support are straightforward and based on common imperatives: structural safety and operability and cost-oriented considerations. They can be summarised as follows:

1. The overall structural stability, safety and the minimal clearance profile must be granted in all situations by the applied support system.

2. Conventional materials and construction methods should be used, and the applied concept should not be different from the other support concepts applied in the tunnel.

3. The load-displacement relationship of the entire support system, and therefore of the yielding elements, should be easily adaptable – in accordance to the observed system behaviour.

4. The support resistance should be maximized, in order to reduce the displacement magnitude fluctuations in heterogeneous ground and reduce ground disintegration in the vicinity of the excavation. In addition, the required overcut of the profile is minimised.

5. The load-displacement relationship of the yielding elements should be adjusted to the time-dependent shotcrete strength development and the overall displacement characteristic of the ground. Generally said, low initial stiffness (in order to prevent overstressing of the young shotcrete) followed by a smooth and steady ductile region are favourable. The load-displacement relationship should not feature strong oscillations, in order to prevent the entire system "jumping" into the next "valley" and producing avoidable fluctuations in final displacements (Figure 1).
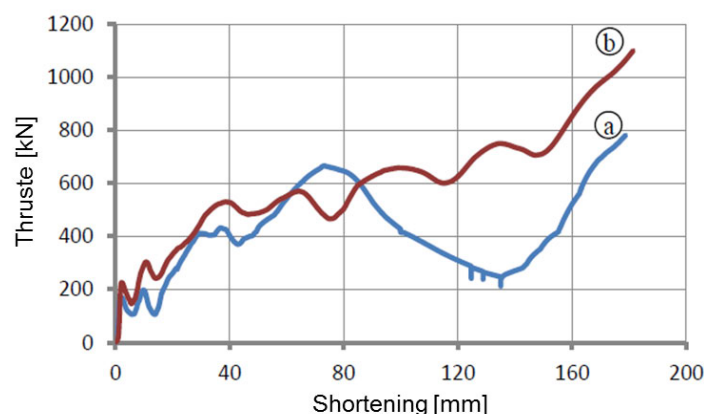
Figure 1. Unfavourably oscillating (a) and favourable (b) load-displacement relationship, with regard to the overall support resistance and final displacement prediction.

3. BASIC EFFECT OF DUCTILE LININGS

The application of open deformation gaps or installation of ductile elements allow the otherwise too stiff shotcrete lining to deform in such degree that an equilibrium with the relaxing ground can be attained. As the experience has proven time and again, the usual approach, common for conventional structural analysis, of increasing the capacity of the structure until the loads can be sustained, leads to additional stiffness increase and attraction of additional loads. Simply put: the effort of devising a support which would be able to withstand the ground pressure is a race which is either impossible to win or very costly.

In case open gaps are used, the contribution of the lining is very limited and support mobilisation of the lining is governed by shear bond between the ground and the shotcrete and shear resistance of the rock bolts. Hence, system behaviour is very sensitive to changes in the ground quality, and the displacement field of the tunnel support can strongly change within a few meters of advance. This leads to additional stress-redistribution processes triggered in the ground (since stiffer rock mass portions attract additional stresses and are prone to brittle failure), and lining cracks due to incompatible displacement differences between two adjacent areas. Additional disadvantages are the occurrence of long-lasting displacements (since the support pressure is low) and presence of a kinematically free lining system in case of sudden failure (Schubert & Riedmüller 1995).

The application of yielding elements (or open gaps) results in certain kinematical peculiarities which have to be accounted for. The "absorption" of tangential strains by the yielding elements inevitably results in relative displacements (slip) developing between the shotcrete and the ground, and additional shear loading of the installed rock bolts. The occurring slip and its consequences have a significant influence on the axial forces in shotcrete segments and the overall support mobilisation. In addition, if only the top heading is excavated, the axial loading of the shotcrete is usually unsustainable by the ground beneath the lining feet, and they penetrate into the ground considerably. This leads to the generation of two additional "yielding elements" and translational movement of the entire support (Figure 2).
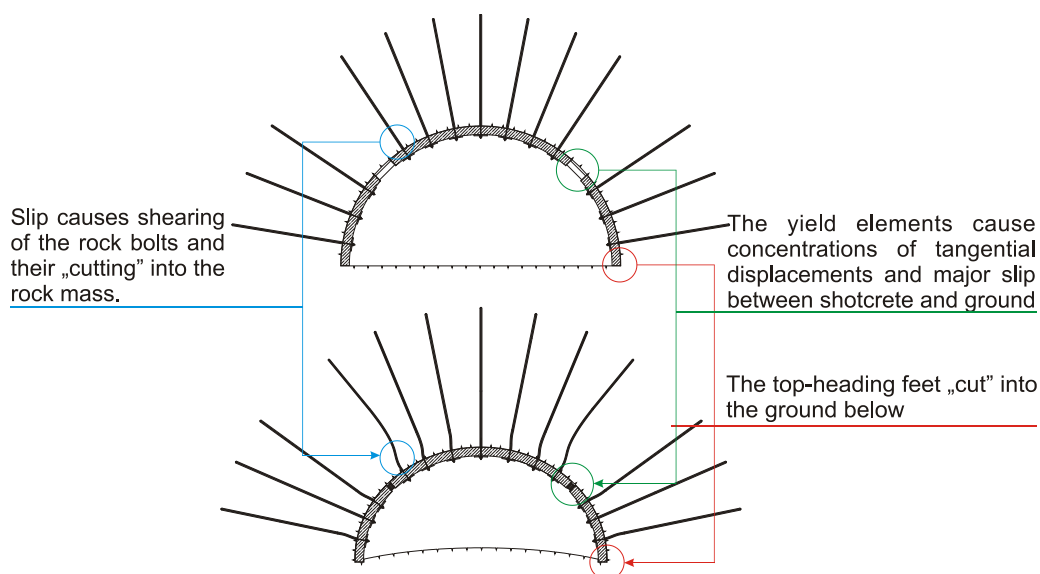
Figure 2. Large deformations and their influence on the lining incorporating yielding elements; Top: undeformed system state; Bottom: deformed system state.

4. DESIGN

4.1. Boundaries of conventional support

Many criteria for fast determining whether a ductile support must be used or not have been published over the years, some based on the idea of critical radial strain (Hoek 2001, Aydan et al. 1993) or on the definition of a critical ground classification number (Singh et al. 1992, Goel et al. 1995). However, all of the proposed methods fail to recognise that the ground forms an integral part of the ground-support system, and that the yielding support is simply required when the conventional one is not able to economically and safely withstand the loads. Simply put: the application boundaries for a ductile support are defined by the capacity of conventional support methods being applied at the time, and should be changed in accordance to the progress of material technology.

Radoncic (2011) conducted a Monte-Carlo simulation with this "inverse" reasoning in mind: first the maximum capacity of different conventional support concepts (immediate ring closure, top heading, top heading with temporary invert) has been determined, and then the ability of the chosen concept to attain equilibrium with the randomly chosen set of ground parameters has been checked. The results show a clear trend, featuring a clear boundary defined by overburden and radial strain, calculated for the case of unsupported ground (Figure 3).
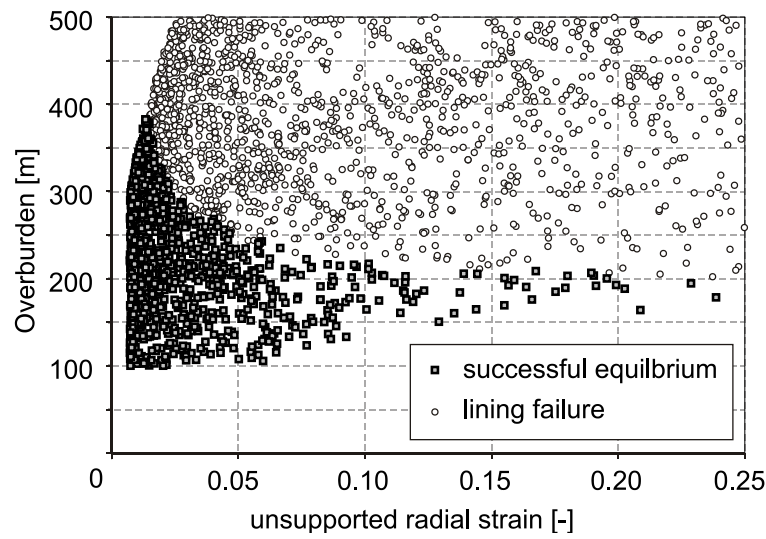
Figure 3. Results of Monte-Carlo sampling, showing a clear boundary between lining failure and equilibirum.

The systematic analysis allows the drawing of the pre-design chart depicted in Figure 4 and the definition of the relationship (Equation 1).
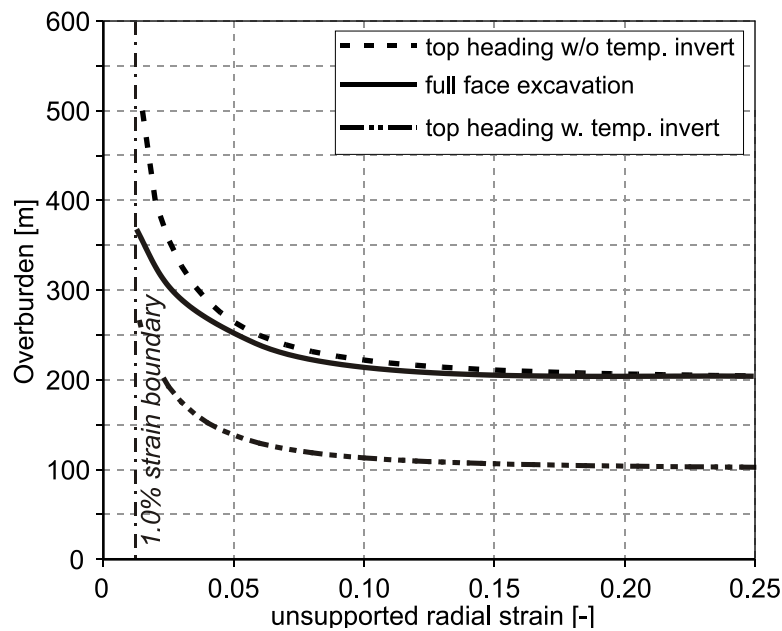
Figure 4. Boundaries of support failure for a friction angle of 15°.

The relationship includes friction angle as an parameter since the study has shown that the boundaries move "up" – the ability of the support to attain an equilibrium with the ground rises with the increasing friction angle.

$$H_{crit} = (H_0 + H^* \tan\varphi) - 75 \cdot \left[1 - \left(\frac{X}{X + \varepsilon - \varepsilon_0} \right)^2 \right]$$

Equation 1

The corresponding parameters for different support concepts are given in Table 1.

Table 1. Parameters defining the critical overburden H_{crit}.

	X [-]	ε_0 [-]	H_0 [m]	H^* [m]
Full-face excavation	0.062	0.035	100	680
Top heading	0.062	0.045	100	680
Top heading w. Invert	0.030	0.030	75	375

4.2. Pre-design

Radoncic et al. (2009) have presented a method based on extensions to the convergence confinement method, allowing incorporation of the influences of the ground conditions, advance rate, time-dependant shotcrete strength and overall support layout into the analysis.
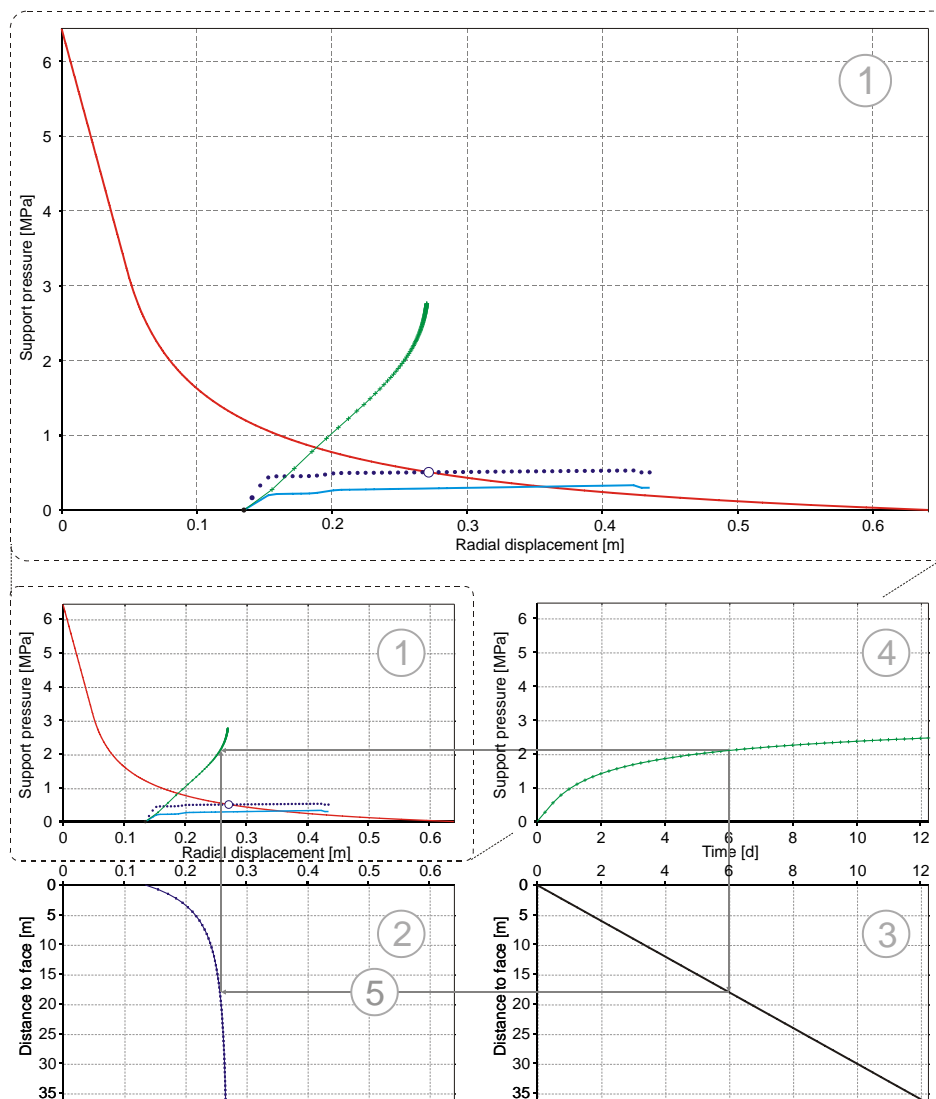
Figure 5. **Determination of the shotcrete thrust capacity (blue line: maximal mobilised shotcrete thrust dotted line: total support resistance, green line: available shotcrete thrust capacity).**

Radoncic (2011) added additional improvements, incorporating the influence of shear bond between ground and shotcrete and dowel action of the rock bolts (Figure 6).
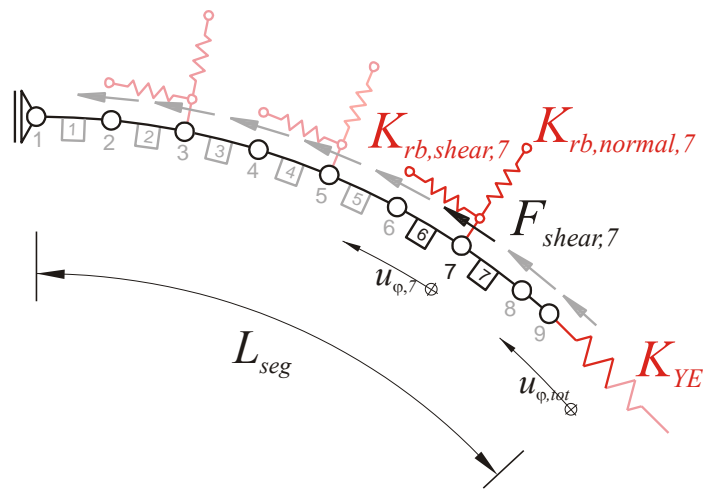
Figure 6. Applied discretisation of a shotcrete half-segment, with rock bolts acting like non-linear springs (both with regard to axial deformation and to tangential shear).

The applied discretisation scheme allows the determination of the shotcrete thrust distribution over the entire length of the shotcrete segment (Figure 7), while still being directly combined with thedesign graph presented in Figure 5.
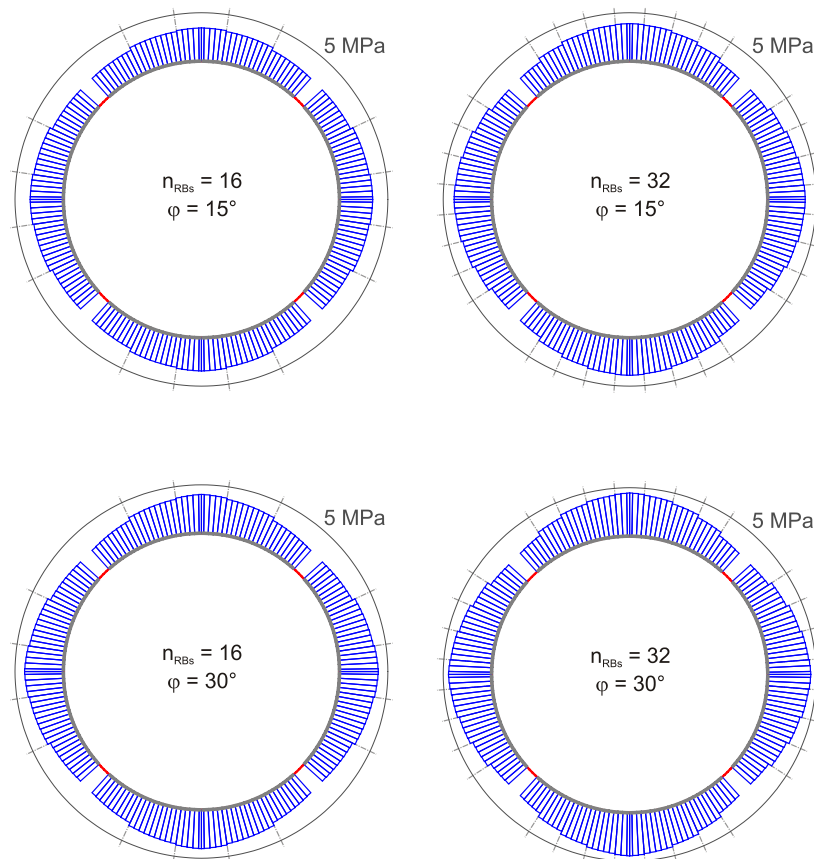
Figure 7. Influence of rock bolting density and friction angle at the rock mass lining contact surface on the thrust distribution in shotcrete (UCS equals 1 MPa, Yielding element thrust of 900 kN, tunnel radius of 5 meters).

4.3. Design and fine tuning

The internal anisotropy of the tectonic faults causes a pronounced mechanical anisotropy. This has a strong effect on the system behaviour, influencing the final displacements, displacement development and the overall contrast in the radial displacements. The internal shear bands act as natural planes of movement and suppress the re-distribution of shear stresses. Hence, in case of an advance perpendicular to the fault orientation, the displacement field tends to be homogenous and the displacements tend to be low, however strong initial displacements can be expected. In the opposite case (parallel advance), the highest radial displacements occur perpendicularly to the internal structure, and the displacement development is long-lasting. Such effects should be accounted for in the final stage, and yielding element layouts should be prepared for the most likely cases.

4.4. Construction and monitoring

It indisputable that in case tunnelling through highly heterogeneous faults, the observational approach represents the only feasible design method. Hence, the design has to be constantly updated – based on the observed system behaviour. In this case, the issues of required over-excavation and shotcrete utilisation / support resistance represent the key issues. Due to already discussed kinematic peculiarities, the shotcrete utilisation and section forces cannot be back-calculated from the absolute displacement monitoring, since the tangential displacements and strains of the shotcrete shell (at the yielding elements position) feature a discontinuity of an unknown magnitude. Hence, it is strongly recommended to install additional displacement monitoring points at both sides of the yielding elements, allowing direct and straightforward determination of the support resistance. Strain gauges can used for gaining additional information, allowing direct determination of the section forces in shotcrete and supplementing the observations with absolute displacement monitoring.

5. CONCLUSIONS

Following recommendations and conclusions are deemed generally applicable in case of designing and constructing a tunnel with integrated yielding elements:

1. Although appearing as a trivial conclusion, the roles of proper investigation, ground characterisation and ground behaviour determination cannot be overstressed. Both the investigation programme and the lab test programme have to be custom-tailored to the envisioned analysis means and identified failure mechanism. This renders the design, especially in the early project stages, an iterative process: after all possible mechanisms of stress re-distribution and displacement development have been identified; additional effort has to be invested into determining reliable parameters for the best-suited calculation model.

2. Proper determination of ground behaviour is an excellent starting point for the basic support design: after the influences of structure, rheological behaviour and water have been determined, the basic layout of lining should follow the anticipated deformation pattern. The layout of the yielding elements within the cross section does NOT have to be symmetrical, but to orientate itself on the kinematics of a ductile lining subjected to unsymmetrical deformation field.

3. The yielding element load-displacement characteristic must comply to the time-dependent development of shotcrete capacity and the displacement development characteristic of the system. Displacement monitoring (especially if including the respective element shortening) should be frequently and systematically conducted and evaluated by competent personnel. A great room for optimisation with regard to overexcavation dimensions, associated support measures and risk minimization is present when the measurement data are evaluated on time and the right conclusions are drawn.

4. The chosen excavation sequence has to closely follow the envisioned support mobilisation. Advancing a top heading with yielding elements of extreme capacity without taking care about the proper abutment of the top heading feet is basically meaningless. The systematic rock bolting, temporary invert installation and/or elephant feet have a limited effect on the top heading resistance mobilisation. While the temporary invert causes adverse support geometry, the elephant feet and rock bolting are intrinsically bound to the ground properties and can have a strongly varying effect. Above a certain level of thrust required in the lining, a short bench and early ring closure should be envisioned, however this does not immediately imply that full-face excavation

should be used. It is associated with several operational problems: use of heavy machinery, low accessibility of the crown and shoulders, a great amount of immediate displacement (and energy release) and heavy face support are the usual consequence.

5. The rock bolt pattern has to adhere to the chosen yielding element layout. Long and stiff rock bolts should be either installed far from the yielding elements, or other means of preventing the combined thrust and shear loading should be used. The general rock bolting concept should combine frequent short rock bolts (with the goals of homogenizing the rock mass and increasing its ductility in the vicinity of the excavation, where the strains are highest) and several strong and long rock bolts for the overall stability (thus anchoring the shotcrete segments and the loosened weight of the rock mass).

References

[1]   Schubert, W. & Riedmüller, G. 1995. Geotechnische Nachlese eines Verbruches – Erkenntnisse und Impulse. Proc. 10th Christian Veder Kolloqium, Semprich et al. (eds.). Graz.

[2]   Hoek, E. 2001. Big tunnels in bad rock. 36th Karl Terzaghi Lecture, ASCE Journal of Geotechnical and Geoenvironmental Engineering. ASCE. Seattle.

[3]   Goel, R.K., Jethwa, J.L. & Paithakan, A.G. 1995. Tunnelling through the young Himalayas – a case history of the Maneri – Uttarkashi power tunnel. Engineering Geology 39. pp. 31-44.

[4]   Radoncic, N., Moritz, A.B. & Schubert, W. 2009. Ductile lining design. Geomechanics and tunnelling 2 (5). pp. 561–577.

[5]   Radoncic, N. 2011. Tunnel design and prediction of system behaviour in weak ground. PhD Thesis, Institute for Rock Mechanics and Tunnelling, Graz University of Technology.

[6]   Aydan, Ö., Akagi, T. & Kawamoto, T. 1993. The squeezing potential of rock around tunnels: theory and prediction. Rock Mechanics and Rock Engineering 2. pp. 137–163.

Authors

Dipl.-Ing. Dr.techn.
Nedim Radončić

Geoconsult ZT-GmbH
GTU Koralmtunnel
Hölzlstraße 5
5071 Wals bei Salzburg
Austria

nedim.radoncic@geoconsult.at

O.Univ.-Prof. Dipl.-Ing. Dr.mont.
Wulf Schubert

Graz University of Technology
Institute for Rock Mechanics and Tunnelling
Rechbauerstraße 12
8010 Graz
Austria

schubert@tugraz.at

Proceedings Workshop "Characterization of Fault Zones"

October 9th 2013, Salzburg, Austria